PL-TR-93-2208

SITE EFFECTS ON REGIONAL SEISMOGRAMS RECORDED IN THE VICINITY OF WESTON OBSERVATORY

Matthew R. Jacobson-Carroll
Alan L. Kafka

Weston Observatory
Department of Geology and Geophysics
Boston College
Weston, MA 02193

30 September 1993

Scientific Report No. 4

PHILLIPS LABORATORY
Directorate of Geophysics
AIR FORCE MATERIEL COMMAND
HANSCOM AIR FORCE BASE, MA 01731-3010

The views and conclusions contained in this document are those of the authors and should not be interpreted as representing the official policies, either expressed or implied, of the Air Force or the U.S. Government.

This technical report has been reviewed and is approved for publication.

JAMES F. LEWKOWICZ
Contract Manager
Solid Earth Geophysics Branch
Earth Sciences Division

JAMES F. LEWKOWICZ
Branch Chief
Solid Earth Geophysics Branch
Earth Sciences Division

DONALD H. ECKHARDT, Director
Earth Sciences Division

This document has been reviewed by the ESD Public Affairs Office (PA) and is releasable to the National Technical Information Service (NTIS).

Qualified requestors may obtain additional copies from the Defense Technical Information Center. All others should apply to the National Technical Information Service.

If your address has changed, or if you wish to be removed from the mailing list, or if the addressee is no longer employed by your organization, please notify PL/IMA, 29 Randolph Road, Hanscom AFB MA 01731-3010. This will assist us in maintaining a current mailing list.

Do not return copies of this report unless contractual obligations or notices on a specific document require that it be returned.

REPORT DOCUMENTATION PAGE

Form Approved
OMB No 0704-0188

1. AGENCY USE ONLY (Leave blank)	2. REPORT DATE	3. REPORT TYPE AND DATES COVERED
	30 September 1993	Scientific No. 4

4. TITLE AND SUBTITLE

Site Effects on Regional Seismograms
Recorded in the Vicinity of Weston Observatory

5. FUNDING NUMBERS

PE 62101F
PR 7600
TA 09
WU AL

F19628-90-K-0035

6. AUTHOR(S)

M.R. Jacobson-Carroll and A.L. Kafka

7. PERFORMING ORGANIZATION NAME(S) AND ADDRESS(ES)

Weston Observatory
Department of Geology and Geophysics
Boston College
Weston, MA 02193

8. PERFORMING ORGANIZATION REPORT NUMBER

9. SPONSORING/MONITORING AGENCY NAME(S) AND ADDRESS(ES)

Phillips Laboratory
29 Randolph Rd.
Hanscom AFB, MA 01731-3010
Contract Manager: James Lewkowicz/GPEH

10. SPONSORING/MONITORING AGENCY REPORT NUMBER

PL-TR-93-2208

11. SUPPLEMENTARY NOTES

12a. DISTRIBUTION/AVAILABILITY STATEMENT

Approved for public release; distribution unlimited

12b. DISTRIBUTION CODE

13 ABSTRACT *(Maximum 200 words)*

This is one of five scientific reports describing specific research projects conducted at Weston Observatory under Contract No. F19628-90-K-0035. The research covers a range of topics related to seismology in general and to nuclear test monitoring in particular. In this report, we describe a study in which we investigated the variation of amplitudes of seismic waves recorded in the vicinity of Weston Observatory. The data used for this study consisted of seismograms recorded from events (primarily quarry blasts) located at regional distances from the Observatory. The data were recorded on a 0.25 km aperture array that surrounds the Observatory. Seismometers were installed at four concrete piers (anchored into bedrock) and four sites where the sensors are in soil overlying bedrock. We calculated spectral amplitude ratios between channels for cases in which the type of siting varied. We found that spectral amplitudes varied by nearly a factor of two at bedrock sites and by as much as a factor of five at soil-covered sites (where the soil layer thickness was about 5 to 6 m). Based on the lack of an obvious trend toward greater variation in amplitudes for sites separated by greater distances, our preliminary results suggest that, on the scale of a few tenths of a kilometer, site effects play a larger role than propagation effects.

14 SUBJECT TERMS	15. NUMBER OF PAGES
Site Effects, Regional Seismograms, Quarry Blasts, Chemical Explosions	108
	16. PRICE CODE

17. SECURITY CLASSIFICATION OF REPORT	18. SECURITY CLASSIFICATION OF THIS PAGE	19. SECURITY CLASSIFICATION OF ABSTRACT	20. LIMITATION OF ABSTRACT
Unclassified	Unclassified	Unclassified	SAR

TABLE OF CONTENTS

PREFACE

This is one of five scientific reports describing specific research projects conducted at Weston Observatory under Contract No. F19628-90-K-0035. The research covers a range of topics related to seismology in general and to nuclear test monitoring in particular.

This scientific report consists of an M.S. thesis written by Matthew R. Jacobson-Carroll under the supervision of Professor Alan L. Kafka. In this study, we investigated the variation of amplitudes of seismic waves recorded in the vicinity of Weston Observatory. The data used for this study consisted of seismograms recorded from events (primarily quarry blasts) located at regional distances from the Observatory. The data were recorded on a 0.25 km aperture seismic array that surrounds the Observatory. Seismometers were installed at four concrete piers (anchored into bedrock) and four sites where the sensors are in soil overlying bedrock. At three pier sites, multiple seismometers were installed to investigate the differences between instrument responses.

Over 70 blasts were recorded and the 26 with the highest signal-to-noise ratio were analyzed. Seismograms were corrected for instrument response and analyzed in the time and frequency domains. We calculated spectral amplitude ratios between channels for cases in which the type of siting (pier-mount/bedrock vs. soil sites) and inter-sensor distances vary. Complete seismograms of about 20 sec duration, including initial noise segments followed by P, S/Lg, and Rg arrivals, were analyzed to compute the spectral ratios. We found that, due to what appear to be site effects, spectral amplitudes varied by nearly a factor of two at bedrock sites and by as much as a factor of five at soil-covered sites (where the soil layer thickness was about 5 to 6 m). Based on the lack of an obvious trend toward greater variation in amplitudes for sites separated by greater distances, our preliminary results suggest that for this type of experiment site effects play a larger role than propagation effects, at least on the scale of a few tenths of a kilometer.

1. INTRODUCTION

Accurate measurement of amplitudes of seismic waves is an important aspect of various types of seismological studies. For example, amplitudes are used to calculate magnitudes and seismic moments, to determine focal mechanisms of earthquakes, to discriminate earthquakes from explosions, and to characterize ground motion in seismic risk analyses. It is therefore important to understand all of the phenomena that affect amplitudes of seismic waves. In this study, the various factors that affect amplitudes of seismic waves recorded in the vicinity of Weston Observatory are investigated along with systematic evaluation of site effects at several sites located within a small area surrounding the Observatory. The data used for this study consists of seismograms recorded from events located at regional distances from a seismic array that was specifically designed for this study (Figure 1).

Factors that affect the amplitudes of seismic phases recorded at regional distances can be divided into the following four categories:

- effects of source radiation patterns
- effects of the propagation
- effects of near receiver earth structure
- effects of instrument coupling and instrument response.

Accurately correcting for each of these factors is a fundamental problem in seismology, and it is important to understand as much as we can about these factors and the effects that they have on regionally recorded seismograms.

The emphasis of this study is to examine and attempt to quantify the effects of near receiver earth structures as well as instrument coupling and

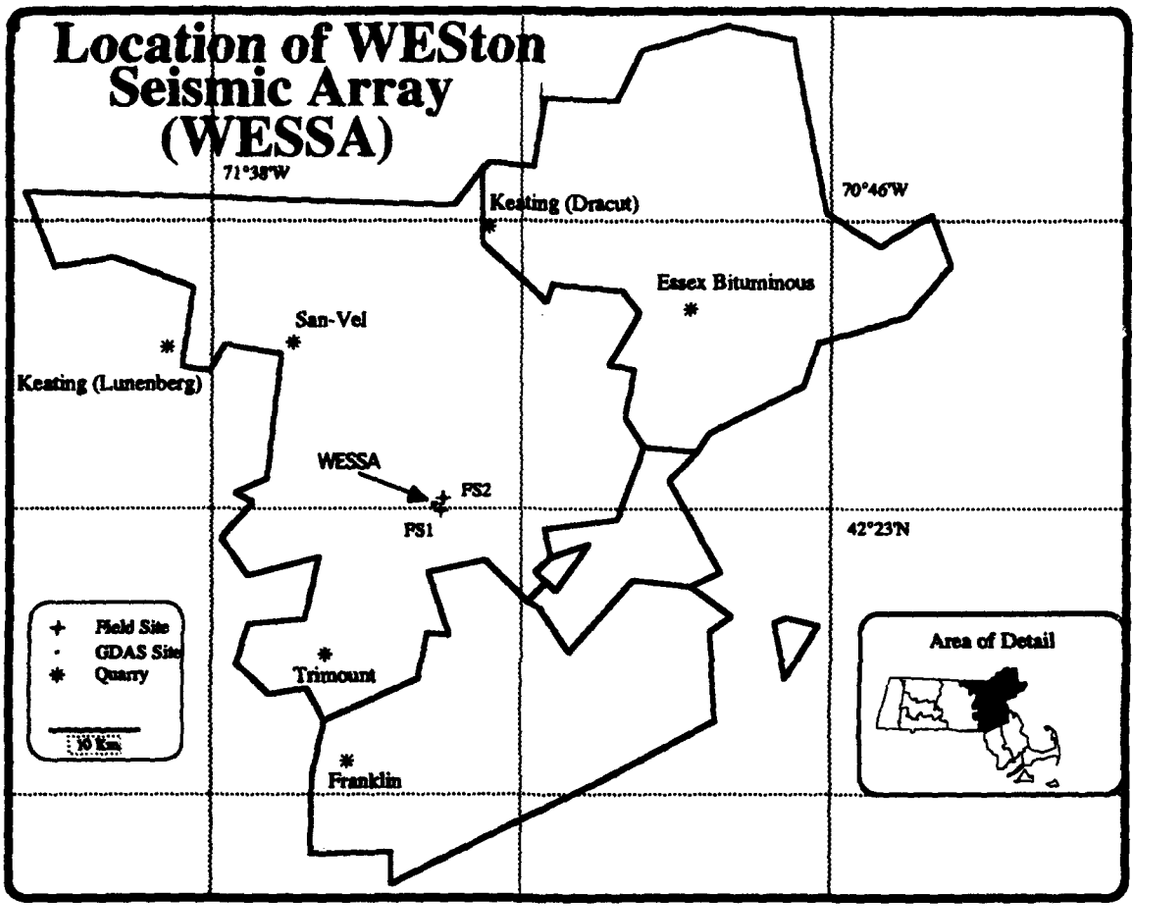

Figure 1: Map of the study area showing the WEStonSeismic Array (WESSA) and the location of the known quarries where blasts were detonated and recorded by the WESSA.

response. By performing a carefully controlled experiment designed to separate these site and instrument effects from the other effects on amplitudes, an investigation on how accurately and precisely we can measure the effect of the near receiver earth structure on amplitudes of seismic phases is performed.

The next section discusses two examples of unresolved problems that illustrate the need to conduct this type of study.

2. TWO EXAMPLES OF WHY THIS TYPE OF STUDY IS IMPORTANT

2.1 Example 1: Magnitudes of Earthquakes Recorded by Station QUA:

Station QUA, located in New Salem, MA, is one of the 30 stations that make up the New England Seismic Network (NESN) operated by Weston Observatory. One of the observations that motivated me to do this study is that the magnitude reported for station QUA is, on average, about 0.43 units higher than the average NESN magnitude for the same event (see Table 1). Figure 2 shows a histogram of the differences between the NESN average magnitude and the QUA magnitude for the events listed in Table 1. The histogram illustrates that, for a given event, the magnitude determined from station QUA is consistently larger than the average NESN magnitude and the differences appear to be randomly distributed around the average difference The scatter around the average suggests that there are random errors that affect these magnitude calculations. Because the average is not close to zero, one (or more) systematic effects is probably present in the magnitude calculations. One or more of the effects on amplitudes mentioned in the previous section may be responsible for this systematic error.

Of those four effects, source radiation pattern and path effects probably do not have a significant effect on the average difference in magnitudes. The event epicenters tend to be randomly oriented around station QUA, and the seismic waves travel across different paths with different path lengths. These effects may be responsible for the random error, but they are probably not sources of the systematic error.

Table 1

Date	Location	HR:MN	Sec	Latitude	Longitude	Dep.	Mn (NESN)	Dist.	Az.	Mn (QUA)	Mn(QUA) - Mn(NESN)
84SEP28	PQ, 5 KM E. OF DISRAELI	0401	00.40	46-01.31	71-25.03	5.00	2.70	403.4	191	2.8	0.1
86APR18	NY, GOODNOW	1250	16.67	43-58.86	74-14.43	11.12	2.50	227.4	138	2.6	0.1
86AUG09	ME, E. SEBAGO	0627	03.26	43-50.00	70-36.00	4.08	2.10	210.3	223	2.5	0.4
86AUG30	NH, 5 KM ESE OF WEBSTER	1440	03.74	43-18.39	71-40.44	4.63	2.40	110.4	211	2.8	0.4
87MAY30	NH, 5 KM ESE OF WARNER	0815	32.15	43-16.14	71-46.02	2.94	2.70	102.9	209	3.1	0.4
87JUN27	NH, 10 KM E. OF CENTER HARBOR	2340	22.22	43-41.00	71-26.63	4.20	2.10	155.9	209	2.4	0.3
87SEP25	NY, 10 KM W. OF LAKE PLEASANT	2056	14.94	43-29.00	74-33.35	0.42	2.90	211.2	123	3.3	0.4
87OCT21	NH, 10 KM NE OF CONCORD	0451	18.27	43-13.17	71-29.61	6.37	2.00	111.2	220	2.2	0.2
87NOV03	ME, 29 KM NW OF TURNER	2326	10.42	44-24.71	70-31.78	7.06	3.00	263.6	215	3.2	0.2
88FEB18	NH, 9 KM W OF JACKSON	0420	23.79	44-08.63	71-18.41	7.63	2.50	206.4	205	3.4	0.9
88AUG02	CT, 10 KM S. OF NORWICH	0425	02.48	41-20.01	71-58.61	7.34	3.40	129.2	345	3.7	0.3
88AUG22	NY, 25 KM SW OF ALBANY	1511	25.21	42-33.91	74-11.30	14.70	2.70	149.7	95	3.3	0.6
89FEB21	CT, 10 KM W. OF WATERBURY	1946	24.77	41-33.17	73-25.71	9.71	2.30	133.1	41	2.3	0.0
89APR15	NH, 10 KM SW FROM LACONIA	1635	06.57	43-27.34	71-33.67	7.23	3.00	129.2	211	3.5	0.5
89APR19	NY, SE OF LONG ISLAND	2301	41.13	40-18.98	72-04.86	17.09	3.50	239.1	354	3.9	0.4
90AUG27	NH, 5 KM NORTH OF CONCORD	0639	11.38	43-18.53	71-36.77	7.93	2.60	113.2	213	3.0	0.4
90SEP17	NH, PITTSFIELD	2301	37.64	43-23.86	71-32.19	7.25	3.10	124.9	213	3.6	0.5
90OCT07	PQ, 18 KM SW OF LA MINERVE	0847	30.65	46-18.03	75-13.50	7.97	3.70	483.6	152	4.3	0.6
90OCT23	DE, SE OF JENKINS	0134	49.56	39-34.71	75-23.05	5.00	3.40	407.8	38	4.1	0.7
90DEC26	NY, BLAST QUARRY #49	1941	51.53	42-23.64	73-42.11	8.66	3.20	109.5	86	3.6	0.4
91MAR06	PQ, 60 KM N OF PEMBROKE	0526	53.77	46-17.14	76-52.05	8.19	3.70	555.9	140	4.2	0.5
91MAR26	NY, BLAST QUARRY #50	2018	52.84	42-27.29	73-55.92	2.34	2.80	128.0	90	3.3	0.5
91APR12	NY, 5 KM S OF MOUNT KISCO	1112	11.62	41-09.03	73-39.20	9.36	3.20	179.9	36	3.7	0.5
91MAY17	PQ, BROWNSBURG	1808	46.47	45-38.88	74-29.70	0.31	3.10	393.0	154	3.5	0.4
91MAY23	ME, 10 KM NW OF BEDDINGTON	0737	34.25	44-51.04	68-08.84	2.00	2.60	432.3	232	3.1	0.5
91JUN03	RI, 7 KM SE OF BLOCK ISLAND	1328	09.15	41-03.09	71-26.64	1.26	3.30	174.3	334	4.0	0.7
91JUN17	NY, SUMMIT	0853	19.18	42-35.05	74-38.70	12.27	4.50	187.1	94	5.1	0.6
									Average Difference		0.43

Station QUA has been calibrated four times since 1986: twice in the summer of 1986, once on July 9, 1987 and finally on August 21, 1990. The two estimates of the gain at 1-Hz calculated in 1986 differ from each other by a factor of two (see Table 2). Although there were no records of the amplifier gain settings, it is suspected that the difference between these two estimates results from a change made in the amplifier gain. It is interesting to note that the magnitude residuals for station QUA are smaller (0.1 magnitude units) before the summer of 1986, and that during and after that summer the magnitude residuals jumped to 0.4 magnitude units. It is therefore possible that instrument response (i.e. a transcription error) is at least part of the

cause of the systematic error observed in the magnitude residuals for station QUA.

Table 2

Date	Gain (Counts per micron at 1-Hz)
August 1986	120.8
August 1986	223.3
July 9, 1987	223.3
August 21, 1990	223.3

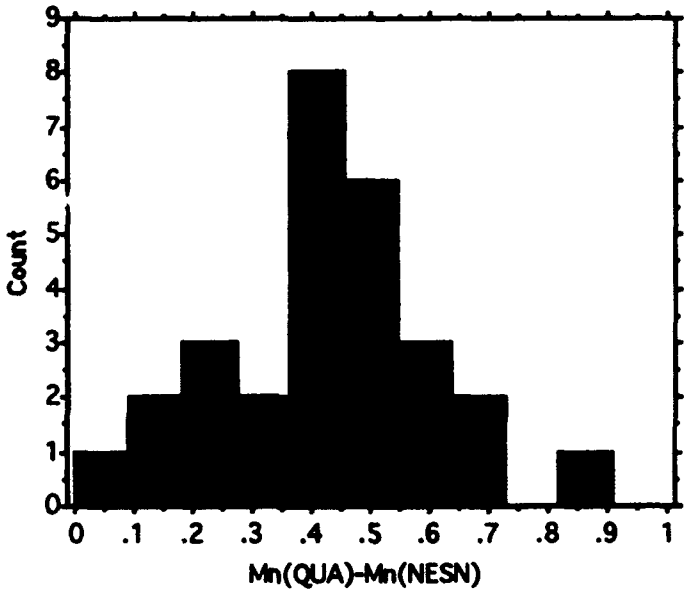

Figure 2: Histogram of the magnitude residuals for station QUA for the events listed in Table 1. Residuals are calculated as the difference between the magnitude calculated for station QUA and the average magnitude calculated for the NESN (Mn[QUA] - Mn[NESN]).

The effect of near receiver earth structure is also a likely candidate for the cause of the systematic error. Because all of the seismic wave energy recorded by QUA must pass through the near receiver earth structure, each seismogram, independent of source distance, size, or azimuth is affected by this factor. Station QUA is installed in soil, and (as will be demonstrated below) the results of this study indicate that at a site installed on sediments, seismic wave

amplitudes tend to be amplified relative to amplitudes recorded at a site installed on bedrock. Also, there may be earth structures in the bedrock beneath the site that focus seismic energy towards QUA. In order to reconcile the difference between the magnitudes reported for QUA with the NESN average, it is necessary to constrain the site effects at station QUA. This is best accomplished by performing a carefully controlled experiment in the vicinity of QUA, as has been done in this thesis for station WES.

2.2 Example 2: Estimating Attenuation of Seismic Waves:

There are two components of seismic wave attenuation that cause a dissipation of energy. The first component is geometric spreading, which causes a decrease in amplitude of seismic wave energy due to the spreading out of energy as the wave travels further from its source. The second component is absorption, which is the loss of energy due to the anelastic properties (internal friction) of the rocks through which the energy is traveling. Internal friction involves a combination of a number of factors which dissipate mechanical energy. While the factors that contribute to internal friction are difficult to measure individually, together they can be quantified by the coefficient of anelastic attenuation (γ) (e.g. Stacey, 1969). After correcting seismic wave amplitudes for geometric spreading, the residual attenuation is characterized by the value of γ. The coefficient γ is a measure of the anelastic loss of energy as the energy travels along the path from source to receiver.

There have been many studies of γ(Lg), γ(S) and γ(Rg) in various parts of the world (e.g., Båth, 1975; Fowler, 1985; Cicerone, 1980; Nuttli, 1973; Dwyer et al, 1983, to name just a few). The results of these selected studies are summarized in Table 3 and include estimates of γ(Lg) and γ(Rg) for regional

distances (up to 600 km) and at frequencies ranging from 5 to 10-Hz for Lg and near 1-Hz for Rg. For these distances and frequencies it is often difficult to distinguish S waves from Lg waves. I will, therefore, (for the rest of this thesis) refer to both as one complicated wave train using the notation of "Lg" (see Kafka, 1990).

In this study, γ(Lg) for New England has been estimated by measuring the decay of amplitudes of the Lg phase with distance. Seismograms of regional earthquakes were bandpass filtered using a 14th order Butterworth filter. In order to study the frequency dependence of γ(Lg), the seismograms were filtered with a passband of 8 to 12-Hz and then again with a passband of 3 to 7-Hz.

Following Nuttli (1978), the amplitudes measured were the maximum sustained amplitudes, which is defined as being "the largest amplitude which is equaled or exceeded by at least three cycles of wave motion" (see Figure 3).

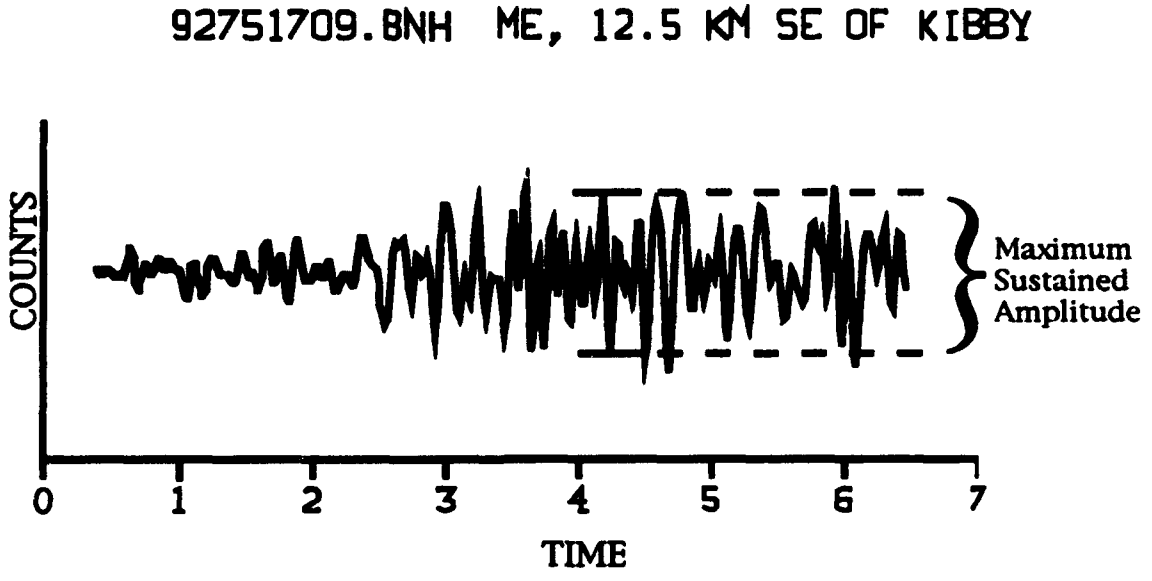

Figure 3: The maximum sustained amplitude is measured as the largest amplitude which is equaled or exceeded by at least three cycles of wave motion. (after Nuttli, 1978; Cicerone, 1980)

The periods of these amplitudes were also measured from the filtered seismogram in order to correct the amplitude measurements for instrument response. The amplitudes were corrected for the instrument gain at the period measured using values for instrument gain obtained through an internal document available at Weston Observatory (Weston Observatory, 1992).

Table 3

GAMMA VALUES FOR VARIOUS PARTS OF WORLD

Author	Wave Type Studied	Gamma (km^{-1})		Area Studied
Båth (1975)	Rg (1.33-Hz)	0.0051	± 0.0090	Sweden
Fowler (1985)*	Rg (1.0-Hz)	0.010	± 0.006	New England
Nuttli (1973)	Lg (1.0-Hz)	0.0006		Eastern U. S.
Dwyer et al (1983)	Lg (1.0-Hz)	0.0007	± 0.0001	Central U. S.
Cicerone (1980)	Lg (5 to 10-Hz)	0.0039	± 0.0004	New England
Dwyer et al (1983)	Lg (10-Hz)	0.0029	± 0.0005	Central U. S.
Ebel (1992)	Lg (about 10-Hz)	0.007	± 0.001	New England

*After recalculating Fowler's results from his published data using a more appropriate geometric spreading factor ($1/r^{1/2}$) (A. L. Kafka, personal communication).

Figure 4 shows typical examples of the plots used to estimate γ(Lg) based on the 8 to 12-Hz filtered data. Instrument corrected Lg amplitudes were corrected for geometric spreading by using a factor of $r^{5/6}$ (where r is the epicentral distance in km). A least-squares regression was performed to fit a line to the log of the corrected amplitudes versus distance. The slope of the fitted line gives an estimate of γ(Lg).

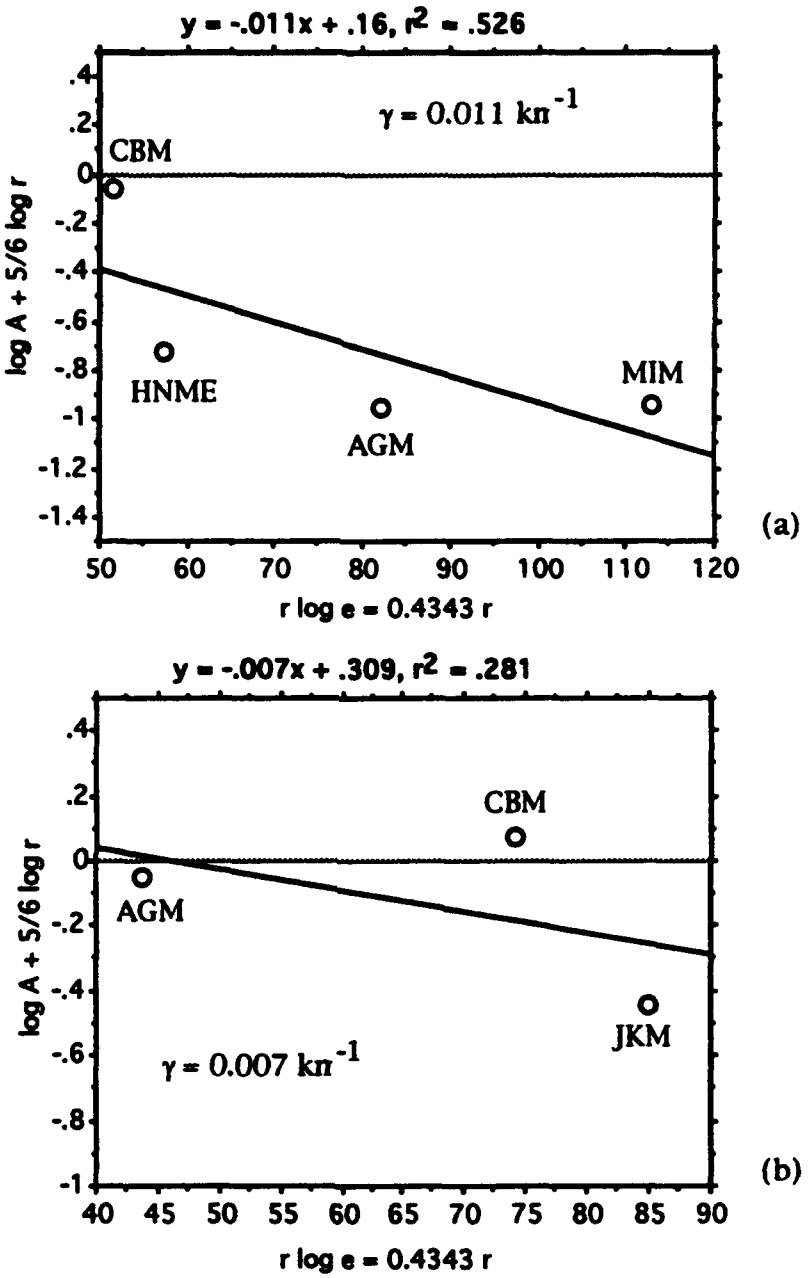

Figure 4: Examples of the plots used to estimate γ in the 8 to 12-Hz frequency band. (a) Event 93150922 - Miramichi, PQ (Mn = 3.2, Mc =2.5). (b) Event 93262305 - Charlevoix, PQ (Mn = 3.4).

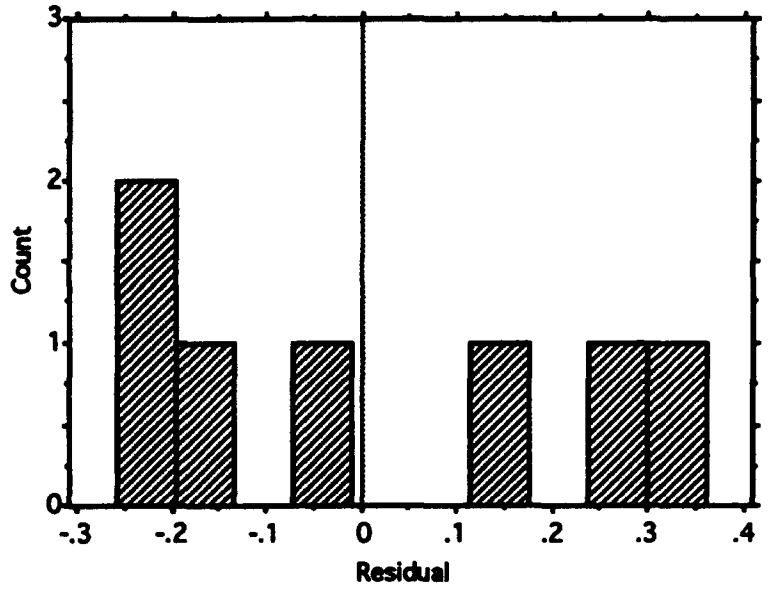

Figure 5: Histogram of the residuals associated with the data used to calculate γ in Figure 4.

Figure 5 shows a histogram of the scatter in the amplitude residuals associated with the data in Figure 4. This scatter is caused by a failure to (accurately) correct for the effects on amplitudes as described in the previous section. In Figure 4 azimuth has been ignored, and therefore the effect of radiation pattern was not corrected for in the results. Since the stations are distributed around the epicenter, rather than in a line radiating from the source, this factor is most likely one of the significant causes of the scatter in the data.

It is also quite probable that there are site effects at each of the stations (similar to those that might exist at station QUA) which have not yet been investigated. In order to accurately compare the amplitudes measured at two or more different stations, these site effects must be more completely understood. Of the 30 NESN stations, the majority are located on soil sites rather than bedrock or concrete piers anchored into bedrock. As will be

demonstrated in a later section, there are large discrepancies between amplitudes measured at soil sites and pier sites which are located in close proximity to each other. The stations used for Figure 4 are located on both concrete pier and soil sites and they are up to 350 km apart from each other. In order to accurately estimate γ(Lg) in New England, experiments must be performed to constrain the site effects and to correct for (or eliminate) the effect of source radiation patterns.

In the next section, each of the factors that affect amplitudes will be discussed in more detail. Further on, this thesis will describe the experimen used to isolate and quantify these effects for seismograms recorded in the vicinity of station WES.

3. EFFECTS ON AMPLITUDES

Previously outlined were four factors that affect the amplitudes of seismic phases recorded on regional seismograms: source radiation patterns, propagation, near receiver earth structure, instrument coupling and instrument response. A detailed discussion of each of these factors follows.

3.1 Source Radiation Patterns:

When the seismic wave amplitude radiated by an earthquake or explosion varies as a function of azimuth around the source, the resulting pattern of higher and lower amplitudes is called the source radiation pattern. By examining the radiation patterns of seismic sources, it is possible to obtain information about whether the event was an earthquake or explosion. If the event is an earthquake, the radiation pattern provides information regarding the style of faulting that released the seismic energy.

In principle, an earthquake should have a very different radiation pattern from that of an explosion. Since an explosion is generated by a concentrated pressure pulse that is presumably spherically symmetric, its radiation pattern should be spherically symmetric. Earthquakes, on the other hand, are caused by shearing motion along a fault plane, and the radiation patterns generated by earthquakes are asymmetric. While asymmetric radiation patterns are well documented for earthquakes, it is not necessarily true that radiation patterns generated by explosions are symmetric (e.g. Wallace, 1992). Because of the actual geometry of the individual shots used in a quarry explosion, it is possible (perhaps even likely) that an asymmetric radiation pattern is generated by these sources. If a seismogram can be corrected for the other factors that affect seismic amplitudes, it would be possible to accurately measure radiation patterns generated by explosions.

If all other factors that affect amplitudes have been correctly accounted for, the measurements of amplitudes recorded at different azimuths around a source will reveal the source radiation pattern. While this may be the desired result for source radiation pattern experiments, the purpose of the experiment described in this thesis is to minimize the effects of source radiation patterns in order to study the site effects. For the purposes of this study, the effect of source radiation pattern is minimized by using an array which is only 0.25 km wide and by using sources greater than 25 km away from the array. This gave the array a maximum coverage of about 0.6° of azimuth.

3.2 Path Effects:

The energy released by a regional seismic event travels through the earth's crust and upper mantle to the recording station. In New England, the

regional crustal and upper mantle structure consists of the structures that underlie the Northern Appalachian Mountains.

The Northern Appalachians include a complex group of "lithotectonic terranes" sutured together during the Middle Paleozoic through Mesozoic times. The terranes, which are believed to have once been separate units, came together as a result of massive plate collisions. This suturing of distinct units resulted in a "collage" of geologic subdivisions each with distinct stratigraphy, structure, and style of deformation (e.g. Skehan and Osberg, 1979).

Kafka and Skehan (1990) divided Southern New England into distinct regions based on the results of Rg dispersion studies. They describe the "Bronson Avalon Dispersion Region" (BADR) as the area of Connecticut and Massachusetts east of the Hartford Rift Basin. This study's research area is *completely contained* within the BADR. The geology of the BADR is quite complex. It consists if the following tectonic terranes (see Figure 6):

1. The Bronson Hill Anticlinorium
2. The Kearsarge Central Maine Synclinorium
3. The Merrimak Trough
4. The Putnam Nashoba Terrane
5. The Avalonian Superterrane

Kafka and Dollin (1985), Kafka and Skehan (1990), and Kafka and Bowers (1991) studied the lateral variations in group velocity dispersion of Rg waves in Southern New England. On the scale used in each of these studies, the BADR was found to be very homogenous with respect to Rg group velocity.

D'Annolfo (1992) showed that on a smaller scale it was possible to discern lateral variations in Rg dispersion within the BADR. The results of her study suggested that the variations in group velocity correlate with the geologic structures in the study area. More specifically, the area surrounding

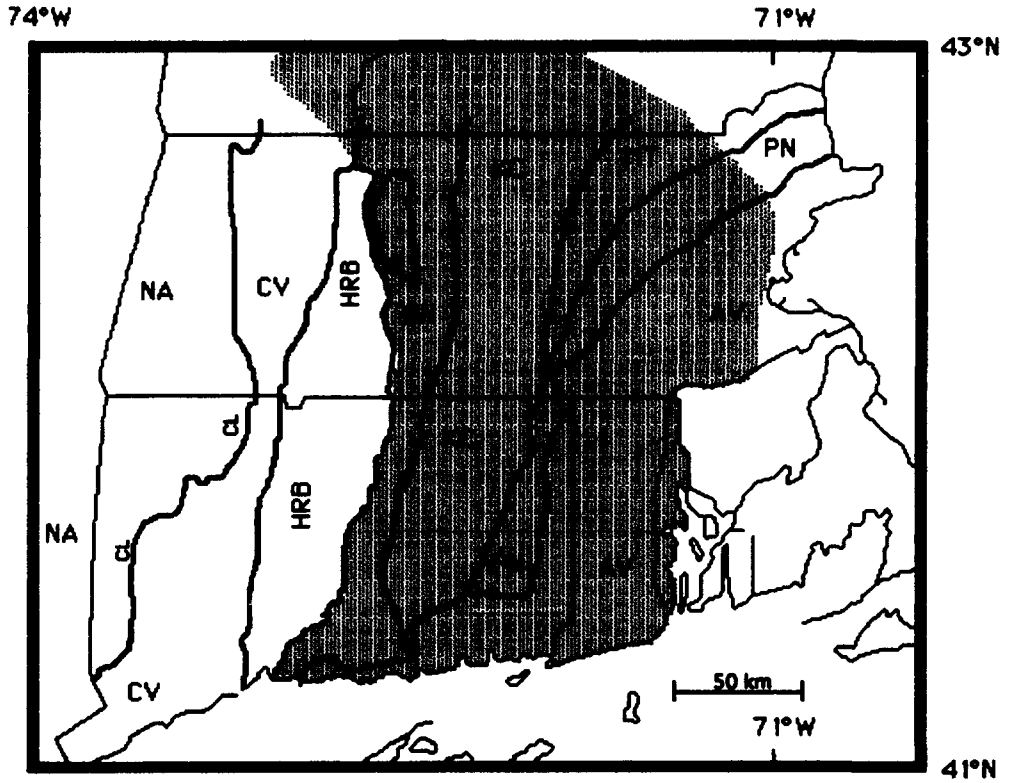

NA = Proto-North American Terrane
CV = Connecticut Valley Synclinorium
CL = Cameron's Line
HRB = Hartford Rift Basin
BH = Bronson Hill Anticlinorium
KC = Kearsarge-Central Maine Synclinorium
MT = Merrimack Trough
PN = Putnam-Nashoba Terrane
AV = Avalonian Superterrane

= BADR

Figure 6: Map of tectonic regions in Southern New England, with the BADR shaded (after Kafka and Skehan; 1990 and D'Annolfo; 1992).

the Clinton-Newbury fault had slower velocities than areas further away from that fault. However, it is important to note that those lateral variations described by D'Annolfo (1992) are quite subtle, and the general conclusion that the BADR is relatively homogeneous still appears to be valid.

Attenuation effects can be separated into the two factors described above: geometric spreading and anelastic attenuation. In the frequency domain, the factor that describes the effect of geometric spreading on surface waves is $r^{-1/2}$, where r is epicentral distance. In the time domain, the factors that describe this effect are r^{-1} for Rg and $r^{-5/6}$ for Lg.

The other path effect on amplitudes, anelastic attenuation, was described above as the loss of amplitude (or energy) due to "internal friction". In the experiment described in this thesis, both of these factors have been minimized by using distant sources and a small aperture array. The maximum difference *in path length differs* only by the aperture of the array (0.25 km). Since the minimum source-receiver distance is 25 km, the extent of the array represents (at most) one percent of the total path length. Assuming a relatively large value for γ of 0.01, the total difference in amplitude from one side of the array to the other, due to geometric spreading and attenuation is only about 1%.

The velocity structure along the path is assumed to be nearly identical for each seismogram recorded by the array. This assumption is based on the facts that the array has a small aperture and that the shallow crustal structure in the study area does not appear to be characterized by large lateral variations in the seismic velocity structure.

Additional evidence that the path effects seem to be minimized is that the f-k spectra (calculated from seismograms recorded by the array) show that

the azimuth of approach is very close to the true azimuth. Figure 7(a-c) shows the f-k spectra for three events recorded on the array. In each figure, the closed circle represents the source location calculated from the analysis, and the open circle represents the actual location with respect to the array. Using f-k spectral analysis on seismograms recorded on this array, it appears that the source can be located accurately to within about 4 degrees of azimuth. This observation suggests that the amount of lateral refraction of seismic waves recorded by the array is quite small.

3.3 Instrument Response:

In order to accurately estimate site effects, the instrument response of the seismographs used in the study must be well constrained. Although absolute amplitudes are in general important, relative amplitudes (i.e. differences from one site to the next) are most important for this study. Therefore a series of experiments was performed which were designed to provide information on both the relative response between the instruments as well as the absolute magnification of each instrument.

The GDAS recording system was calibrated 10 times during the course of the experiment. A known current was input into the calibration coil of each seismometer and the output response was measured. This procedure was repeated 20 times and the average of the output response was calculated for each channel. Using the methods described by Blaney (1990, 1991 and 1992), a least squares fit is made to the average the response curve. This becomes a theoretical model that is used to correct for instrument response. The details of this procedure are described below in Section 6.

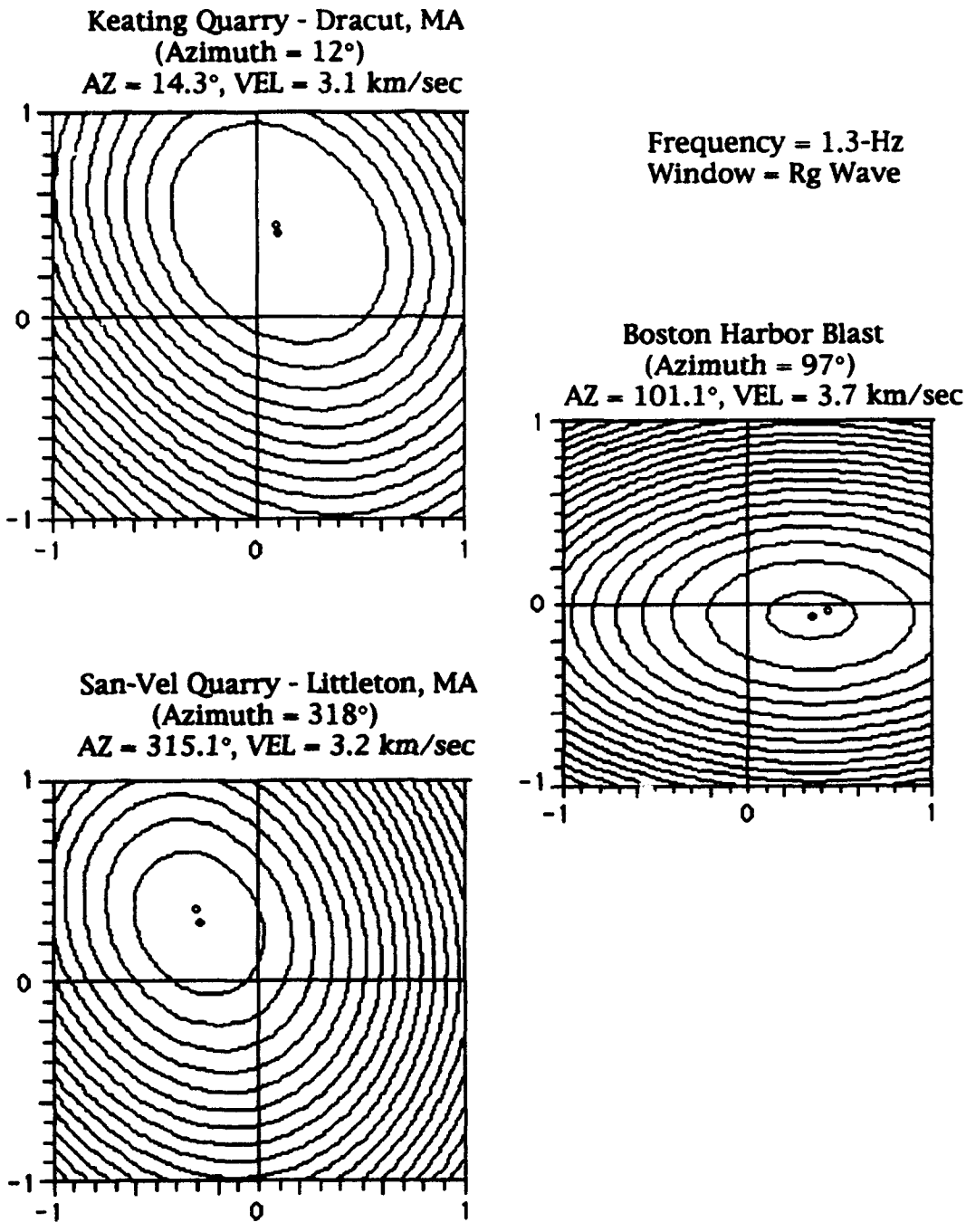

Figure 7: f-k spectra for three events recorded by the WESSA. The closed circle represents the source location calculated by this analysis. The open circle represents the actual location with respect to the array.

In order to test how well the relative instrument response is actually characterized by this procedure, multiple seismometers were "co-located" (i.e., installed directly adjacent to each other on the same pier), and remained co-located throughout the experiment. For each of these channels, spectral amplitude ratios were computed. This was done by correcting the spectral amplitudes for instrument using our model of the instrument response, and comparing them to the corrected amplitudes of the reference channel. The ratio of the corrected spectra provides evidence for evaluating how well instrument response is constrained.

Figure 8 shows the ratios of the corrected spectral amplitudes of channels 8 and 10 to the corrected amplitudes for the reference channel (channel 3). All three of these seismometers were co-located on the same pier. With the exception of the ratios associated with one event, the maximum deviation between the instruments is about 5%. For one of the events, however, the maximum deviation is about 25%, and it is unclear why the deviation is so much larger for that event. This blast was a construction blast detonated in Boston Harbor, and is approximately three times larger than the other blasts studied. The deviation for the Boston Harbor blast is a problem that cannot be resolved at this point. However, for all other events that were analyzed, all of which were quarry explosions, the results for these channels were nearly identical to each other. Therefore this deviation does not seem to be a problem if the analysis is limited to quarry explosions.

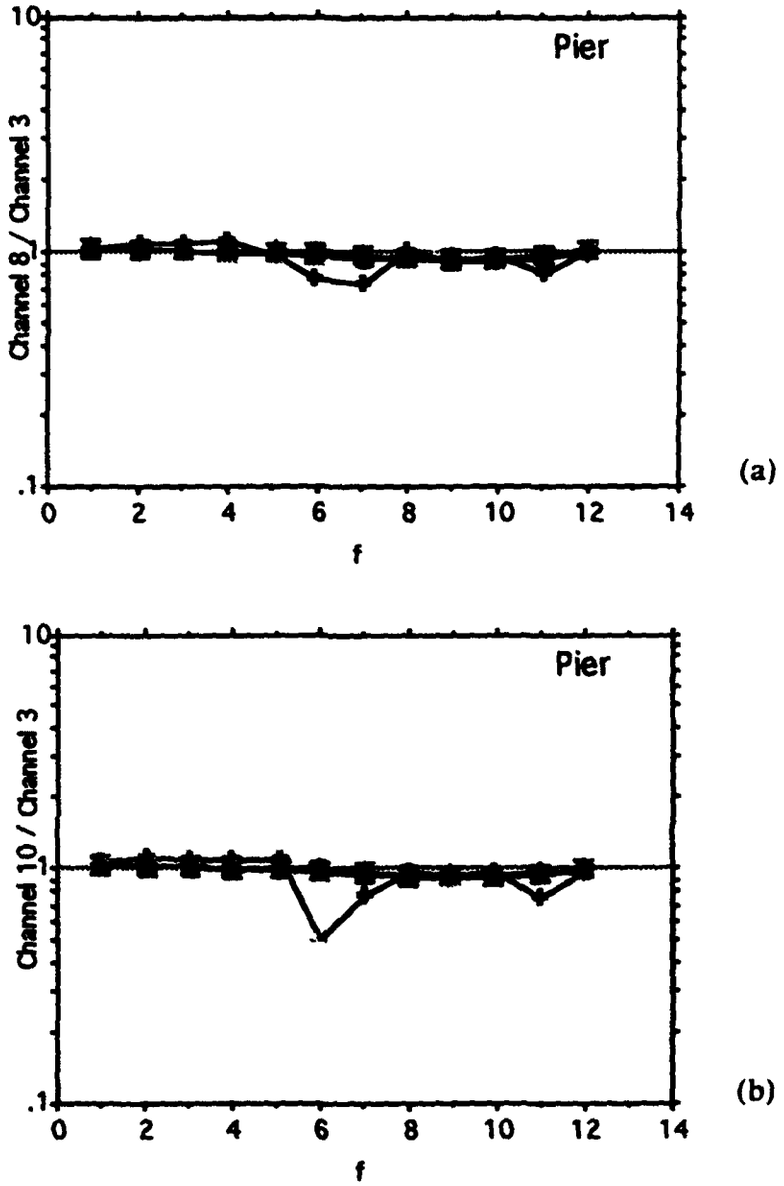

Figure 8: (a) Spectral ratios for Channel 8 / Channel 3, for entire data set. (b) Spectral ratios for Channel 10 / Channel 3, for entire data set. These figures indicate the precision obtained in the instrument response curves. In both cases the anomalous event is 92-103A, the Boston Harbor Blast.

3.4 Recording Site Characteristics:

The primary objective of this study is to investigate the site effects on regional seismograms recorded in the vicinity of Weston Observatory. There

have been a number of previous studies that have shown that recording site characteristics can have a significant effect on the amplitudes recorded on a seismogram. Mayeda et al. (1991), Koyanagi et al. (1992), and Phillips and Aki (1986) studied the amplification of coda waves in different geologic settings. In each study, the authors found that site amplification factors are frequency dependent and can be as high as a factor of 12 to 20 at frequencies of 1.5 to 12-Hz.

The depth to bedrock is known for soil site 1A, and is approximately 0.5 meters. For all other soil sites, depth to bedrock can only be estimated from the Surficial Geology Map of the Concord Quadrangle (Koteff, 1964). The surficial deposits in the study area are primarily glacial till. In the southeastern portion of the quadrangle, where there are significant outcrops of bedrock, the thickness of the till is believed to be no greater than about 5 or 6 meters (Koteff, 1964).

4. RESULTS OF SIMILAR STUDIES

In general, the results of studies similar to this one have shown that soil sites tend to amplify seismic waves more than bedrock sites. Gutenberg (1957) studied earthquakes in California on stations separated by as much as 29 km from the reference station. The estimated depth of the alluvium ranged from zero (for sites on crystalline basement rock) to over 1 km. The average distance between the stations and the reference station was about 9 km, and the average depth of alluvium at soil sites was about 296 meters. For sites where the depth to the water table was known, the ground water table was from 30 to 100 meters below the ground surface.

Gutenberg studied the East/West horizontal component of ground motion on instruments installed on concrete floors and compared them to amplitudes recorded on similar instruments installed at a reference site. He found that the ratio of amplitudes at sites on dry alluvium to those recorded on sites underlain by crystalline rock were on the order of 5:1 or more at frequencies between 0.67 and 1-Hz. For sites on water-saturated alluvium, he found that the amplitudes were closer to 10 times those at the crystalline rock reference site. He also found that the site amplification was dependent on the period of the wave studied, and for frequencies lower than 4-Hz, the difference between amplitudes recorded at other crystalline rock sites did not differ significantly from those at the reference site.

Koyanagi et al. (1992) studied the frequency dependent site amplification on the island of Hawaii using S-wave coda spectral ratios for frequencies between 1.5 and 15-Hz. They used 40 vertical 1-Hz seismometers, and recorded 136 local earthquakes with focal depths greater than 5 km. The stations used in their study were distributed mostly near the calderas or along the flanks of the active volcanoes of Mauna Loa and Kilauea. The distances between the sites ranged from a few km to over 100 km. Although there is little variation in surficial geology in their study area, they found amplification factors as large as 12 times the reference amplitudes for a given frequency. They attributed these to differences in absorption and/or impedance properties beneath the site.

Mayeda et al. (1991) investigated the site amplification using the S-wave coda from small local events (magnitudes ranging from 1.5 to 2.8) located in the Long Valley Caldera Region, California. The station site characteristics vary greatly, ranging from Quaternary alluvial deposits to Cretaceous

crystalline basement rock. Distances between the 15 stations ranged from about two to about 25 km. They found that at 1.5 and 3-Hz, sites within the caldera experienced amplification of ground motion from 5 to 17 times that of the reference site. At higher frequencies, they found that there was less amplification at these sites. They attributed the change from higher to lower amplification to the competing effects of an impedance contrast between the basement and the caldera fill and high absorption in the caldera fill at high frequencies.

Phillips and Aki (1986) studied the coda from local earthquakes in central California to examine site amplification. These earthquakes were recorded on a part of the CALNET network which included over 150 stations distributed over an area of approximately 100 by 300 km. They observed amplification factors as high as 20 times the average station for low frequencies (1.5 to 3-Hz) at sediment sites. They found that for sediment sites, amplification varied inversely with sediment age and that amplification was lowest for Franciscan (basement) sites and sites situated on granite. They also noted a different pattern at high frequencies (6 to 24-Hz). At these frequencies, granitic sites exhibit increasing amplification relative to the average station. Near-site impedance and attenuation were proposed as explanations of their results.

In their study of the Garm region of (what was then) the USSR, Tucker et al. (1984) made observations of hard rock site effects at frequencies between 1 and 40-Hz by comparing the seismograms recorded at sites in tunnels and at sites on outcrops. The tunnel sites were separated by 300 meters horizontally and 20 meters vertically. The experiment used sites whose minimum station spacing started to approach the maximum station spacing used in this study.

Tunnel sites affected the amplitudes of signals by as much as a factor of 3 at frequencies inversely proportional to the tunnel depth. Most of the tunnel effects were explained by interference between direct waves and waves reflected from the surface. Although hard rock sites typically varied by no more than a factor of 3, outcrop sites did record amplifications as high as a factor of 8 times the reference site.

In a related study, King and Tucker (1984) studied the variations in amplitudes recorded across a sediment filled valley for frequencies between 1 and 50-Hz. The stations, in parts of this experiment, were more closely spaced than the stations in the tunnels of the previous study. The closest spacing in this study was a 200 meter line of 4 equally spaced stations stretching across a sediment filled valley. The sediments in the valley were deepest at the middle of the valley where they ranged from 75 to 300 meters thick. They observed that amplitudes at soil sites were amplified by as much as a factor of 10 relative to those recorded at a reference hard rock site. They also found that amplification was dependent on frequency and distance from the valley edge. Local site effects that changed the amplitude of ground motion by about a factor of 2 could be identified in almost all events. Ground motion at the valley edge deviated from the ground motion at the middle of the valley by as much as a factor of 5, even though these sites were separated by less than 200 meters.

5. DESIGN OF EXPERIMENT: THE WESSA

The WESton Seismic Array (WESSA) is an array of 13 1-Hz seismometers installed in the area around Weston Observatory. The array data are recorded by the Geophysical Data Acquisition System (GDAS) described by Blaney (1991). The array was installed in two phases. The seismometers installed in the first

phase extended out to about 0.25 km from the reference site. Installation and calibration of the instruments installed as part of the second phase is nearly complete. The second phase extended the array to about 0.5 km from the reference site. The part of the array that was used for this study (sites occupied in the first phase) consists of 8 sites, 4 on concrete piers which are assumed to be anchored to bedrock, and 4 at soil sites. At three of the pier sites co-located seismometers were installed to allow a comparison of the differences between instruments.

5.1 Description of the Equipment in the Array:

Blaney (1990 and 1991) gives a functional description of the entire GDAS system and its recording capabilities. The aspects of the system described in this section are only those pertinent to this experiment.

The WESSA sensors are Electro-Tech EV-17 1-Hz vertical seismometers. These seismometers are connected by cable to a junction box with a 6 pole 12.5-Hz anti-aliasing filter. The signal from the junction box is sent by cable to the analog to digital converter and sampled at 50 samples per second. The data are recorded on magnetic tape and stored for later analysis.

5.2 Geometry of the WESSA :

Figure 6 shows the geometry of the WESSA. Site A is located on the same pier as station WES of the NESN. For this reason, site A, and in particular channel 3, was chosen to be our reference site for the experiment.

Site B is a pier site located about 70 meters south of the reference site. It is located within 4 meters of the pier used for the World Wide Standardized Seismic Network (WWSSN) station WES. Three seismometers (channels 4, 6 and 13) were co-located at this site. Site C is a pier site located 251 meters south of the reference site. Channel 7 was located at this site.

Site D is a pier site located about 141 meters southeast of the reference site at the Observatory's magnetic observatory pier. This pier differs from the other piers in its geometry. While the other piers had very large surface areas (a few m^2), and were relatively low to the ground surface, this pier was tall (higher from the ground surface) and narrow (relatively small surface area, less than 1 m^2). It is unknown how much the geometry of the pier affected the signals which were recorded.

Site A1 is located 2 meters west of the reference site. It is a soil site which is within about 0.5 meters of bedrock. As described above, this is the only soil site for which the depth to bedrock is well constrained. At the other soil sites, depth to bedrock is believed to be no more than about 5 to 6 meters.

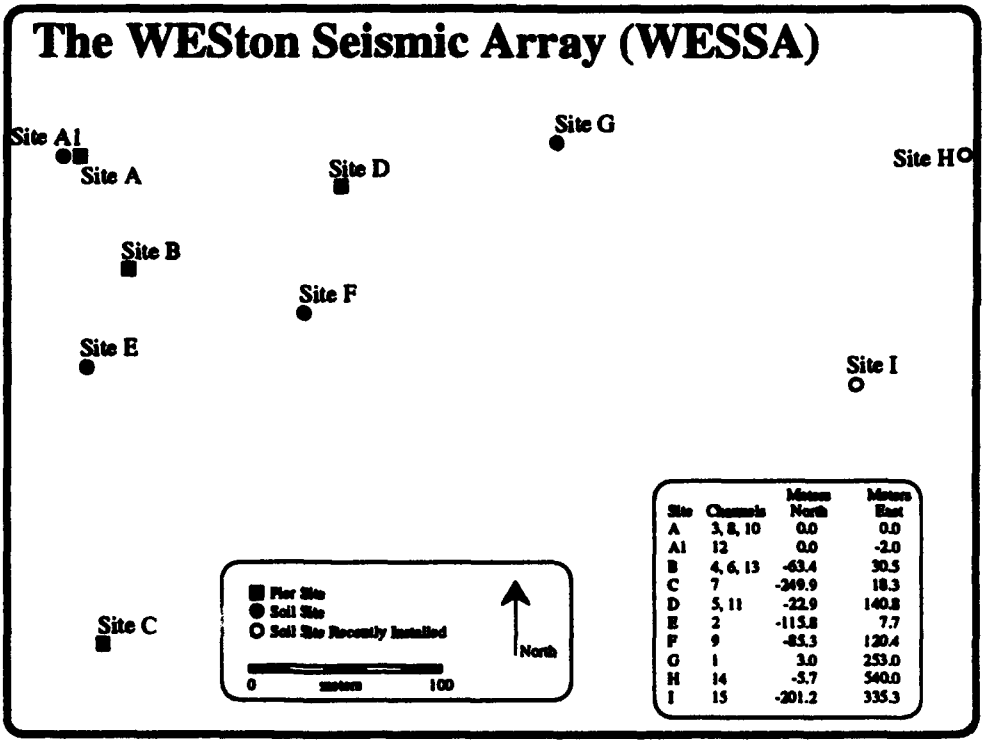

Figure 9: Map showing the geometry of the WESton Seismic Array (WESSA). Closed squares represent pier sites. Closed circles represent soil sites used in this study. Open circles represent soil sites recently installed, and not included in this study.

Site E is a soil site located about 116 meters south of the reference site. This site is located within 53 meters of Concord Road, and is about 8 meters west of the driveway to the Observatory. A significant amount of noise from vehicles may have been recorded by the seismometer located at this site.

Site F is a soil site located 148 meters southeast of the reference site. This site is approximately half way between the site which is furthest south and the site which is furthest east of the reference site. Site G, is the located 253 meters east of the reference site. It is located in a wooded area. Low frequency noise was very prominent on the seismograms recorded at this site.

5.3 Data Acquisition with the GDAS:

Because the GDAS system does not have a trigger mechanism, it was turned on manually to record quarry and construction blasts for which we had advance notice. Several quarry operators had agreed to inform us shortly before they were going to detonate their explosions. In addition to these known times, the GDAS was also turned on periodically to record during times of peak blasting activity, and the seismograms were scanned for events. The GDAS records continuously for one hour before the magnetic tape must be changed. In order to facilitate identifying the times when the blasts occurred, the digital records of the NESN and the analog records of the WWSSN station WES were analyzed for typical blast waveforms.

6. DATA ANALYSIS

Over 70 events were recorded on the WESSA for this study. Of those 70 events, 26 with the highest signal to noise ratios were chosen to be analyzed. Signal to noise ratios were estimated for each event by measuring the highest peak-to-peak amplitude in the window of time that the P, Lg, and Rg phases

arrived. The resulting peak-to-peak amplitudes for these signals were divided by the highest peak-to-peak amplitude measured in the pre-event noise window (see Table 4). The criteria for deciding which events to analyze was to choose the eight events which had the highest signal to noise ratio for the Rg phase, the eight events which had the highest signal to noise ratio for the Lg phase, and the eight events which had the highest signal to noise ratio for the P wave. In addition, seven events from the 1992 field season were analyzed. One of these was the Boston Harbor blast (discussed previously) which was three times larger than any other blast analyzed. The other six from 1992 were analyzed because they were recorded shortly before and shortly after the Boston Harbor blast.

Figures 10-13 show examples of the waveforms and spectra for typical events analyzed in this study. In these figures (and in all other figures in the remainder of this thesis) the seismograms have been corrected for instrument response and processed to appear as if they were recorded by the same instrument (see below). The seismograms have been analyzed in both the time and frequency domains.

6.1 Analysis of Instrument Response:

The GDAS was calibrated regularly throughout the experiment as described by Blaney (1990). The system was calibrated at least 15 times during the experiment, and the 10 calibrations that were used in this analysis were those which were performed during times with the least amount of background noise. Each time the system was calibrated, a known current was applied to the calibration coil of each seismometer and the output of the seismometer was recorded. This was repeated at least 20 times on each day that

a calibration was performed, and the results from each run were stacked. The

Table 4

Event	P S/N	Lg S/N	Rg S/N	
91241A	1.2	4.0	13.0	*
91252A	2.0	4.0	12.5	#
91261B	3.2	7.0	12.2	*
91266B	~1.0	~1.1	12.2	*
91234B	9.0	11.0	12.1	*
91227B	3.8	4.1	12.0	*
91249D	3.5	6.0	12.0	*
91259B	2.8	4.2	11.0	*
91247A	3.0	6.0	10.0	*
91266C	1.7	4.0	9.5	#
91249A	2.0	7.0	9.2	*
91274B	2.2	4.2	9.1	*
91240A	2.0	2.8	9.0	*
91254A	4.0	10.0	9.0	*
91255A	2.2	6.0	9.0	
91277B	2.8	6.1	9.0	
91274A	3.0	12.0	8.8	
91234A	2.9	10.0	7.8	*
91266A	2.2	5.0	7.0	
91212A	1.8	2.3	6.2	*
91249C	~1.0	~1.0	6.0	
91235A	2.1	6.1	5.9	*
91249E	4.0	8.0	5.5	*
91227A	1.5	2.0	5.3	*
91155A	4.3	2.9	5.0	
91344A	1.1	2.8	4.7	
91240C	1.5	2.2	4.6	*
91240E	3.2	3.4	4.5	*
91252B	1.5	3.0	4.0	*
91259A	1.3	1.8	4.0	
91277A	1.8	4.4	3.8	
91252C	1.5	1.5	3.0	
91255B	1.4	2.1	2.7	
91246A	1.0	1.4	2.5	
91240D	3.1	5.5	2.2	
91249B	~1.0	~1.0	1.3	

Events recorded by the WESSA during the 1991 field season. Signal to noise ratios shown for the P, Lg and Rg phases calculated as described in the text. Events marked with an asterisk (*) were analyzed in this study. In addition, 7 events from the 1992 field season were analyzed. Events marked with a pound sign (#) were unable to be analyzed due to loss of data.

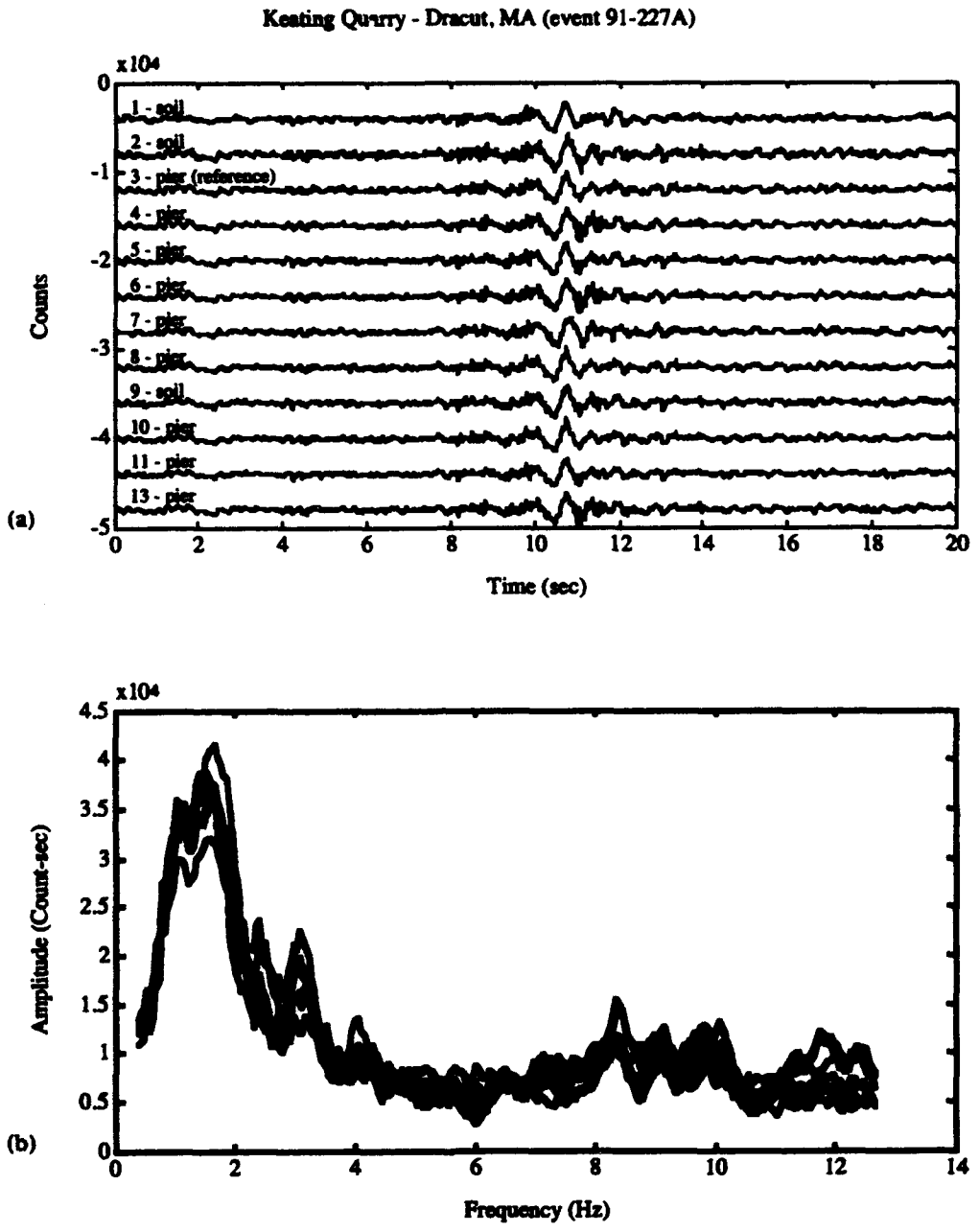

Figure 10: Examples of a typical event recorded on the WESSA. The top figure shows the waveforms for event 91-227A after being corrected to appear as if each was recorded by the same instrument. The bottom figure shows the resulting amplitude spectra for the corrected seismograms.

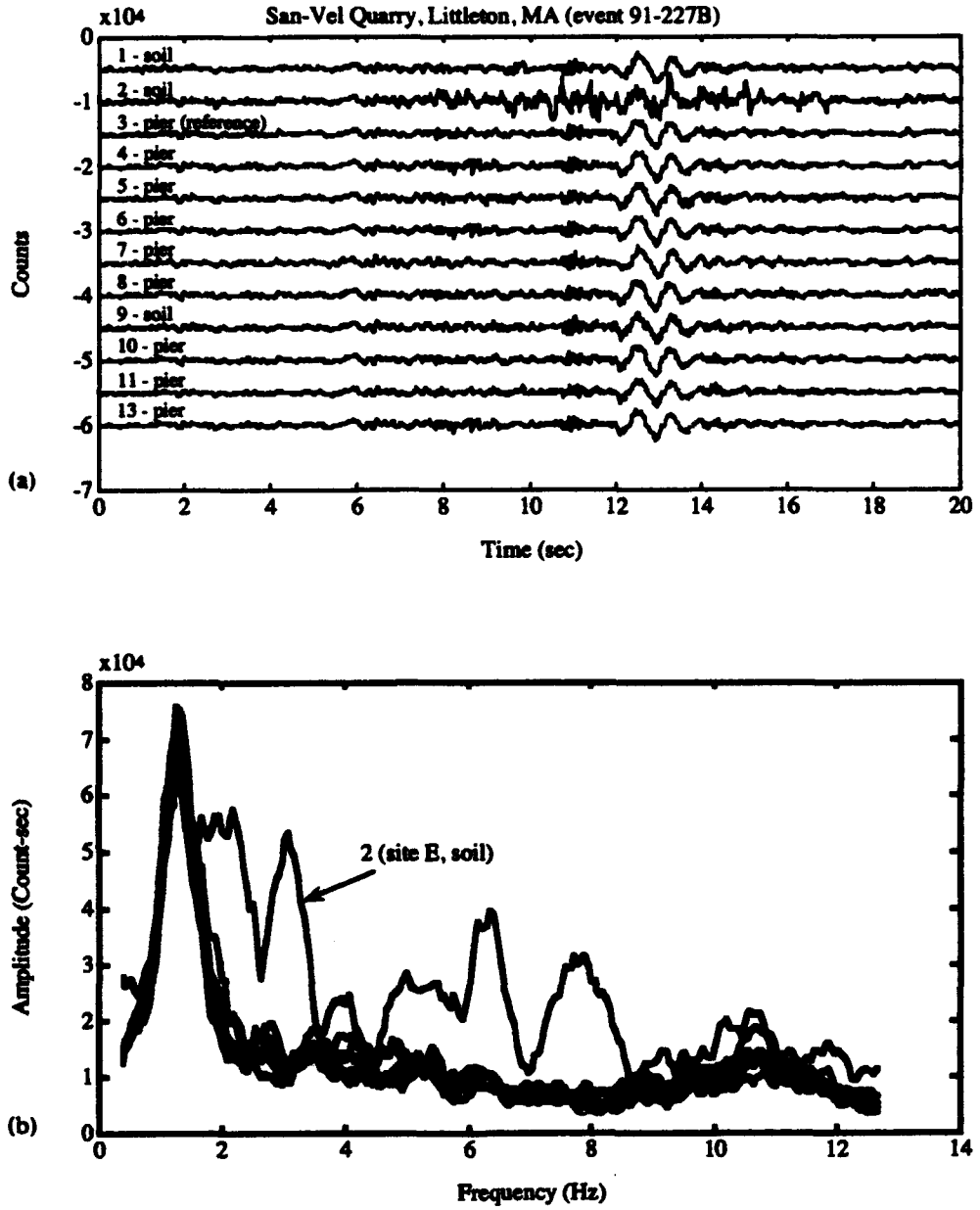

Figure 11: Examples of a typical event recorded on the WESSA. The top figure shows the waveforms for event 91-227B after being corrected to appear as if each was recorded by the same instrument. The bottom figure shows the resulting amplitude spectra for the corrected seismograms.

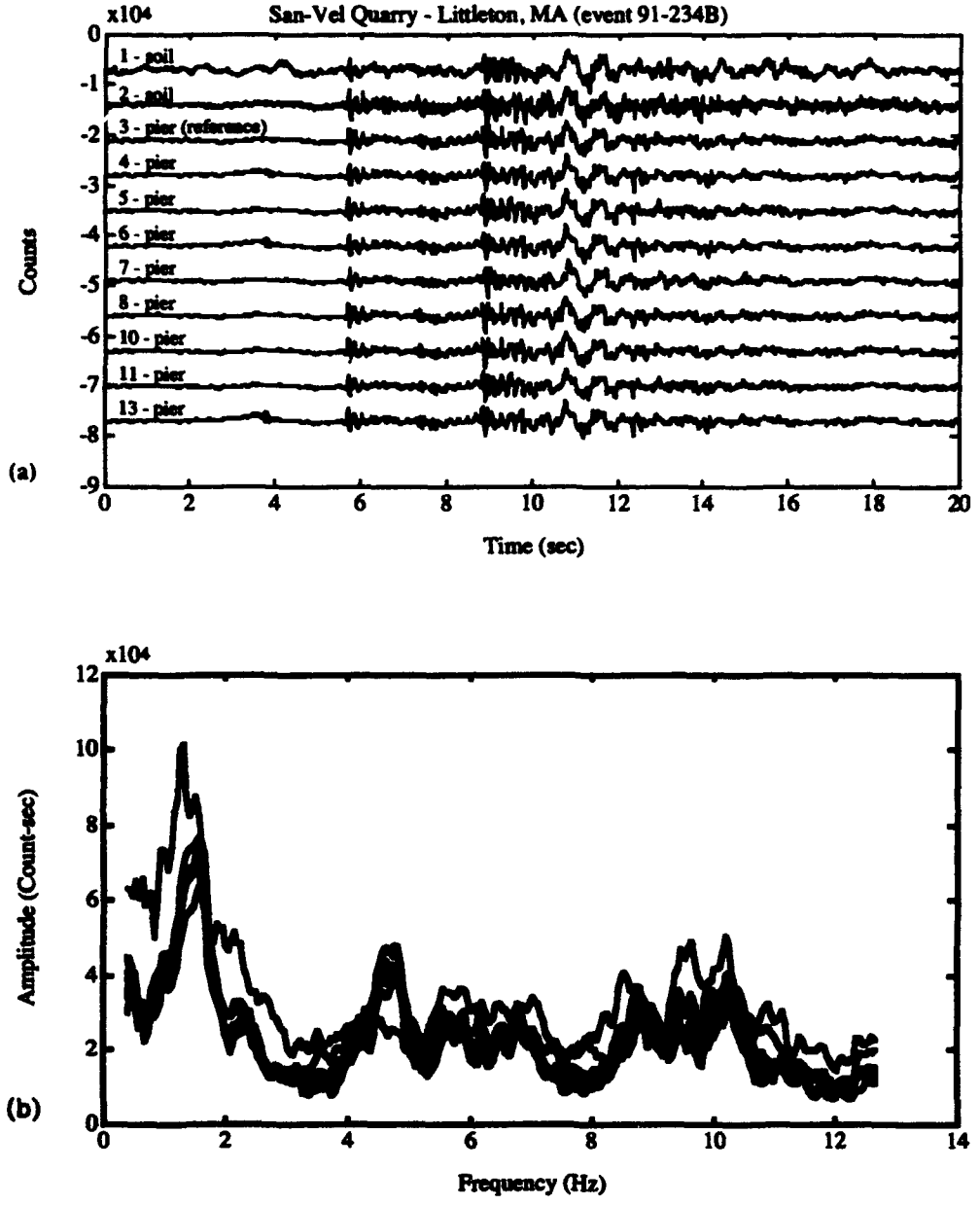

Figure 12: Examples of a typical event recorded on the WESSA. The top figure shows the waveforms for event 91-234B after being corrected to appear as if each was recorded by the same instrument. The bottom figure shows the resulting amplitude spectra for the corrected seismograms.

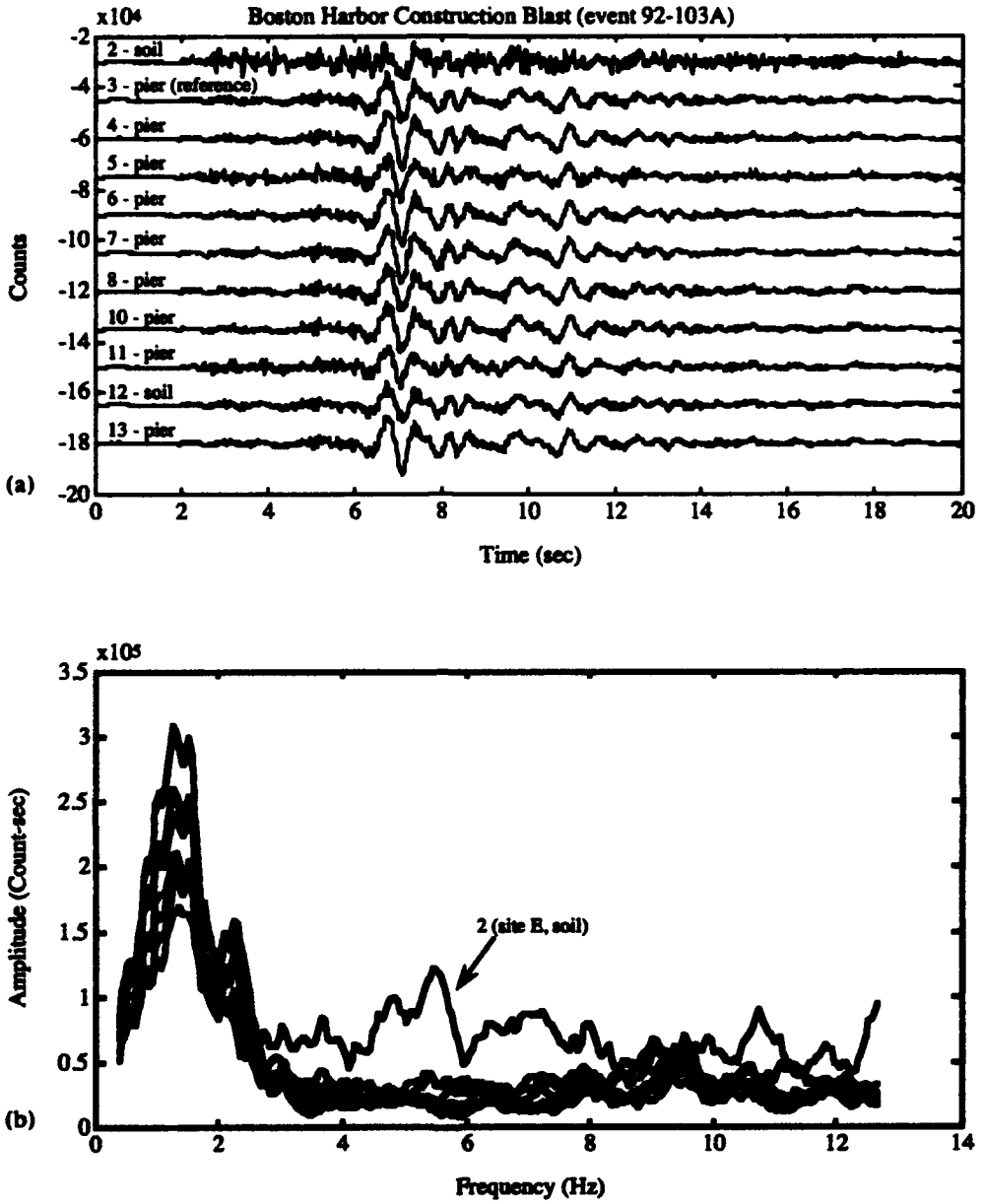

Figure 13: Examples of a typical event recorded on the WESSA. The top figure shows the waveforms for event 92-103A after being corrected to appear as if each was recorded by the same instrument. The bottom figure shows the resulting amplitude spectra for the corrected seismograms.

stacked output is referred to as the daily average pulse (DAP). A least-squares fit of the DAP was used to determine the model instrument response for the individual day (see Blaney, 1990). At the end of the experiment, the model instrument responses were averaged to determine the nominal instrument response (NIR) for each instrument.

Figures 14-16 show the results of the calibrations for three of the channels. In the top of each figure the response of the individual DAP is shown as well as the resulting NIR for each instrument. The bottom portion of each figure shows the NIR as well as the average response determined from the DAP's.

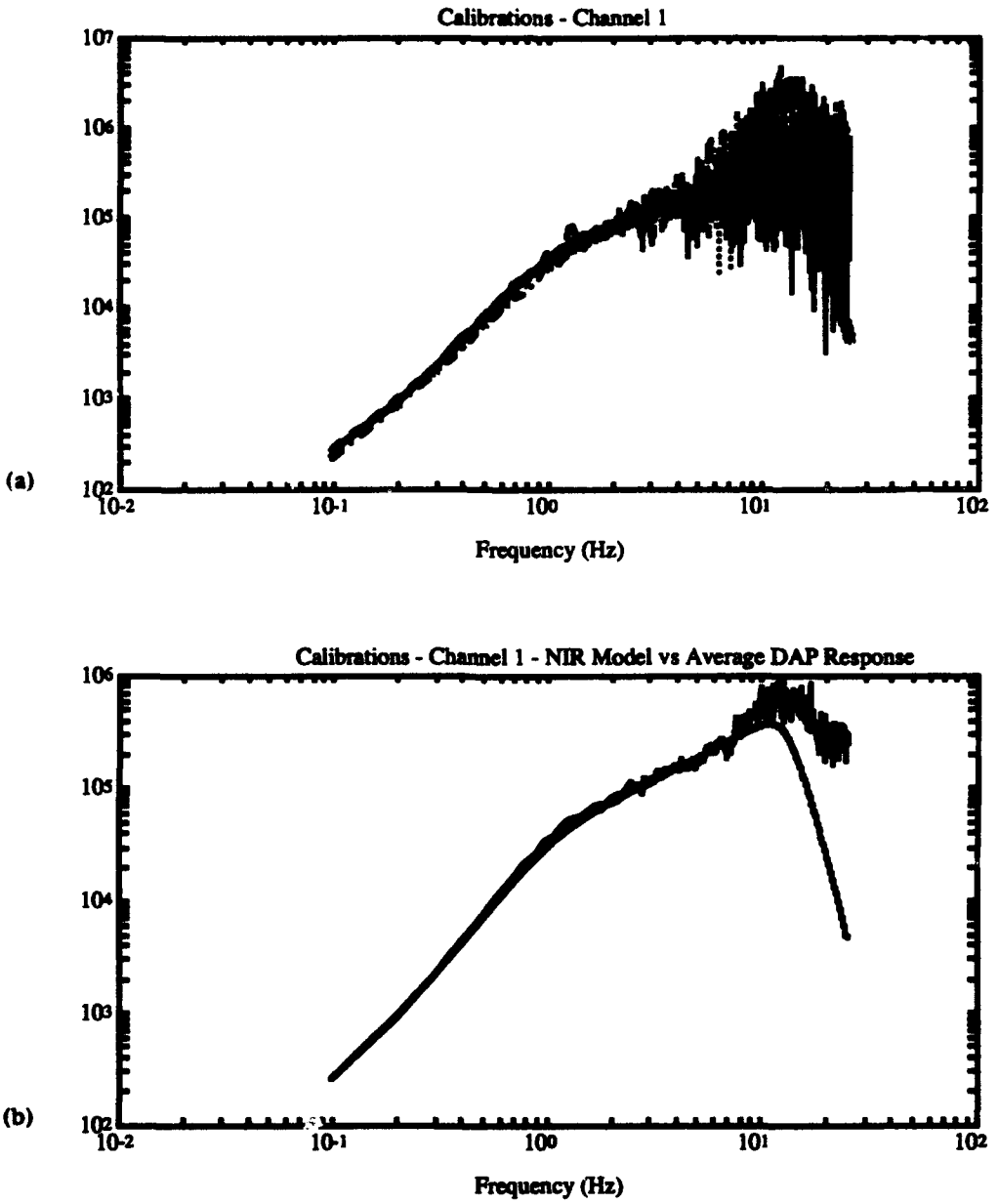

Figure 14: Example of calibration results for channel 1. The top figure shows the response of the individual Daily Average Pulse (DAP) as well as the resulting Nominal Instrument Response (NIR) for each instrument. The bottom figure shows the NIR as well as the average response of the DAP's.

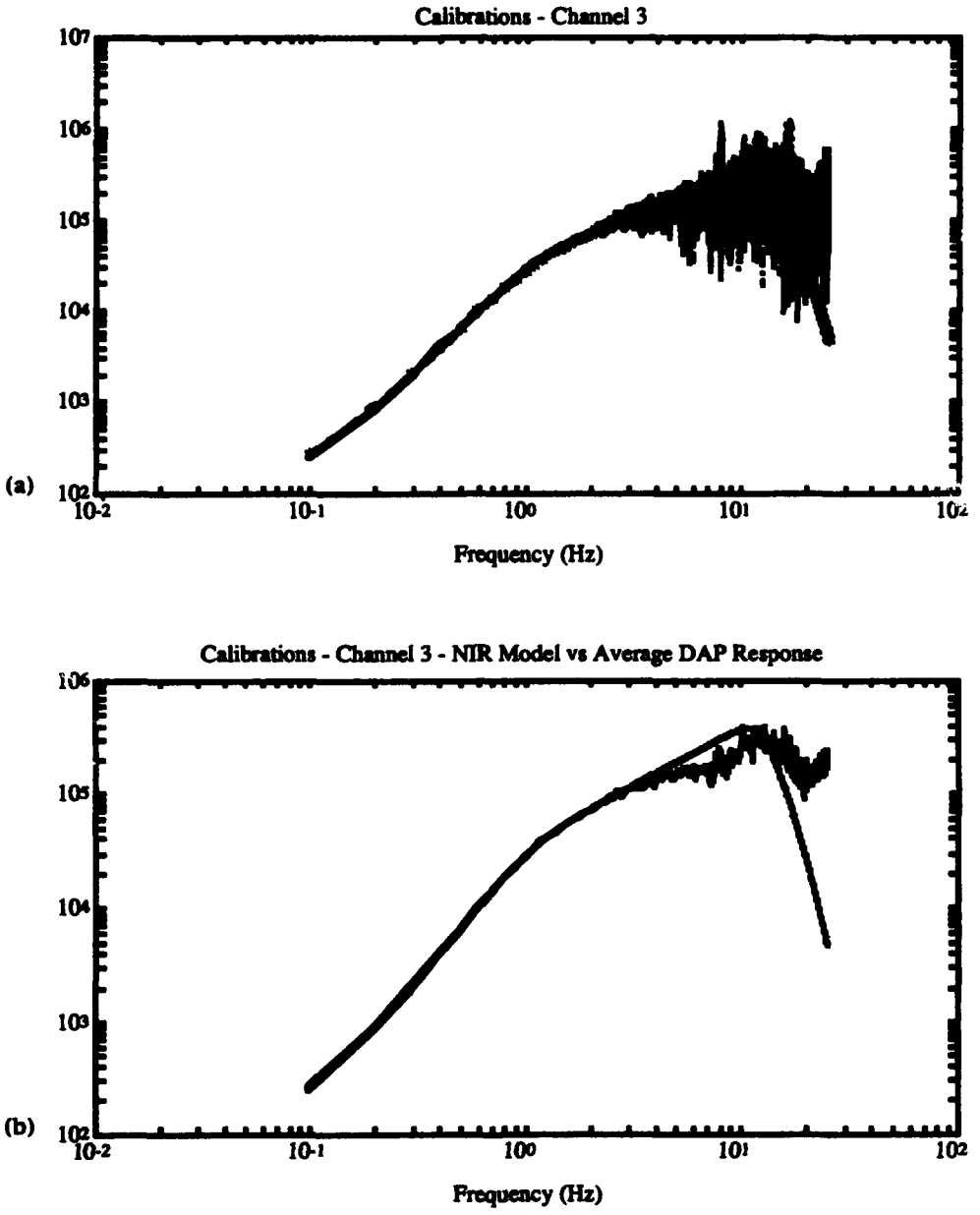

Figure 15: Example of calibration results for channel 3. The top figure shows the response of the individual Daily Average Pulse (DAP) as well as the resulting Nominal Instrument Response (NIR) for each instrument. The bottom figure shows the NIR as well as the average response of the DAP's.

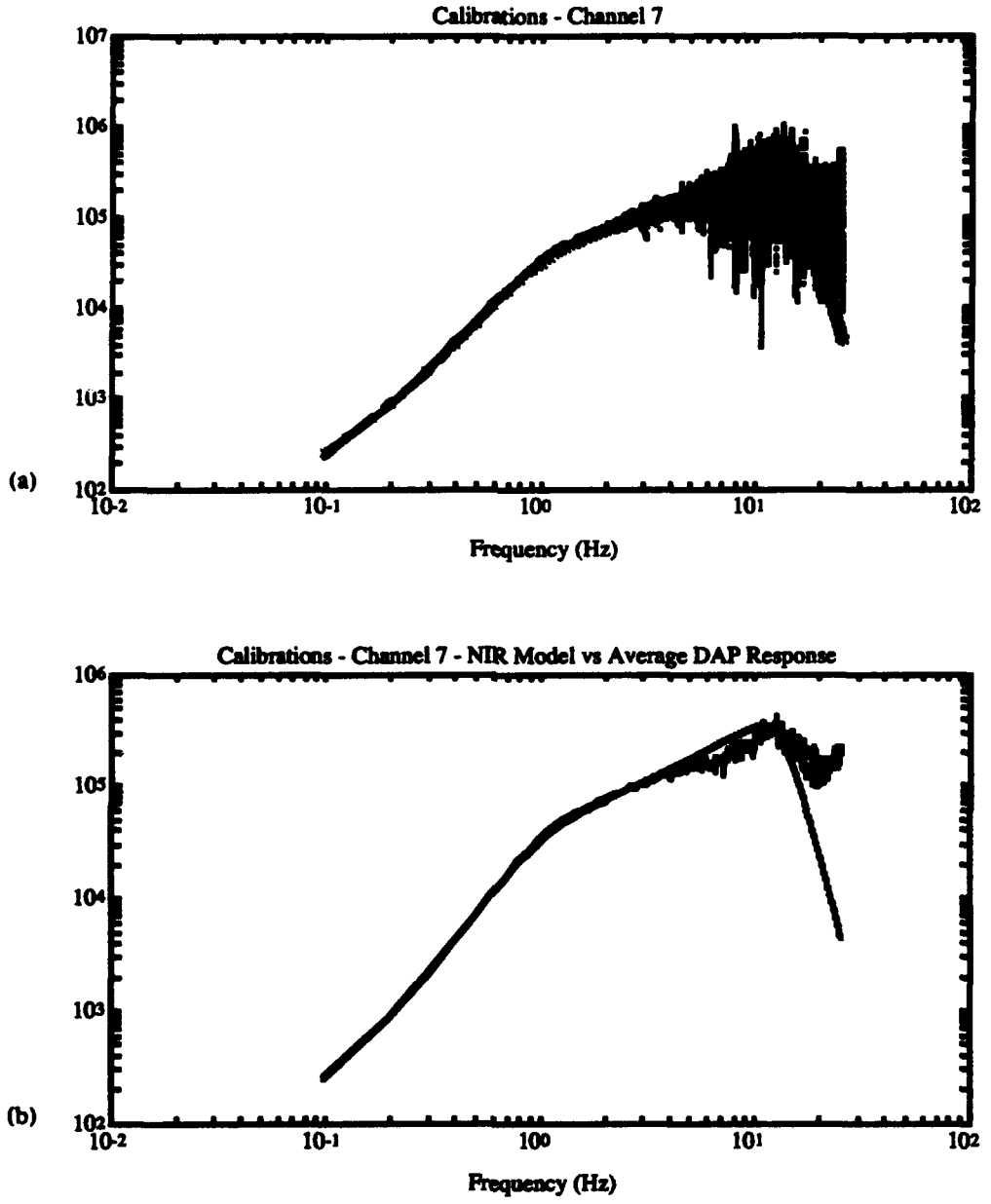

Figure 16: Example of calibration results for channel 7. The top figure shows the response of the individual Daily Average Pulse (DAP) as well as the resulting Nominal Instrument Response (NIR) for each instrument. The bottom figure shows the NIR as well as the average response of the DAP's.

6.2 Effects of Errors in Instrument Response Curve:

Figure 17 shows an example of the variation of spectral ratios when three different estimates of instrument response are used to correct to ground motion. The first estimate is the NIR described above in Section 6.1. The second estimate is based on averaging all the DAP estimates as described in Section 6.1. The last estimate is based on calculating instrument response using the average of all calibration pulses for the season.

The maximum difference between the three estimates is about 20% for frequencies below 6-Hz. At frequencies greater than 6-Hz, the difference between the estimates becomes more significant and the maximum difference is about 75%. As will be discussed below, this suggests that some of the differences in amplitudes at frequencies above 6-Hz could be as much due to instrument as to site effects. It is also important in this regard to consider the spectral ratios of channel 8 to channel 3 and for the ratios of channel 10 to channel 3 (see Figure 8). All three of these channels are co-located on the reference pier. With the exception of one event, which was a construction blast detonated in Boston Harbor (see Section 3.3), the maximum deviation in these ratios is less than 5%. Between 0 and 4-Hz and above 11-Hz, the ratios for channels 8 and 10 are very close to 1.0, but between 4 and 11-Hz, the ratios drop to a minimum of about 0.95 (which occurs near 9-Hz). Thus, it appears that although the differences between different types of methods of estimating instrument response can be as great as 20% at low frequencies and 75% at high frequencies, the actual difference between the amplification of the instruments is much smaller.

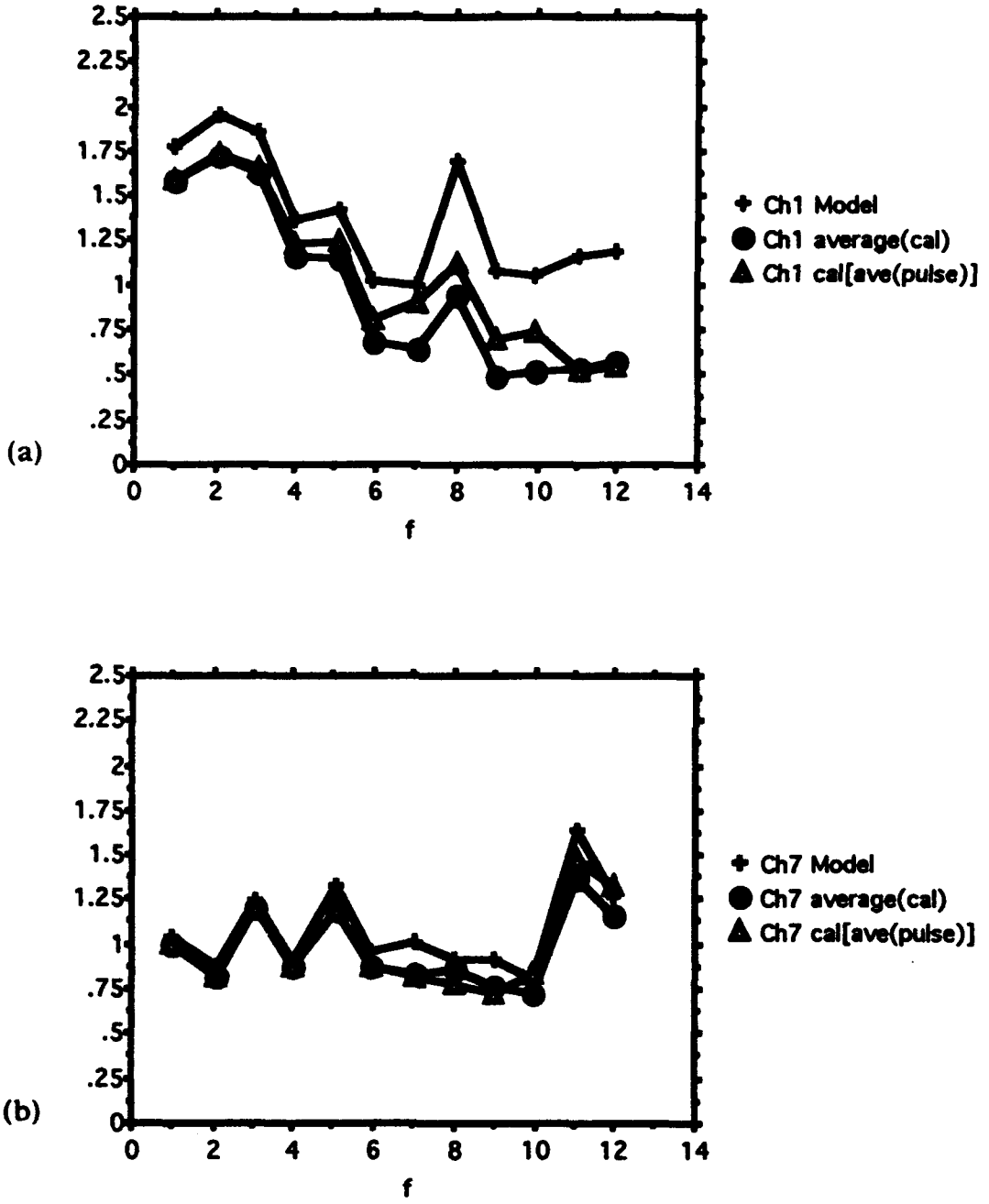

Figure 17: An example of the variation of spectral ratios when three different estimates of instrument response are used to correct to ground motion. The top figure shows the results for channel 1, the bottom figure shows the results for channel 7.

6.3 Frequency Domain Analysis:

The amplitude spectrum was calculated for each of the 26 high signal-to-noise seismograms recorded by the WESSA. Each spectrum was then smoothed with a 9 point moving average filter in order to reduce numerical noise which had a significant effect on ratios between spectra. Figure 18 shows the smoothed and unsmoothed spectrum for a typical event recorded on channel 3 (the reference site).

For each channel, ratios between the spectral amplitudes at that site and the spectral amplitudes of the reference site (channel 3) were computed. Channel 3 was chosen as the reference channel because it is located on the same pier as the seismometer for station WES of the NESN. In addition to the full spectral ratios, ratios were computed at discrete frequencies to yield a data set that could be statistically analyzed (see Section 7). The discrete frequencies used for this aspect of the study were the frequencies closest to the whole number frequencies between 1 and 12-Hz.

Figures 19(a)-22(a) show selected spectral ratios for the events shown before in figures 10-13. In each figure, the spectrum of the individual channel was divided by the spectrum of the reference channel and the resulting ratio was plotted on a logarithmic scale.

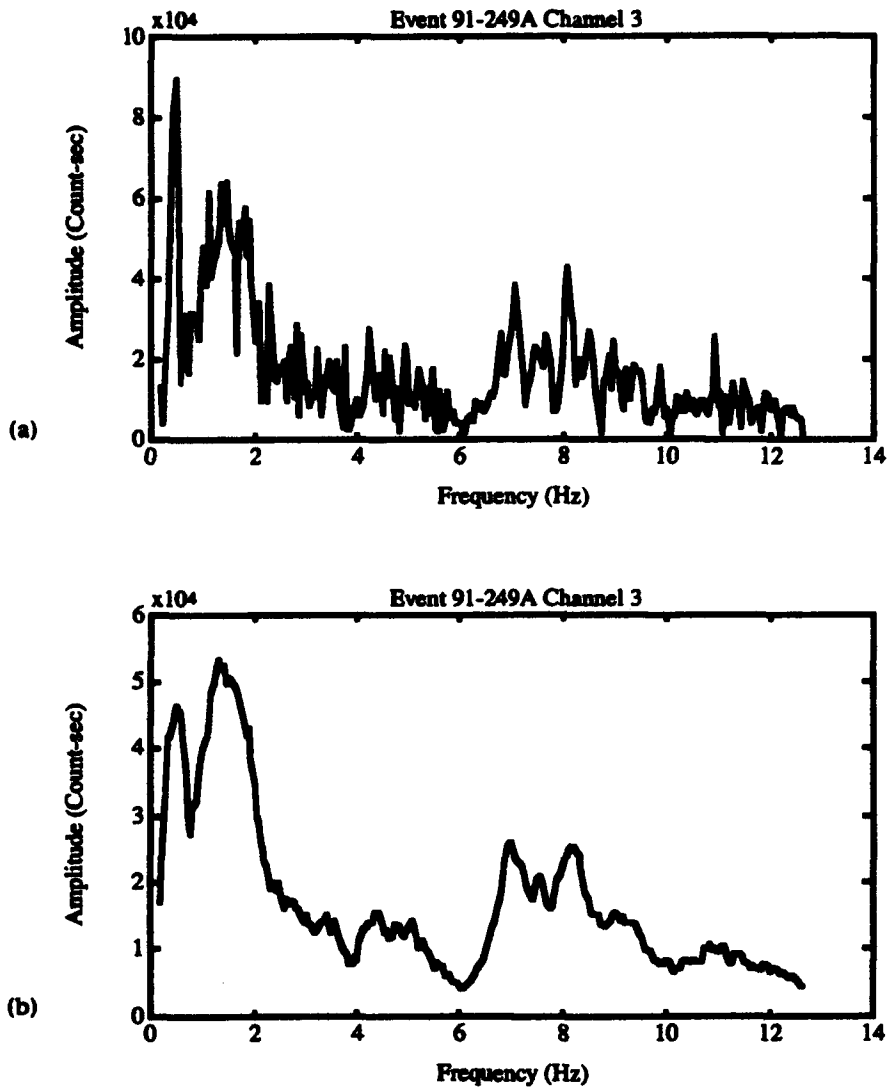

Figure 18: (a) Spectrum of channel 3 for event 91-249A. (b) Spectrum of channel 3 for event 91-249A after filtering with a 9 point moving average filter to reduce numerical noise when calculating ratios.

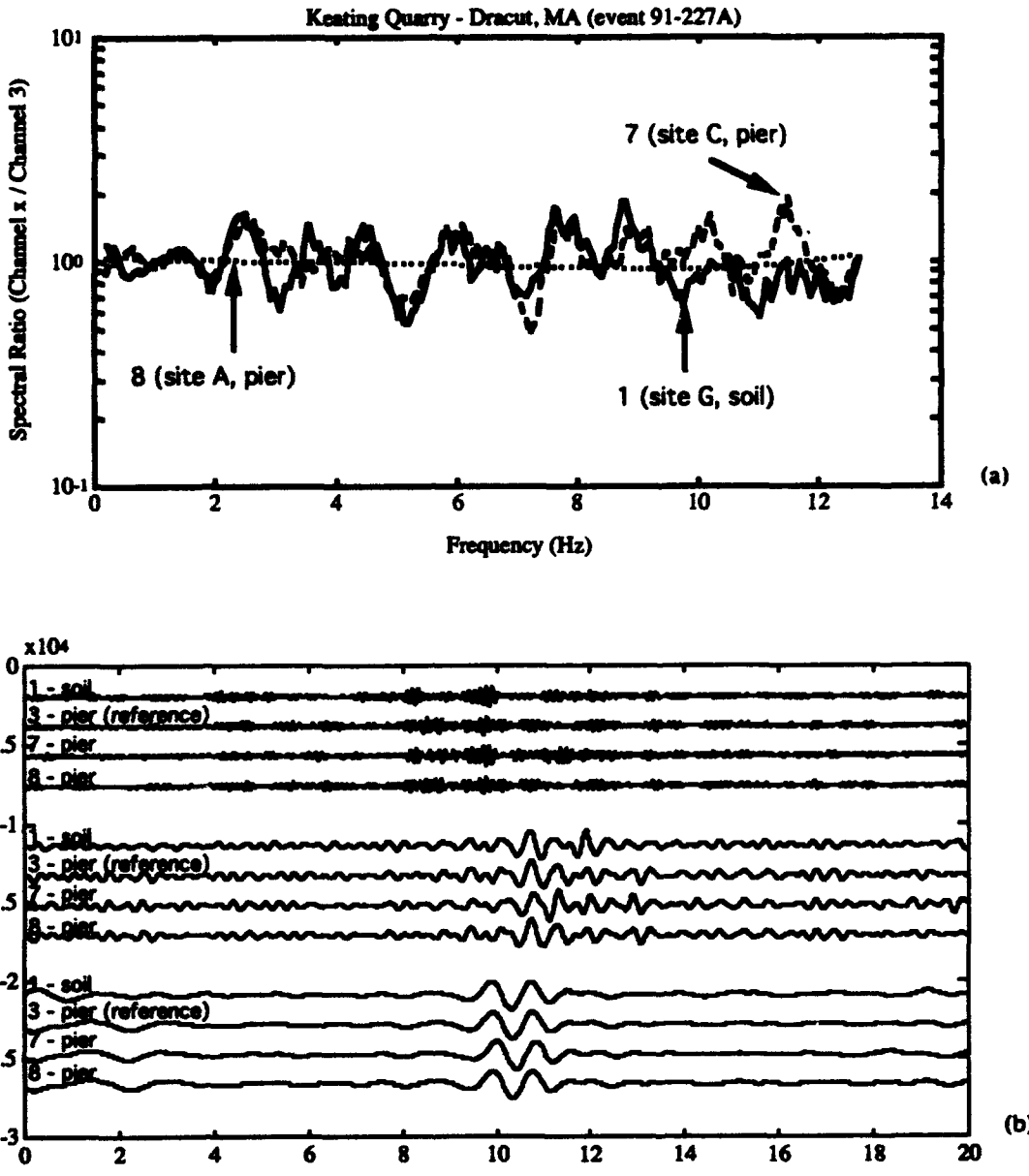

Figure 19: (a) Selected spectral ratios for the event shown in Figures 10. The spectrum of each individual channel was divided by the spectrum of the reference channel and the resulting ratio was plotted on a logarithmic scale. (b) Seismograms filtered with the following bandwidths: 0.5 to 1.5-Hz, 1.5 to 4.5-Hz, 5.5 to 10.5-Hz. Using the filtered seismograms, it is possible to observe the differences in waveforms which correspond to the differences seen in the frequency domain analysis.

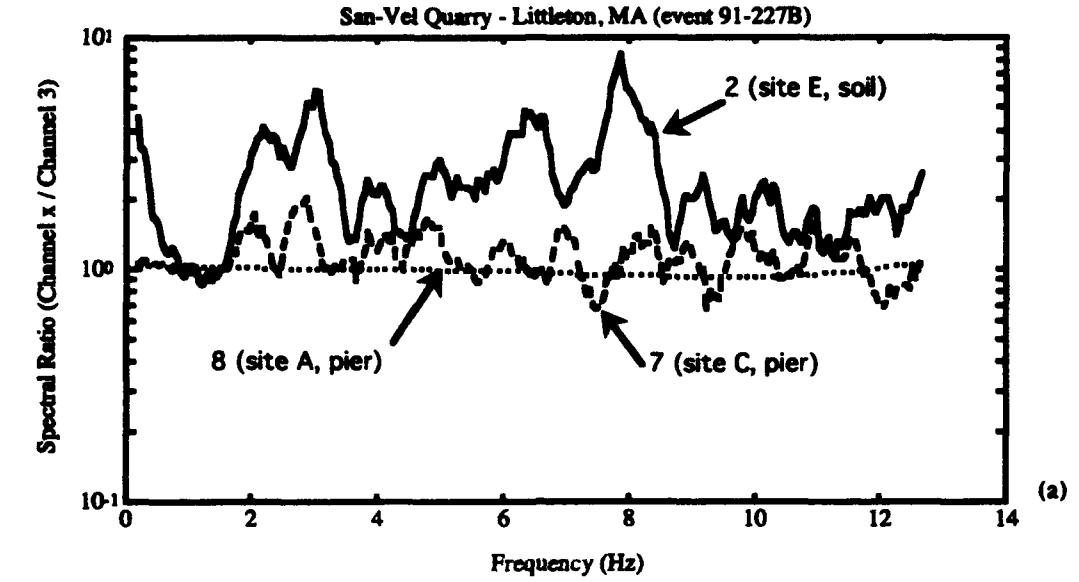

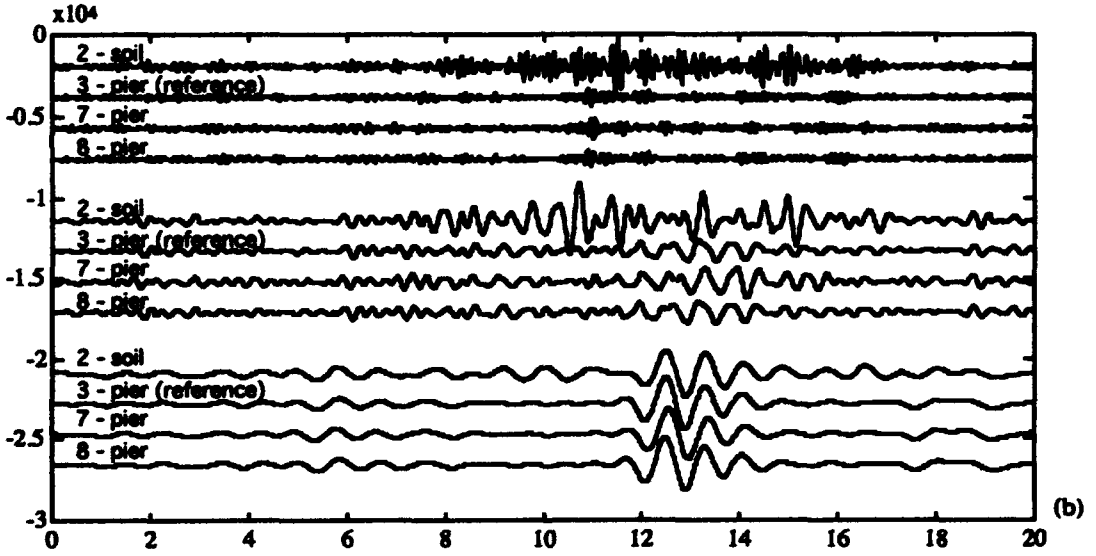

Figure 20: (a) Selected spectral ratios for the event shown in Figures 11. The spectrum of each individual channel was divided by the spectrum of the reference channel and the resulting ratio was plotted on a logarithmic scale. (b) Seismograms filtered with the following bandwidths: 0.5 to 1.5-Hz, 1.5 to 4.5-Hz, 5.5 to 10.5-Hz. Using the filtered seismograms, it is possible to observe the differences in waveforms which correspond to the differences seen in the frequency domain analysis.

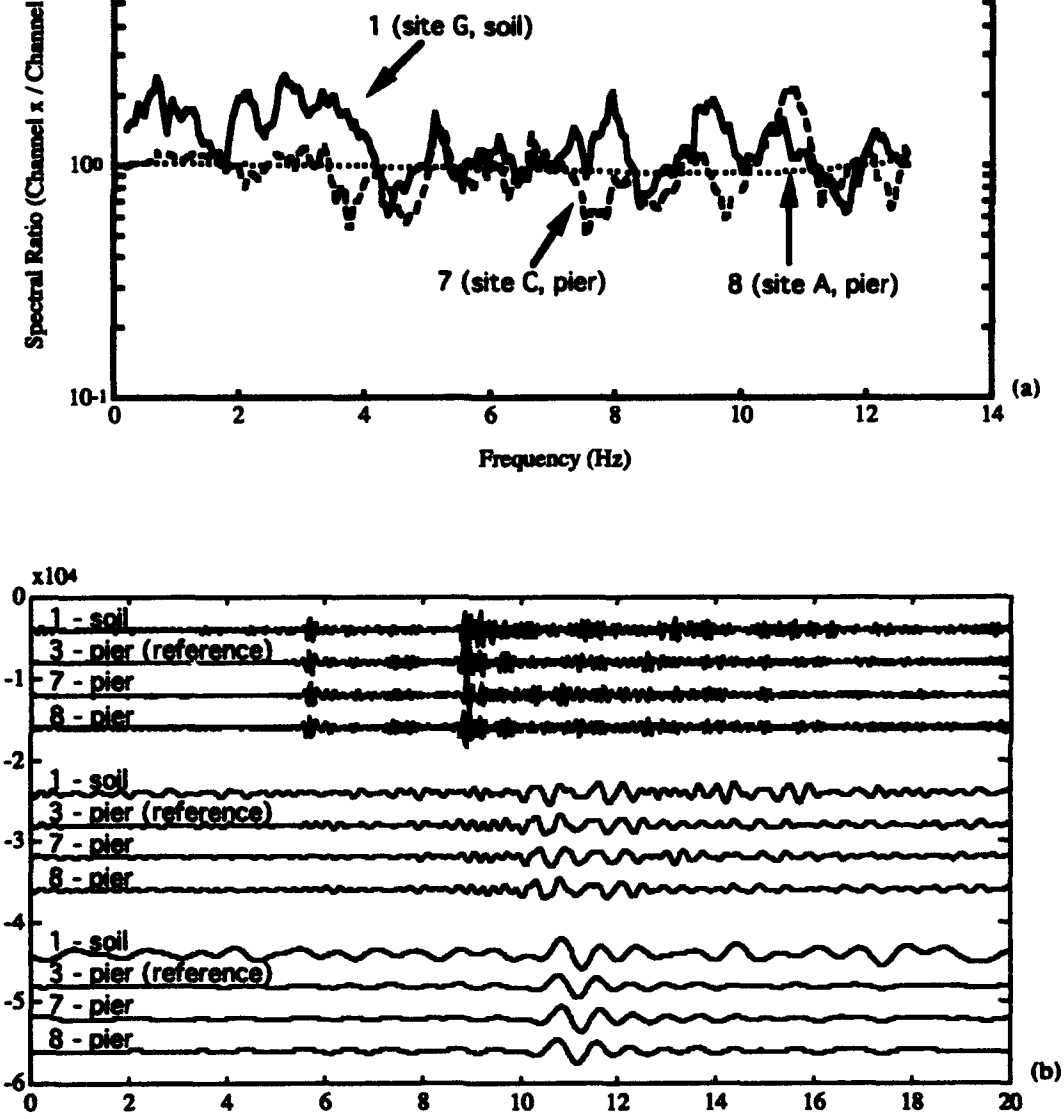

Figure 21: (a) Selected spectral ratios for the event shown in Figures 12. The spectrum of each individual channel was divided by the spectrum of the reference channel and the resulting ratio was plotted on a logarithmic scale. (b) Seismograms filtered with the following bandwidths: 0.5 to 1.5-Hz, 1.5 to 4.5-Hz, 5.5 to 10.5-Hz. Using the filtered seismograms, it is possible to observe the differences in waveforms which correspond to the differences seen in the frequency domain analysis.

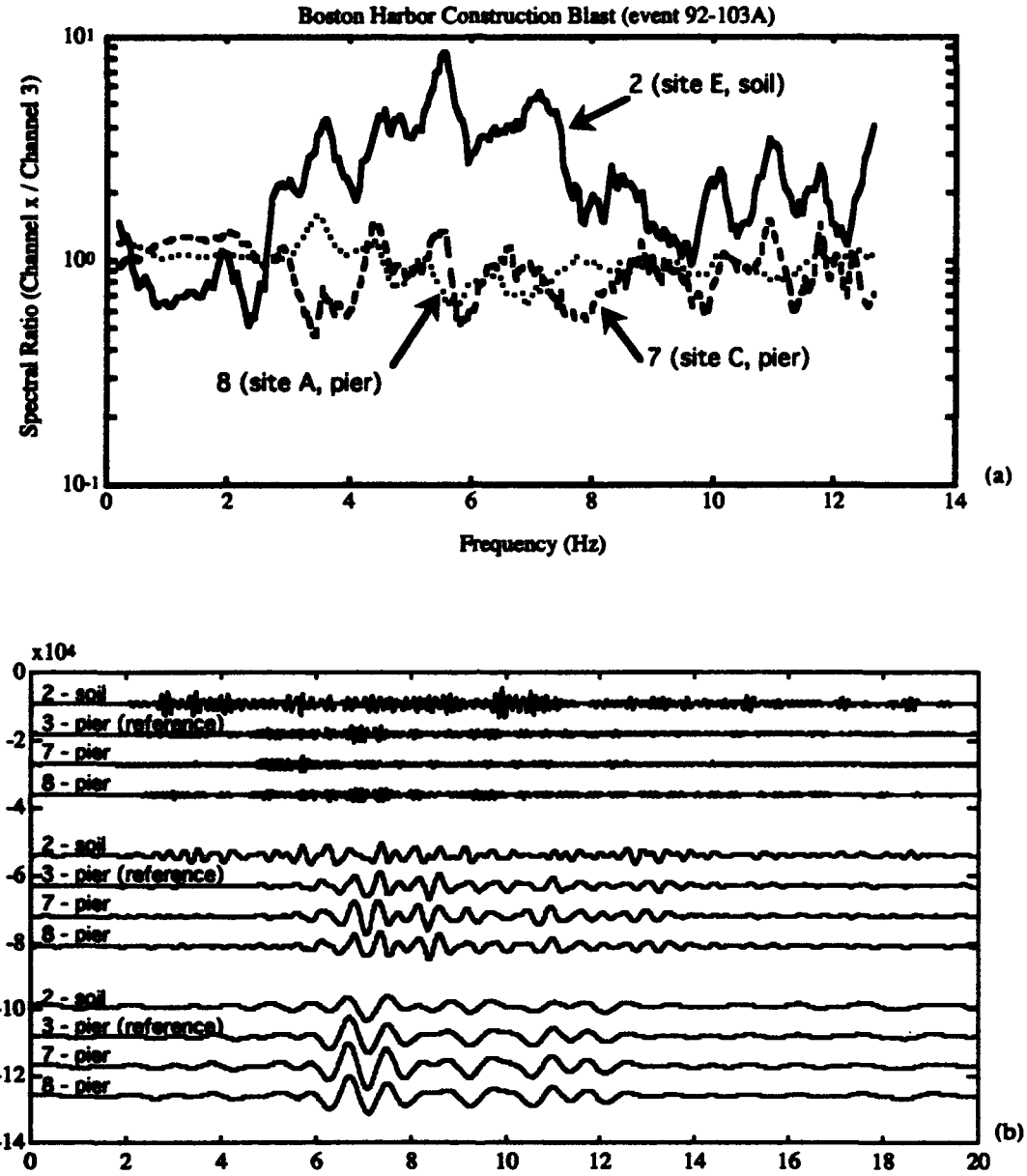

Figure 22: (a) Selected spectral ratios for the event shown in Figures 13. The spectrum of each individual channel was divided by the spectrum of the reference channel and the resulting ratio was plotted on a logarithmic scale. (b) Seismograms filtered with the following bandwidths: 0.5 to 1.5-Hz, 1.5 to 4.5-Hz, 5.5 to 10.5-Hz. Using the filtered seismograms, it is possible to observe the differences in waveforms which correspond to the differences seen in the frequency domain analysis.

6.4 Time Domain Analysis:

For time domain analysis, the signals recorded by the WESSA were processed to appear as if they were recorded by the same instrument. This was accomplished by deconvolving the instrument response from each signal, and then convolving the resulting ground motion with a theoretical instrument which has a similar response to that of the reference instrument. The theoretical instrument is a 1-Hz seismometer, with 0.77 damping, which has a gain of 15,364 counts/micron at 1-Hz, and a 12.5-Hz anti-aliasing filter.

After the signals were corrected to the same standard instrument, they were filtered using Butterworth band pass filters with the following bandwidths: 0.5-1.5-Hz, 1.5-4.5-Hz, 5.5-10.5-Hz. Figures 19(b)-22(b) are examples of seismograms filtered by this method. By observing the filtered seismograms, it is possible to see the differences in waveforms which correspond to the differences seen in the frequency domain analysis described in the previous section.

7. RESULTS

7.1 Analysis by Event Location:

As described above in Section 5.3, the GDAS was turned on to record when advanced notice was received from quarry operators. In addition, the GDAS was also turned on during peak blasting times to record events from other quarries. Therefore, the catalog of seismograms includes data from events with known and unknown locations. In order to test for systematic

effects associated with events recorded from specific quarries, events from known quarries were analyzed separately.

7.1.1 Events from the San-Vel Quarry, Littleton MA

The San-Vel Quarry, is located about 25 km northwest of the WESSA. Six known blasts from this quarry were recorded on the WESSA during the summer of 1991. Of these events, four were analyzed for this study. The others were not analyzed because a significant portion of the WESSA had not yet been installed when these blasts occurred. Additionally, channel 12 was installed for only one of the analyzed blasts, and was therefore ignored in the statistical analyses presented in this section.

7.1.1.1 Pier Sites

Figure 23(a-d) shows the ratios for the four pier sites for the four known San-Vel Quarry blasts. Each of the plots in Figure 23 is the instrument corrected spectrum for an individual channel divided by the corrected spectrum for the reference channel (channel 3), and plotted on a log scale. Figure 23(a) is this ratio for channel 8, plotted for each of the four San-Vel Quarry blasts. Channel 8 and channel 3 are co-located on the same pier. The ratios show a characteristic response for channel 8, which is discussed in more detail below in Section 7.2.1. The ratios are close to 1.0 across the entire frequency band analyzed, which indicates that the two instruments are recording nearly identical ground motion (once they are properly corrected for instrument response). The maximum difference between channel 8 and channel 3 is only 5%, which occurs between 8 and 10-Hz. Between 0 and 4-Hz the maximum difference is only 2%.

Figure 23(b), shows the ratios for channel 4, which is the closest pier site to the reference site. By examining only San-Vel Quarry blasts, I have

analyzed events for which the propagation path is nearly identical. Nonetheless, there is up to a factor of 2 difference between the response at channel 4 relative to the response at the reference channel. This suggests that we are seeing a site response effect. That is, the small amount of difference in the earth structure over only several tens of meters between the two sites appears to be creating the observed differences in spectral amplitudes. Between 0.5 and 2-Hz, the ratios indicate that amplitude variations are no greater than 12%, and between 2 and 6-Hz, the ratios do not vary from 1.0 by more than 25% and the curves generally have the same shape.

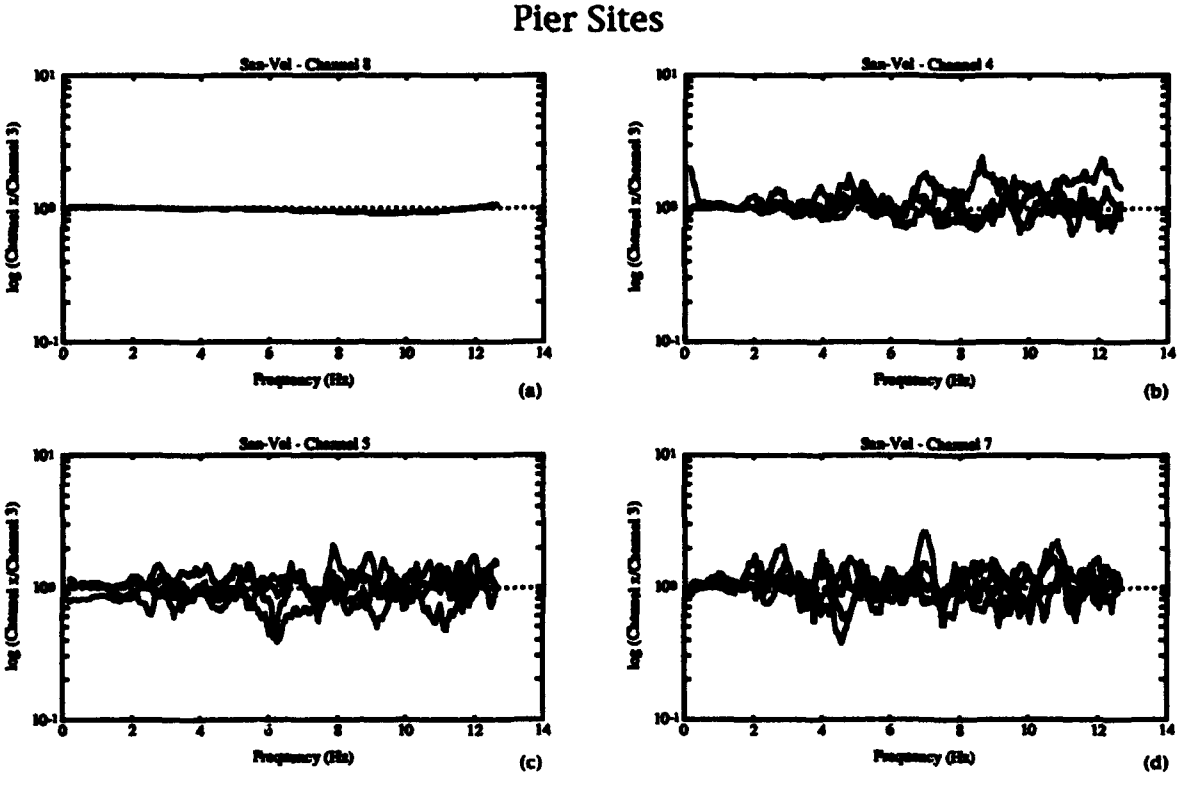

Figure 23: The ratios for the pier sites for the known San-Vel Quarry blasts. Each of the plots is the instrument corrected spectrum for an individual channel divided by the corrected spectrum for the reference channel (channel 3), and plotted on a log scale.

At about 5-Hz, the ratios are nearly identical for each of the San-Vel Quarry blasts. Above 6-Hz, the ratios vary by as much as a factor of 2 from each other, and the shapes of the curves vary significantly.

Figure 23(c) shows the ratios for channel 5, a pier site further away from the reference site than channel 4. For three of the curves, the ratio between 0 and 1.5-Hz is less than 8%, but somewhat surprisingly, one of the curves is offset from the others by about 18%. Although the total difference between the curves for the different events is at least as large as those of channel 4, the ratio curves generally follow the same pattern throughout all the frequencies of interest. As with channel 4, the ratios show the most variation at higher frequencies (above 6-Hz).

Figure 23(d) shows the ratios for the pier site farthest away from the reference pier. At higher frequencies, i.e. beyond about 2-Hz, the ratios for this site exhibit slightly more variation than channels 4 and 5. Also, the ratio curves do not appear to have a consistent shape. The ratios vary from each other by up to a factor of 2.5, although between 0 and 1-Hz, they vary from each other by less than 20%.

7.1.1.2 Soil Sites

Figure 24(a-c) shows the ratios for the three soil sites for the known San-Vel Quarry blasts. Figure 24(a) shows the ratios for channel 2, the closest soil site to the reference site. For these events, this site shows the greatest amount of variation from the reference site of any site. Between 2 and 3.5-Hz, and near 8-Hz, the ratio of the amplitude at channel 2 relative to the amplitude at the reference site approaches an order of magnitude for one of the events. At the pier sites, the ratios were approximately randomly distributed above and below 1.0, which indicates that there is as much amplification of the signals at

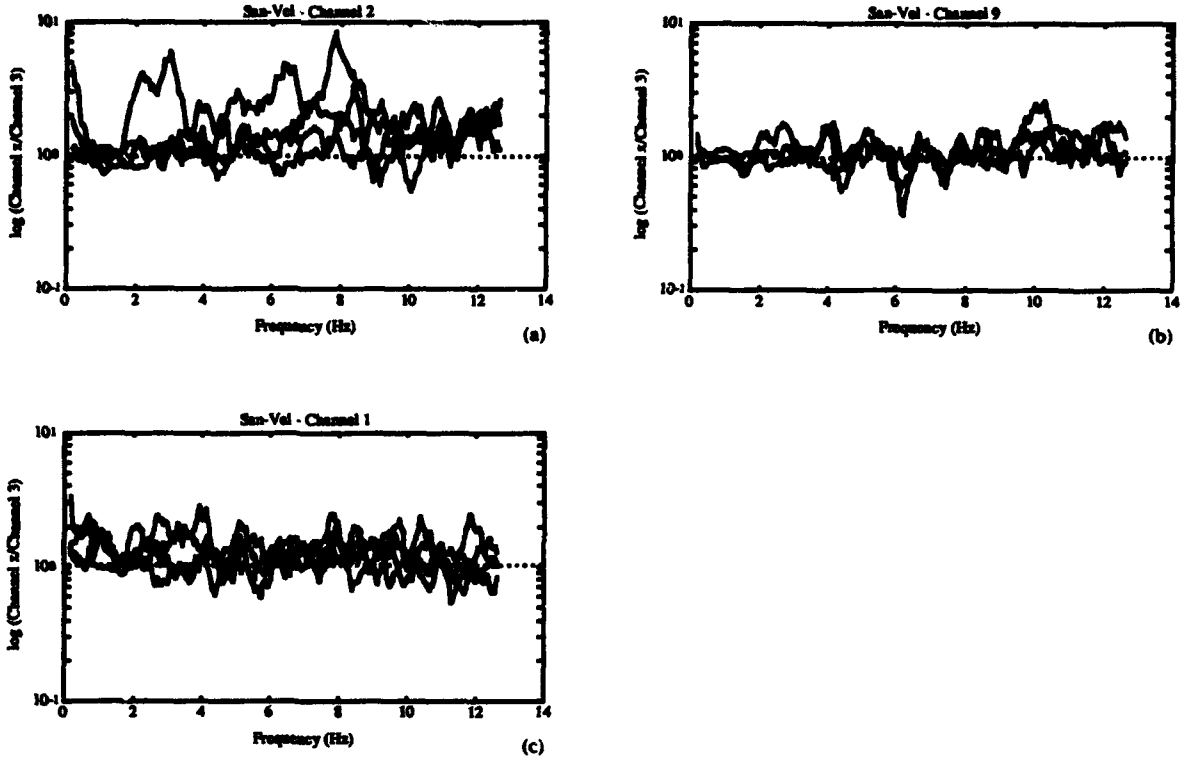

Figure 24: The ratios for the soil sites for the known San-Vel Quarry blasts. Each of the plots is the instrument corrected spectrum for an individual channel divided by the corrected spectrum for the reference channel (channel 3), and plotted on a log scale.

these sites as there is a decrease in signals. However, at this soil site (as well as the other soil sites) there is a significant amount of amplification of the signals. This amplification is evident because the ratios are greater than 1.0 in nearly all cases for a large part of the frequency band analyzed. There are two bands where the ratios for all of these events are close to each other: between about 1 to 1.5-Hz, and above 11-Hz.

Figure 24(b) shows the ratios for channel 9, a soil site at an intermediate distance from the reference site (148 m). These ratios exhibit a more uniform

pattern than at the other soil sites. The deviation and amplification at this site is not as great as at the other soil sites [Figures 24(a) and 24(c)].

Figure 24(c) shows the ratios for channel 1, the farthest soil site from the reference site. These ratios do not exhibit an obvious pattern across the frequency band analyzed, and at most frequencies there is an amplification by a factor of about 1.5 to 2.0 relative to the reference site. There seems to be a slight linear trend in the ratios from higher amplification at lower frequencies to lower amplification at higher frequencies. This may be the result of a significant amount of low frequency noise which appears on the seismograms from this site. Also, for the narrow frequency band between 6.5 and 7.5-Hz, the ratios are nearly the same for each of the four events.

7.1.2 Events from the Keating Quarry, Dracut MA

The Keating Quarry in Dracut, MA is about 34 km north of the WESSA. There were six known blasts from the Keating Quarry. Of these, only three were successfully recorded on the WESSA. As with the known blasts from the San-Vel Quarry (discussed above), channel 12 was not installed at the time these three blasts were recorded.

7.1.2.1 Pier Sites

Figure 25(a-d) shows the amplitude ratios at the pier sites for confirmed blasts from the Keating Quarry. The channels co-located with the reference channel show virtually the same shape curve as those for the San-Vel Quarry blasts [compare Figure 25(a) and 23(a)].

The Keating Quarry blast ratios for channel 4 are shown in Figure 25(b). Overall, the curves for the three events generally have the same shape. Below 4-Hz, the ratio is very close to 1.0 and varies by about 5 to 12%. Above 4-Hz, the ratios vary above and below 1.0, with frequency bands where the ratios

for the different events are very close to each other, and other frequency bands where the ratios deviate from each other by up to about 50%. Between 5 and 6-Hz, near 8.5-Hz, and above 11-Hz, the ratios show the most amount of variation between the different events. Below, 4-Hz, between 6 and 8-Hz, and around 9-Hz the ratios show the least amount of deviation.

The ratio curves for channel 4 generally vary by similar amounts for the San-Vel Quarry and the Keating Quarry blasts [compare Figures 23(b) and 25(b)]. With the exception of one event for San-Vel, all ratio curves at channel 4 vary by no more than 10% from each other up to about 4-Hz.

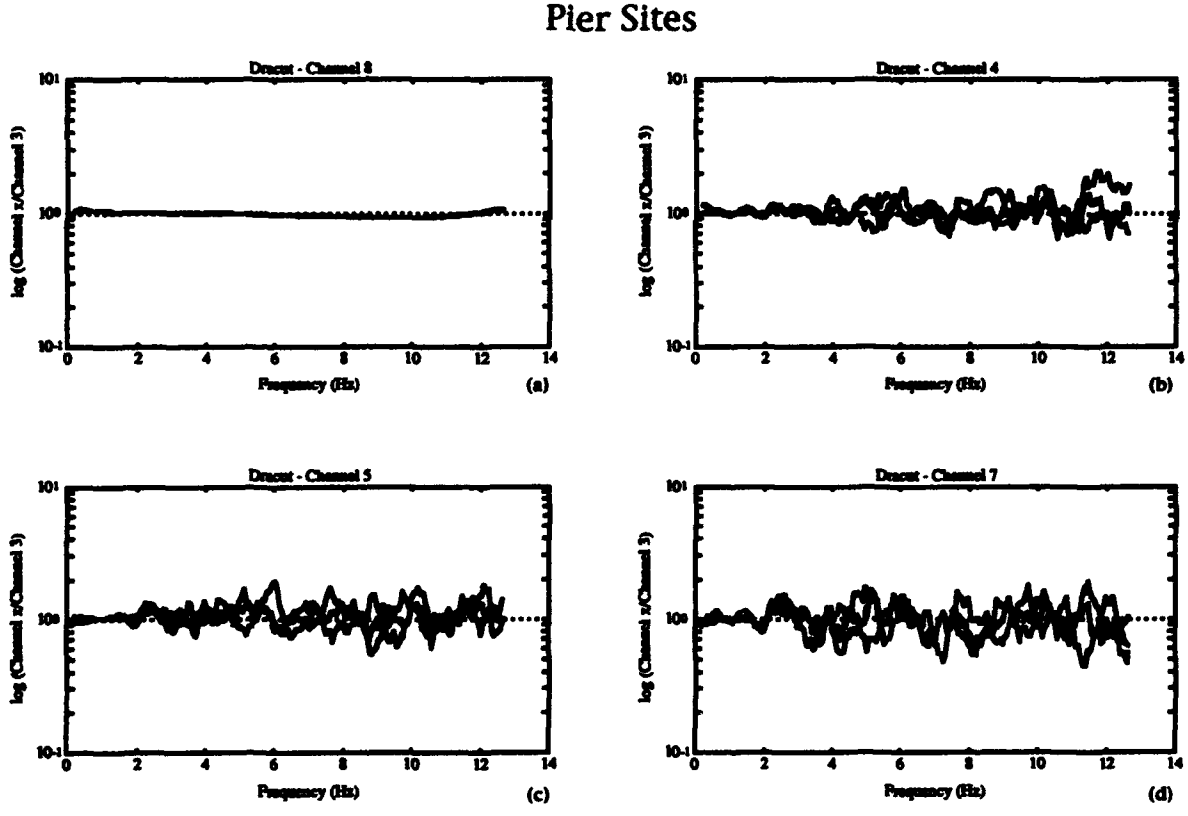

Figure 25: The ratios for the pier sites for the known Keating Quarry blasts. Each of the plots is the instrument corrected spectrum for an individual channel divided by the corrected spectrum for the reference channel (channel 3), and plotted on a log scale.

Furthermore, at frequencies below 4-Hz, for all but one curve, the total variation is less than 10%. This suggests that the one anomalous event is so because of cultural noise at channel 4 (which is located inside an Observatory building). Thus, in the absence of a significant amount of noise and for events from the same location, differences in site effects between channel 3 and channel 4 may be as small as 10% at frequencies below 4-Hz.

Figure 25(c) shows the ratios for channel 5. As with channel 4, there is less deviation at lower frequencies. In the case of channel 5, there seems to be a distinct cut off at about 3-Hz, below which the variation is limited to only a few percent. The maximum deviation between the curves occurs between about 9 and 10-Hz, and is on the order of a factor of 2. Above 3-Hz, there does not seem to be a characteristic pattern in the shape of the amplitude ratio curves.

The ratios for channel 7 are shown in Figure 25(d). As with the previous two channels, the lower frequencies (i.e. below 3-Hz) show the least deviation between different ratio curves. There also seems to be some frequency bands in which the ratios behave similarly for all these events. For example, below 3-Hz, near 6-Hz, and around 11-Hz, the curves for all three events have similar ratios.

7.1.2.2 Soil Sites

The ratios for the soil sites that recorded the Keating Quarry blasts are shown in Figure 26. Channels 1 and 9 exhibit variations that are, in general, not significantly greater than those for the pier sites. Channel 2, on the other hand, showed the greatest amount of variation of all the sites, which was also the case for the San-Vel Quarry blasts.

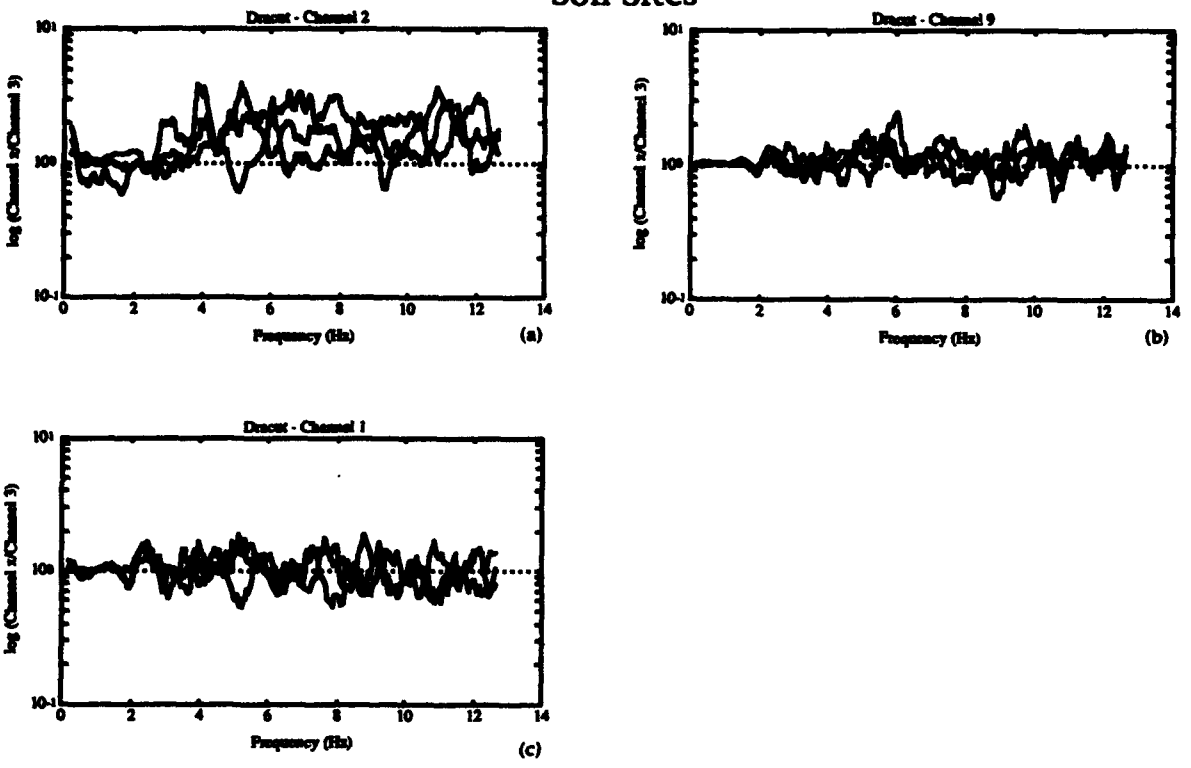

Figure 26: The ratios for the soil sites for the known Keating Quarry blasts. Each of the plots is the instrument corrected spectrum for an individual channel divided by the corrected spectrum for the reference channel (channel 3), and plotted on a log scale.

In the case of channel 2, the ratios for each event deviate from each other by no more than 66% below 4-Hz. Above 4-Hz, the ratio between amplitudes at this site and at the reference site is generally greater than 1.0, indicating signal amplification at this site. Above 4-Hz, there is also more deviation between the individual events than at lower frequencies, and the ratios generally increase with increasing frequency. The ratios tend to level off near 6-Hz, although there is some oscillation above 6-Hz. In general above 6-Hz, the ratios show amplification of the signals recorded at this site.

Figure 26(b) shows the ratios for channel 9. This site shows the least amount of deviation of all the soil sites, and it is comparable to a pier site in terms of these amplitude ratios. Below 2-Hz there is very little deviation between the different ratio curves. Above 2-Hz there is more variation (up to about a factor of 2) between the events, but the variations still follow a general pattern that seems characteristic of events recorded at this site from the Keating Quarry.

The ratios for channel 1, shown in Figure 26(c), show more deviation from each other than those for channel 9, but overall they show about the same amount of maximum deviation from the reference channel as those for channel 9. Below 2-Hz, the ratios vary by no more than 30% from 1.0, and by no more than 25% from each other. The amplitudes vary by no more than about a factor of 2.0 from those at the reference channel above 2-Hz. As with all of the sites for Keating Quarry events, the lower frequencies show the least amount of deviation, either between the site and the reference channel or between individual blasts from the same quarry.

7.2 Analysis by Site:

7.2.1 Pier Sites:

Figures 27(a-d) show all of the sampled spectral ratios, as a function of frequency, for each pier site in the study. In general, the spectral ratios for pier sites in this study show less amplification (and sometimes a slight decrease in amplitudes) than the soil sites which are discussed in the next section.

Channels 8 and 12 are co-located with the reference channel at Site A, and with the exception of one event (92-103A), seem to have a characteristic response. The spectral ratios of all the events (except 92-103A) vary by less

than 5% from the reference channel, and less than 1% from each other. It is unclear why 92-103A, which was a construction blast detonated in Boston Harbor, deviates from the pattern of the spectral ratios of events before and after it.

Channels 4, 6 and 13 were co-located on a pier (Site B) about 70 meters from the reference pier. These channels are generally consistent among themselves, but show greater variation than the channels co-located with the reference channel. There is slightly more scatter at higher frequencies (above 6-Hz) than at lower frequencies. The ratios for this event indicate that amplitudes at this site vary by no more than a factor of 2 from the reference site at higher frequencies and by no more than about 50% at lower frequencies.

Channels 5 and 11 were co-located on a pier (Site D) which is about 143 meters from the reference pier. These channels did not correspond to each other as well as the other groups of co-located seismometers. The spectral ratios for channel 5 were on average about 5-10% lower than those for channel 11. The ratio curves had similar shapes, and were only offset from each other. This probably indicates a failure to accurately correct for instrument response in one or both of the channels. At low frequencies (below 2-Hz) and at higher frequencies (above 6-Hz) both of these channels exhibited more scatter than the other pier sites.

Channel 7 was located at Site C, a pier which is about 251 meters from the reference pier. The spectral ratios for this site exhibited the highest amount of scatter in the 2-4-Hz range. At higher and lower frequencies, the spectral ratios were less than those of channels 5 and 11 which were located at 143 meters from the reference site (half the distance of this channel). This

suggests that, at this scale, distance may not play a significant role in the variation of spectral ratios between different pier sites.

Figure 28(a-d) shows histograms of the spectral ratios in three frequency bands for each channel located on a pier site. In general, it can be seen that the ratios are scattered more at higher frequencies than at lower frequencies. These figures also clearly indicate whether the signals tend to be amplified with respect to the reference channel.

Channel 8 shows slight amplification at 1-Hz and between 2 and 4-Hz. Between 6 and 10-Hz, the histogram for channel 8 shows there is a general decrease in the signal amplitudes. The spectral ratio histograms for channel 10 (not shown here) are very similar to those for channel 8. The results for channel 12 (buried near bedrock, just two meters from channel 8) are discussed below in the section describing the soil sites.

Channels 4, 6, and 13 also show more variation in spectral ratios at higher frequencies than at lower frequencies. Channel 4 does not, on average, show significant amplification in any frequency band. In other words, the mean of the ratios is very close to zero, and the variation is symmetrically distributed around the mean.

Channel 11 (not shown here) exhibits, on average, significant decrease in amplitudes of signals in each frequency band. Channel 5 exhibits less of this effect. The difference between the two channels was described earlier and may be attributed to a failure to accurately correct for instrument response in one or both of the instruments.

The histograms of spectral ratios for channel 7 are fairly symmetric, and the mean ratio is close to zero for all frequency bands. This observation

seems to indicate that the site, which is 251 meters from the reference site, is not amplifying the signals.

7.2.2 Soil Sites:

Figure 29(a-d) shows the spectral ratios for the soil sites used in this study. With the exception of Channel 12 (Site A1), the soil sites show both an amplification of signals as well as more scatter in the spectral ratios than do the pier sites. Figure 30(a-d) are the spectral ratio histograms for the same sites. The histograms are useful in showing the amount of amplification a channel exhibits.

Channel 12 is located at the closest site (Site A1) to the reference site. Site A1 is located within 2 meters of the reference pier, and within 0.5 meters of bedrock. The spectral ratios for channel 12 have only slightly more scatter than those of channels 8 and 10 which are co-located with the reference channel. At higher frequencies there seems to be, on average, a slight decrease in the spectral amplitudes relative to the reference site. As with channels 8 and 10, the event which has the greatest variation is 92-103A, the Boston Harbor Blast. Because of the proximity to bedrock, and possibly the proximity to the reference site, this site behaves more like a pier site than it does a typical soil site.

Channel 2 is located at site E, approximately 116 meters from the reference site. Channel 2 shows more scatter in the spectral ratios than any of the pier sites, and also shows some amplification of the signals at mid to higher frequencies (above 2-Hz). At 1-Hz the signals are not significantly amplified.

Channel 9 is located at site F, about 148 meters from the reference site. With the exception of the Boston Harbor Blast, the spectral ratios for this channel do not show as much variation as do channels 1 and 2. Also, this site

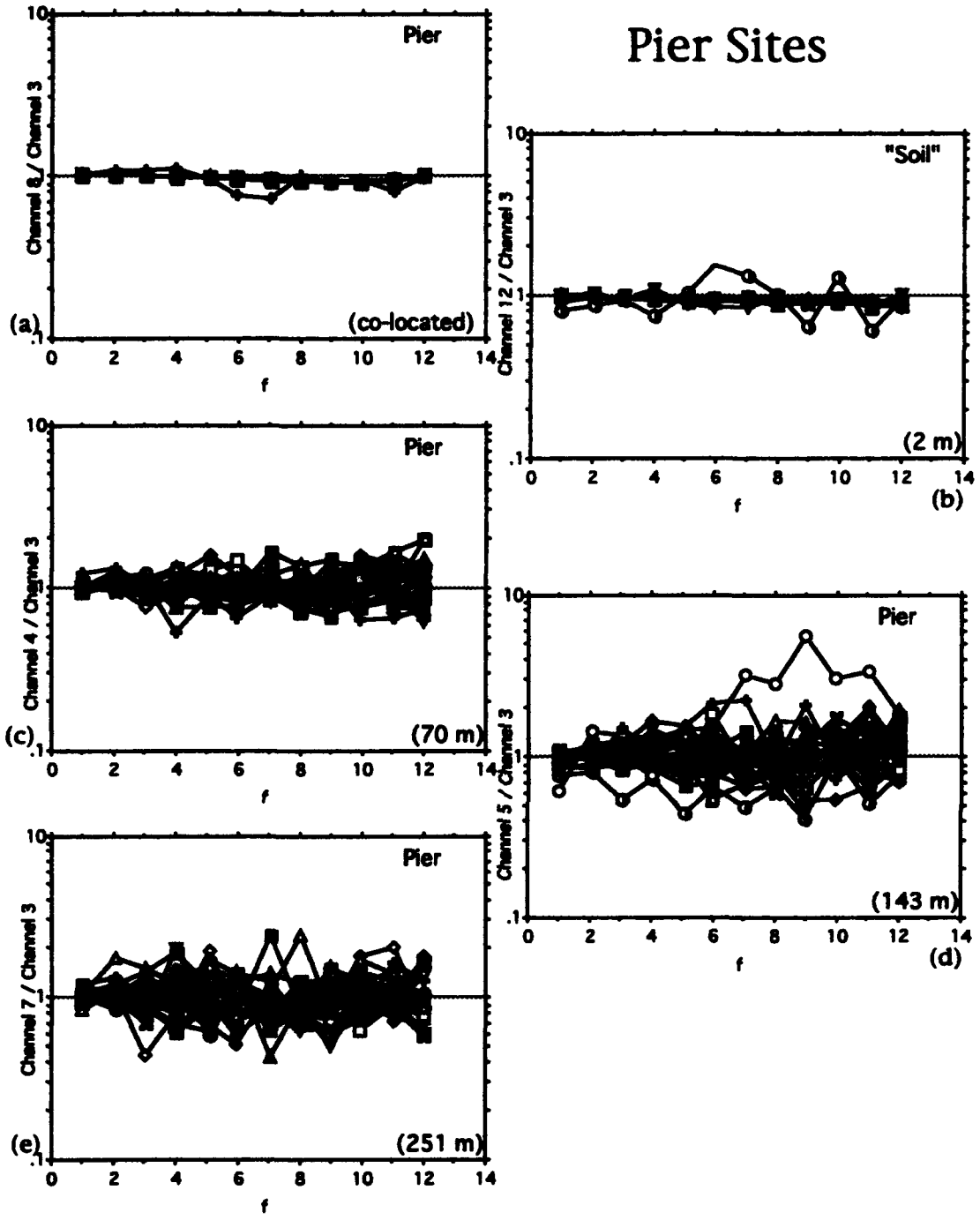

Figures 27 (a-e): Individual spectral ratios for each pier channel in the study.

Channel 8

co-located

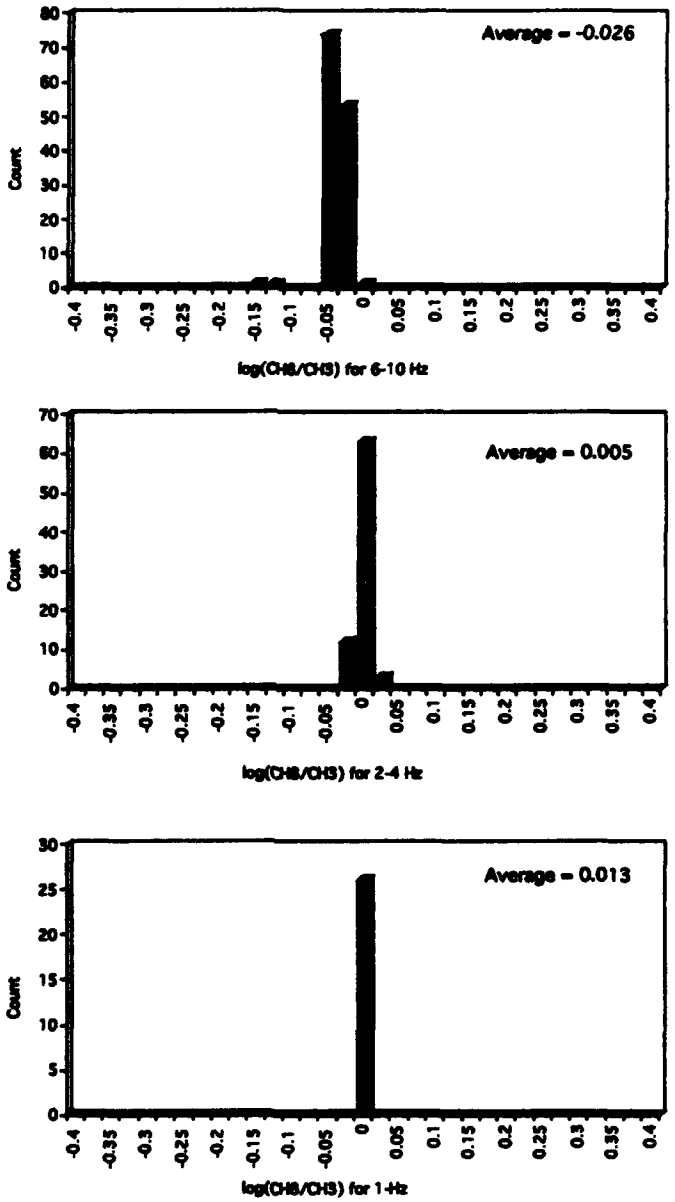

Figure 28 (a): Histograms of the spectral ratios for pier channel 8. The top figure is 6-10 Hz, middle is 2-4 Hz and bottom is 1Hz.

Channel 12

2 meters

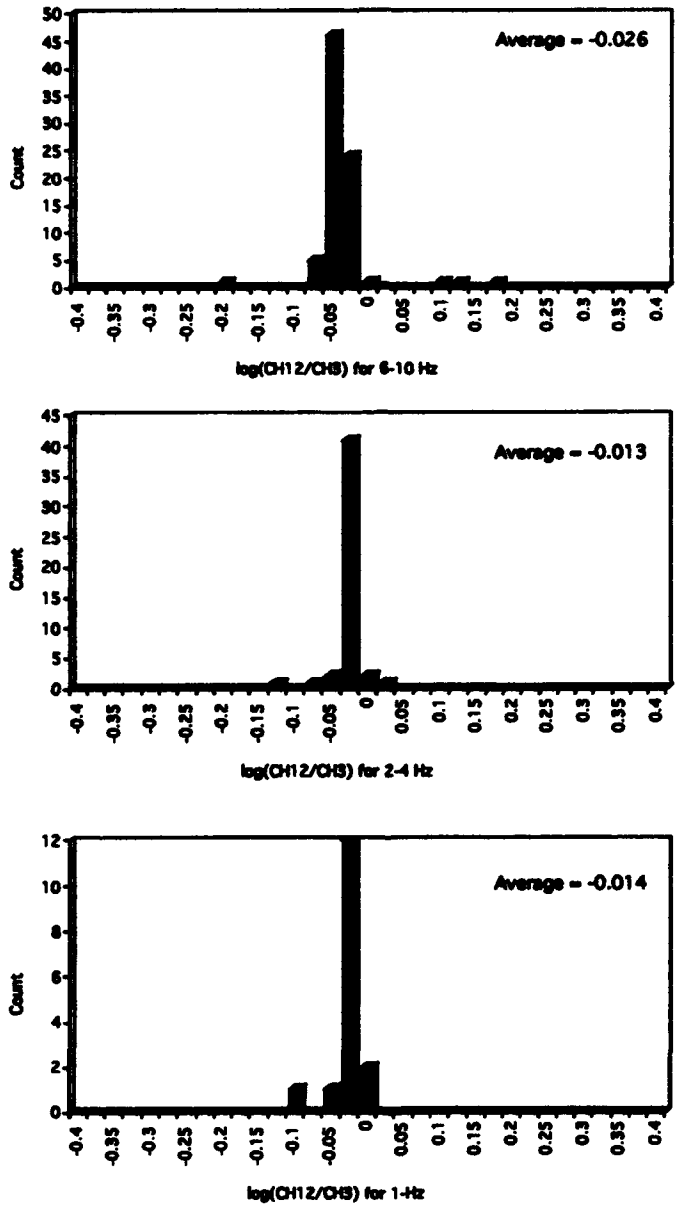

Figure 28 (b): Histograms of the spectral ratios for "soil" channel 12. The top figure is 6-10 Hz, middle is 2-4 Hz and bottom is 1Hz.

Channel 4

70 meters

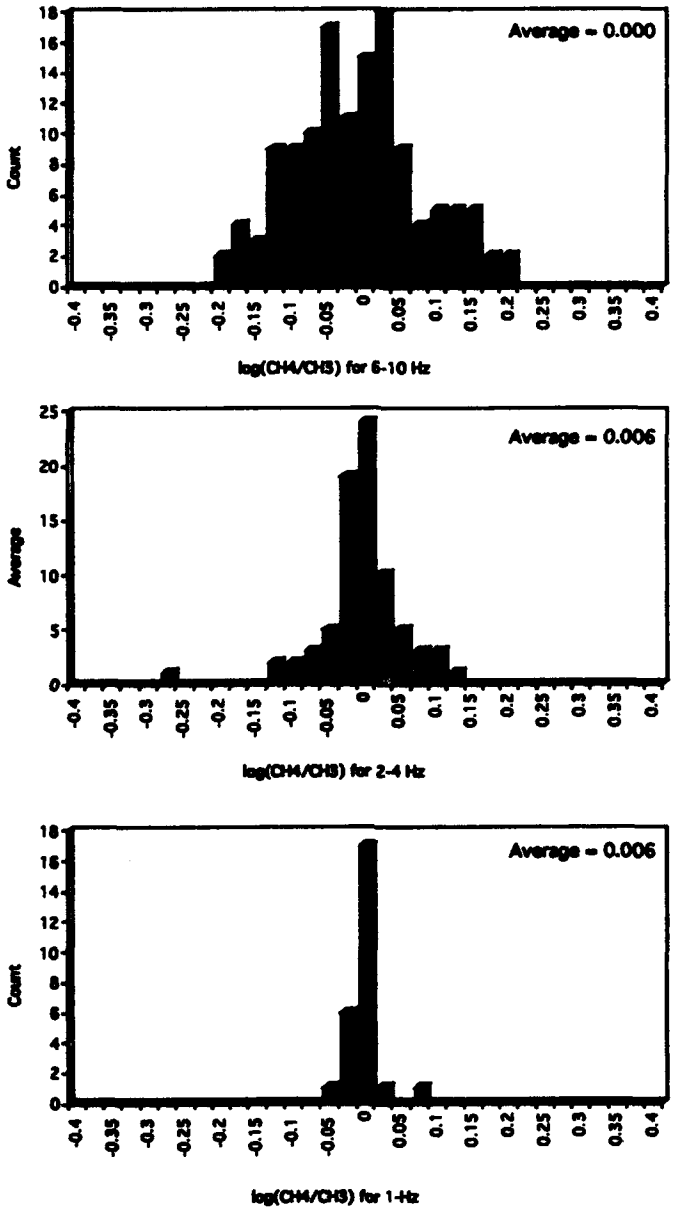

Figure 28 (c): Histograms of the spectral ratios for pier channel 4. The top figure is 6-10 Hz, middle is 2-4 Hz and bottom is 1Hz.

Channel 5

143 meters

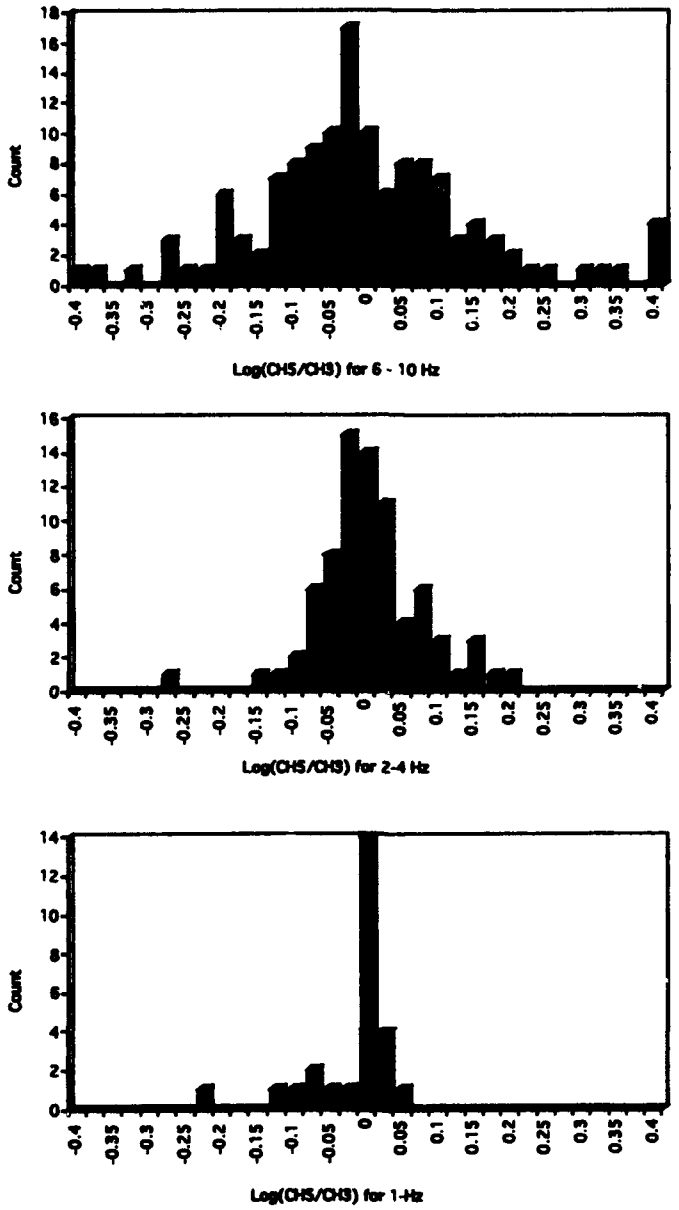

Figure 28 (d): Histograms of the spectral ratios for pier channel 5. The top figure is 6-10 Hz, middle is 2-4 Hz and bottom is 1Hz.

Channel 7

251 meters

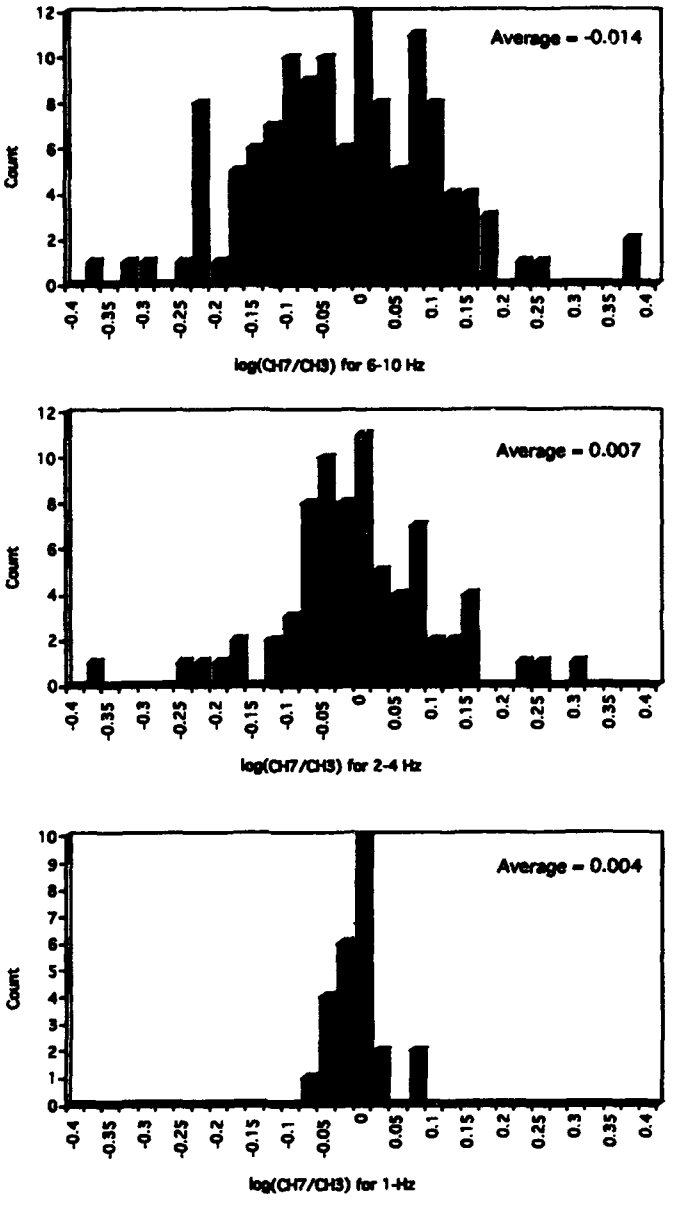

Figure 28 (e): Histograms of the spectral ratios for pier channel 7. The top figure is 6-10 Hz, middle is 2-4 Hz and bottom is 1Hz.

does not show as much amplification as the other soil sites. At 1-Hz there may be a slight decrease in amplitudes, and at higher frequencies amplification is minimal.

Channel 1 is located at site G, which is about 253 meters from the reference site. This site shows the greatest scatter of all sites in the study. The signals are usually amplified compared to the reference channel. This site is located within a wooded section of the Observatory, and there is significant low frequency background noise superimposed on the signals. The amplification evident in the four ratios may be as much due to this noise rather than signal amplification.

7.3 Temporal Analysis:

7.3.1 Effects of Rainfall:

It may be possible that soil moisture affects the site response of the soil sites. Therefore, the ratios were investigated as a function of time and compared to precipitation data to see if the ratios seemed to change when the rainfall was highest. The data discussed in this section is the set of ratios at the sampled frequencies closest to integer values between 1 and 12.

In the top portion of Figures 31-33 the ratios of the pier and soil sites are plotted against the Julian day of the year for blasts that occurred during 1991. Each figure shows a separate frequency band, and for each figure the average ratio for all frequencies in that band is plotted for each channel, on a given day. Plotted below each of the ratios is a bar graph which shows the amount of precipitation that was recorded by the nearest NOAA weather station in Waltham, MA (approximately 6.6 km from the array, U. S. Department of Commerce; 1991).

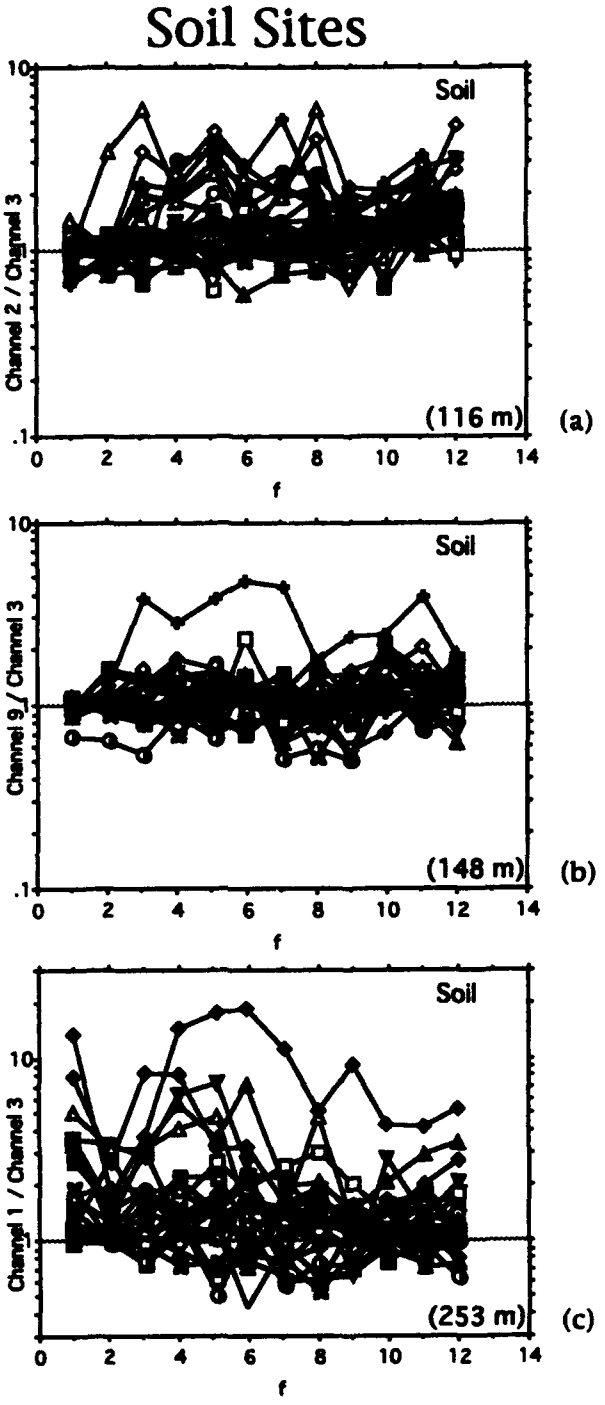

Figure 29 (a-c): Individual spectral ratios for each soil channel in the study.

Channel 12

2 meters

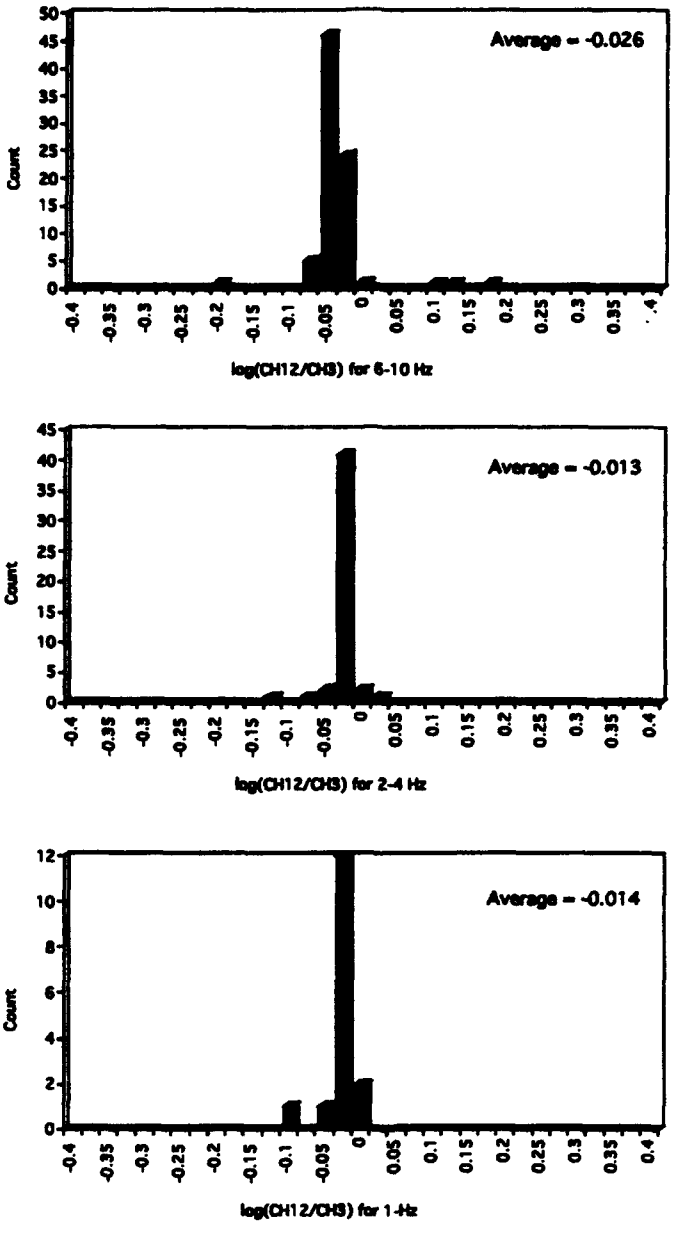

Figure 30 (a): Histograms of the spectral ratios for "soil" channel 12. The top figure is 6-10 Hz, middle is 2-4 Hz and bottom is 1Hz.

Channel 2

116 meters

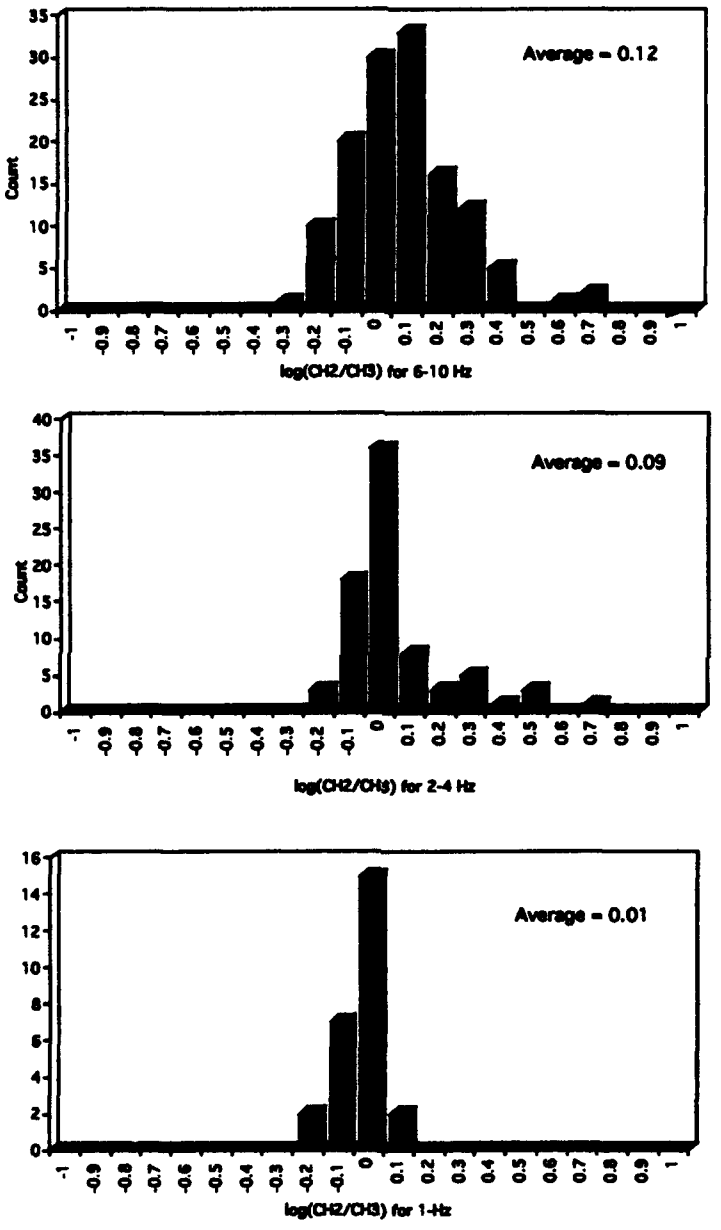

Figure 30 (b): Histograms of the spectral ratios for soil channel 2. The top figure is 6-10 Hz, middle is 2-4 Hz and bottom is 1Hz.

Channel 9

148 meters

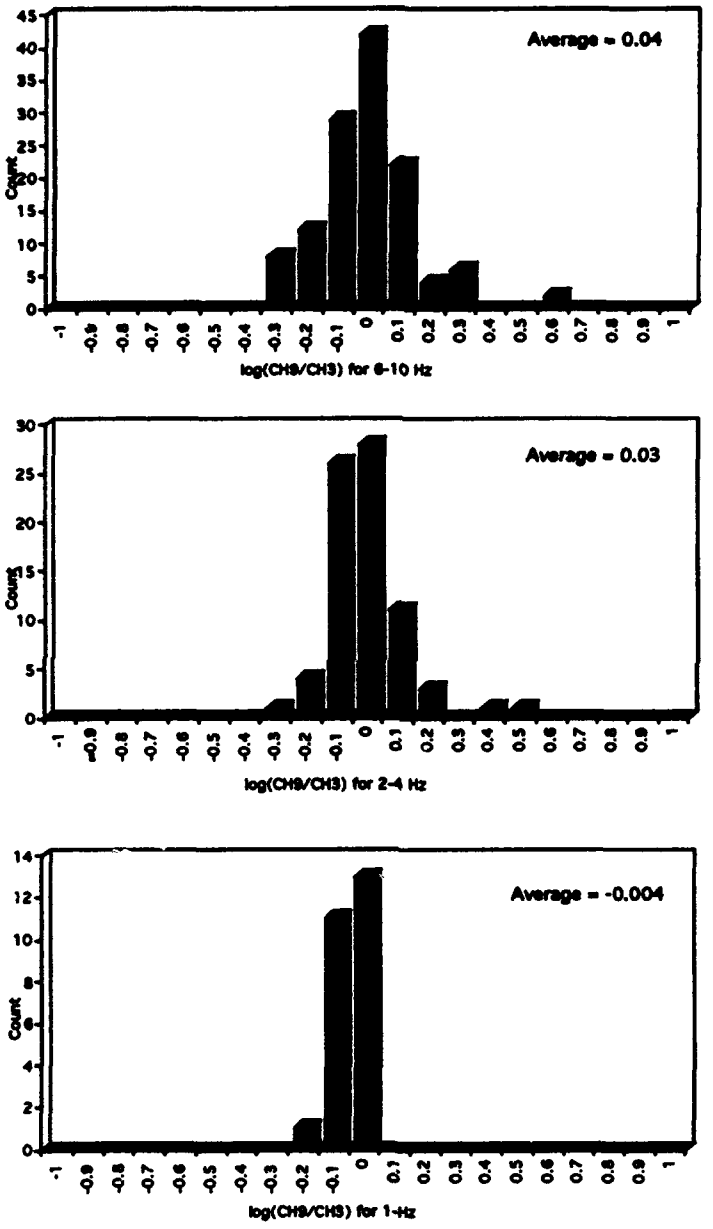

Figure 30 (c): Histograms of the spectral ratios for soil channel 9. The top figure is 6-10 Hz, middle is 2-4 Hz and bottom is 1Hz.

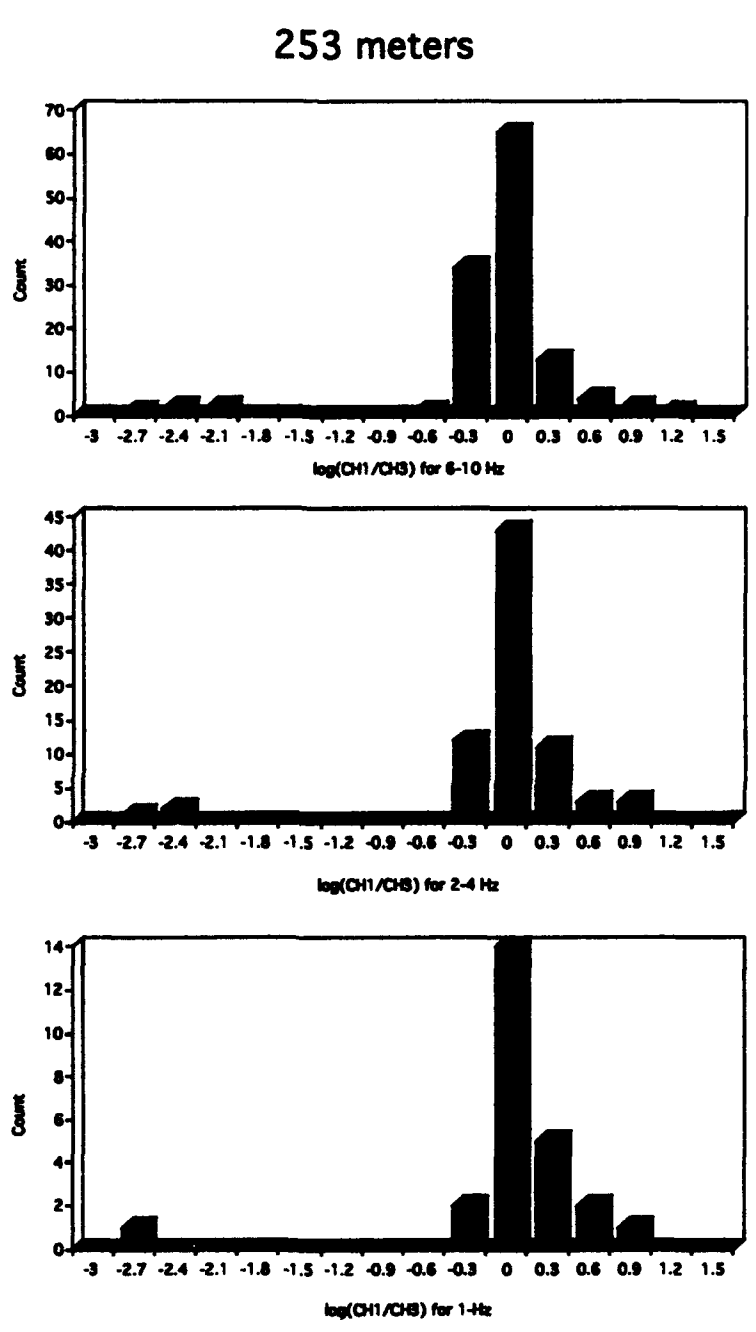

Figure 30 (d): Histograms of the spectral ratios for soil channel 1. The top figure is 6-10 Hz, middle is 2-4 Hz and bottom is 1Hz.

There are times of very significant precipitation during the period of time analyzed. The first occurred around day 230, the second was around day 263. For both of these times, there was some precipitation before and after the peak amount. On day 244 there was nearly 1.25 inches of precipitation, without any on preceding days or days immediately following. On days 256 and 257 there was precipitation which totaled over one inch, however it is unknown how much precipitation is needed to saturate the soil at the sites, nor is it known how long the soil remains saturated.

Figure 31(a) shows the ratios for the pier sites in the frequency band of 6-10-Hz. There does not seem to be any systematic relationship between changes in the ratios and precipitation data. With the exception of channel 5 for the first event, all of the pier sites behave similarly on any given day. There also does not seem to be significant variation in the ratios which correspond systematically to the four most significant precipitation events.

The ratios for the 6-10-Hz band for soil sites are shown in Figure 31(b). These sites also do not exhibit any significant pattern in the variation of the ratios for any given day or period of time. For most of the soil sites, there is little evidence of systematic changes in the ratios corresponding with precipitation. This may be best illustrated by observing ratios for the events that surround the precipitation centered on day 263. Days 260-264 have the largest total precipitation of any time period in the entire data set, yet the ratios for the soil sites 12 and 9 in the 6-10-Hz band do not vary significantly before during or after this period of time. Soil sites 1 and 2 do vary during this time period. Site 1 shows an increase in the amplitude ratios. However, for the second biggest precipitation event, this trend seems to be reversed. After the precipitation event which occurred around day 230, the ratios for site 1

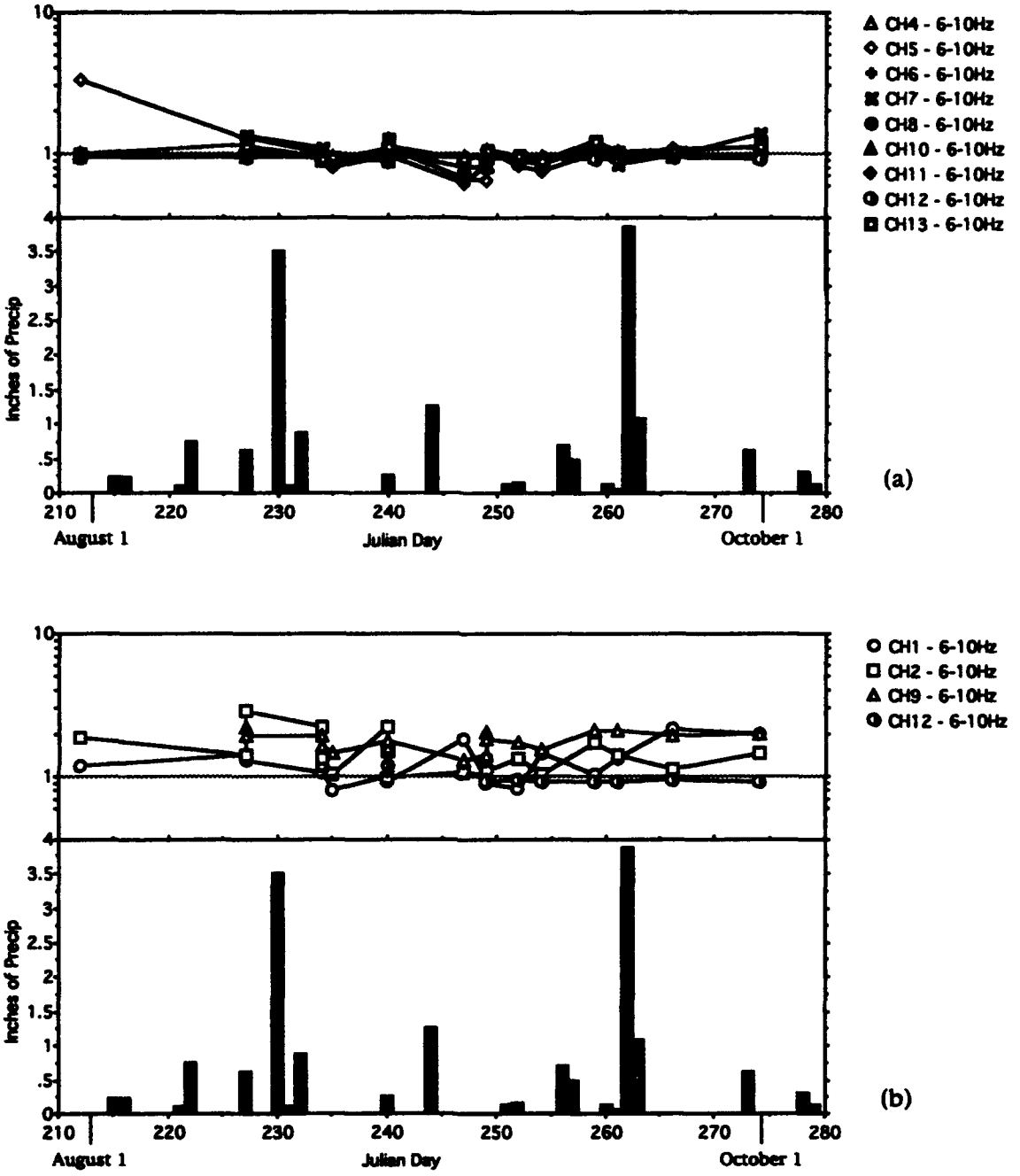

Figure 31: In the top portion of each figure, the ratios in the 6 to 10-Hz frequency band for the pier and soil sites are plotted against the Julian day of the year for blasts which occurred during 1991 are shown. The bottom portion of each figure is a bar graph which shows the amount of precipitation which was recorded by the nearest NOAA weather station in Waltham, MA approximately 6.6 km away from the array (U. S. Dept. of Commerce, 1991).

decrease rather than increase. Site 2 shows a decrease in amplitude ratios for both precipitation periods, although it shows an increase in amplitude ratios during the next two smaller precipitation events.

Figure 32(a) shows the ratios in the 2-4-Hz band for the pier sites. There does not appear to be a systematic relationship between the amount of precipitation and the ratios for the pier sites. It is significant to note that with the same exception of channel 5 on the first event, the ratios for the channels seem behave similarly for any given day.

Figure 32(b) shows the ratios in the 2-4-Hz band for the soil sites plotted against Julian day. There is more variation between the individual channels on any given day then in the previous data sets. However, there is little evidence for any systematic changes in the ratios that are related to the precipitation. The ratios do not change significantly before or after the occurrence of precipitation around day 263. In contrast, there is more variation of the ratios around the precipitation event which occurred on day 230.

Figure 33(a) shows the ratios at 1-Hz for the pier sites plotted against Julian day. With the exception of channel 5 for the first event, and channel 13 for the event on day 262, there is very little variation between the individual channels for a given day or between days. Figure 33(b) shows the ratios for 1-Hz for the soil sites plotted against Julian day. With the exception of channel 1, there is significantly less variation between the individual channels, and between individual days than at other frequency bands. For channel 1, there may possibly be some correspondence between precipitation and the ratio. However, at this frequency, this may be due more to background noise rather than amplification of signals. Channel 1 is located within a wooded area, and

has significant low frequency background noise on many seismograms. Since periods of high precipitation can be associated with high winds, it would not be surprising that there is more low frequency wind and tree noise during and after these periods of high precipitation.

It is interesting to note that the ratios in the 6 to 10-Hz band for pier and soil sites show about the same amount of variation between themselves for any given day. That is, for most days, the maximum difference between the ratios of any two sites is about the same. However, this does not imply that the sites which show the maximum and minimum ratios remain the same. This same observation is made for the ratios for pier sites at 1-Hz. If we discount channel 1 because of the high background noise, then the ratios for soil sites at 1-Hz could also be characterized this way. The ratios from 2 to 4-Hz at pier sites and soil sites show more variation on certain days of the year. If we discount channel 1 because of the high background noise, then the ratios for soil sites at 1-Hz could also be characterized this way. The ratios from 2 to 4-Hz at pier sites and soil sites show more variation on certain days of the year.

7.3.2 Events Recorded on the Same Day

Figure 34 and Figure 35 show the ratios for five blasts recorded on day 112 of 1992 (92-112). These events were chosen to be analyzed because they were all recorded within three hours of each other. When analyzing these events, I began by assuming that any variation in the ratios is not due to temporal effects. This appears to be true for all channels except channel 1.

The pier sites, shown in Figure 34, have almost the same amount of variation within the single day of recording as they did for the entire data set analyzed above in Section 7.2.1. Table 5 summarizes the results for the

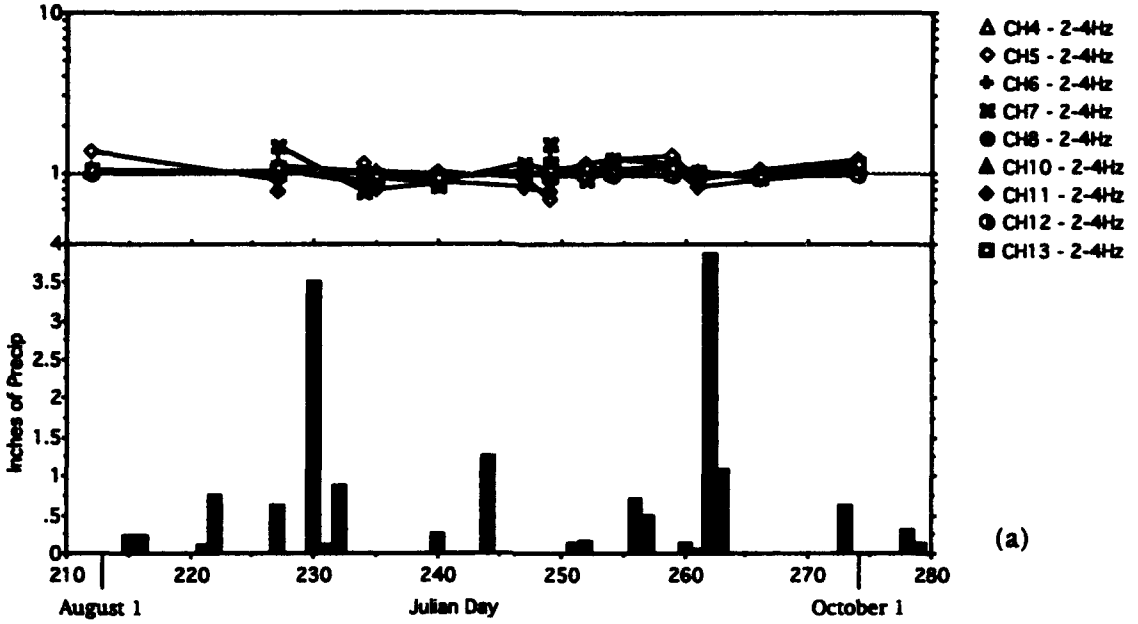

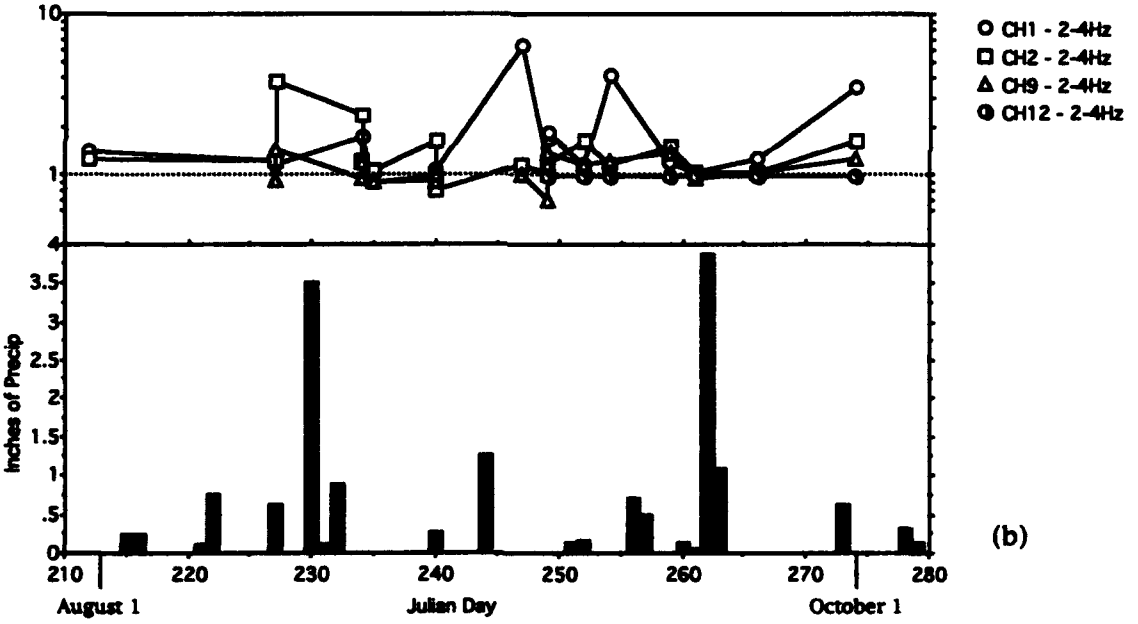

Figure 32: In the top portion of each figure, the ratios in the 2 to 4-Hz frequency band for the pier and soil sites are plotted against the Julian day of the year for blasts which occurred during 1991 are shown. The bottom portion of each figure is a bar graph which shows the amount of precipitation which was recorded by the nearest NOAA weather station in Waltham, MA approximately 6.6 km away from the array (U. S. Dept. of Commerce, 1991).

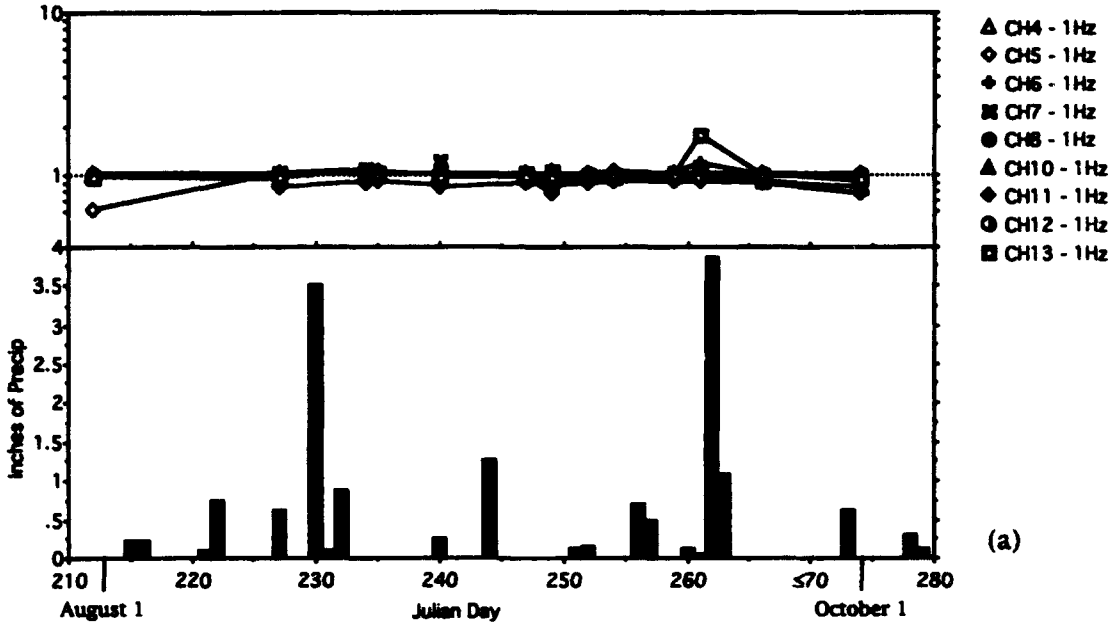

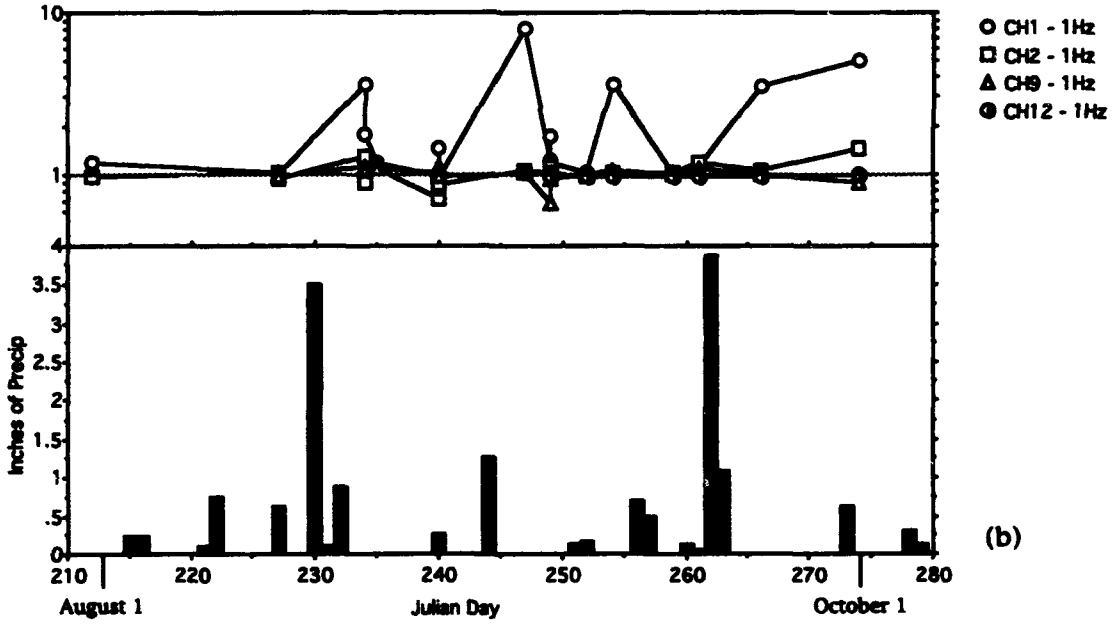

Figure 33: In the top portion of each figure, the ratios at 1-Hz for the pier and soil sites are plotted against the Julian day of the year for blasts which occurred during 1991 are shown. The bottom portion of each figure is a bar graph which shows the amount of precipitation which was recorded by the nearest NOAA weather station in Waltham, MA approximately 6.6 km away from the array (U. S. Dept. of Commerce, 1991).

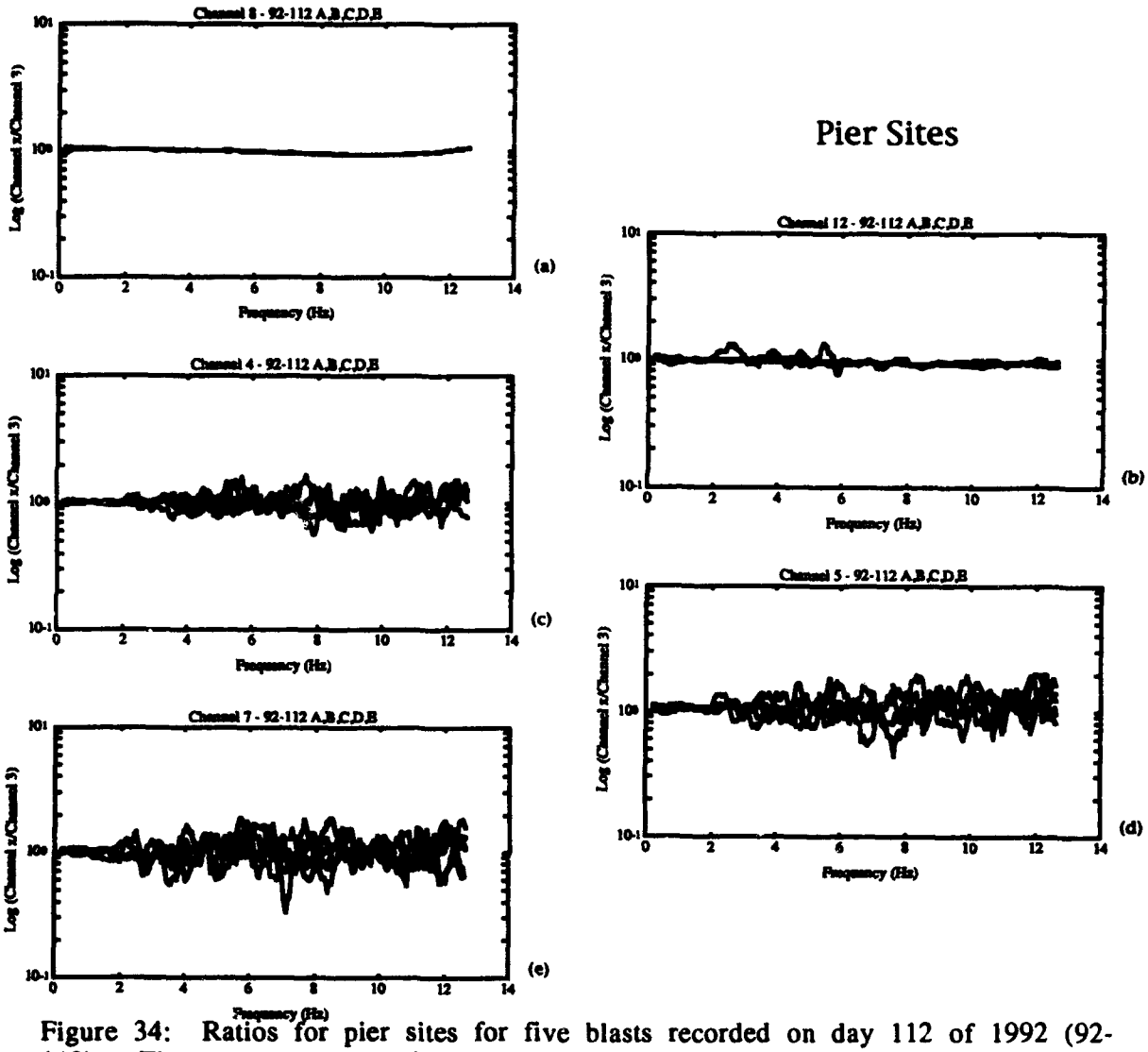

Figure 34: Ratios for pier sites for five blasts recorded on day 112 of 1992 (92-112). These events were chosen to be analyzed because they were all recorded within three hours of each other.

variation of the pier sites for the entire data set and the subset of blasts recorded on day 92-112.

With the exception of one event, the variation for the entire data set of ratios for channel 8 was 5%. The variation was the same for the five blasts recorded on day 92-112. The maximum variation of the ratios for channel 12 was 25%, with the exception of one event that varied by a factor of 2. The variation for channel 12 for day 92-112 was also 25%. In the entire data set,

the ratios for channel 5 varied by a factor of 2 for all blasts except one. For events recorded on day 92-112, the ratios for channel 5 varied by a factor of 2. Ratios for channels 4 and 7 had the same variation for both data sets. For all events the ratios for these two channels varied by a factor of 2.

Table 5

Channel	Entire Data Set Variation	Day 92-112 Variation
8	1.05 (1.3)*	1.05
12	1.25 (2)*	1.25
4	2	2
5	2 (5)*	2
7	2	2

Variation in the ratios of each pier site channel relative to the reference channel. The values of the variation is the maximum variation for the entire data set expressed as a ratio (relative to the amplitude at the reference site).
* Values in parentheses are the maximum ratios for a single event which is anomalous from the rest of the data.

With the exception of channel 9, the ratios for soil sites showed larger differences than the results for the pier sites. The results for the variations of the soil site ratios for the entire data set and the subset of blasts recorded on day 92-112 are presented in Table 6.

The variation of the ratios for channel 2 for the entire data set is about a factor of 5. For day 92-112, the variation of the ratios below 10-Hz is about 66% and is about a factor of 4 above 10-Hz. The maximum variation of ratios for channel 9 is about a factor of 2 for all events except one in the entire data. For that one event, the variation of the ratio for channel 9 is about a factor of 4. For the subset of blasts recorded on day 92-112, the variation of the ratios for channel 9 is about a factor of 2.

Table 6

Channel	Entire Data Set Variation	Day 92-112 Variation
12	1.25 (2)*	1.25
2	5	1.66 (4)†
1	10	4 (10)*
9	2 (4)*	2

Variation in the ratios of each soil site channel relative to the reference channel. The values of the variation is the maximum variation for the entire data set expressed as a ratio (relative to the amplitude at the reference site).
* The values in parentheses are the maximum ratios for a single event which is anomalous from the rest of the data.
† The value in the parentheses are the ratios for frequencies above 10-Hz, the value before the parentheses is for frequencies below 10-Hz

The maximum variation of the ratios for channel 1 is about a factor 10 for the entire data set, and is about a factor of 4 for most of the blasts recorded on day 92-112. For one event recorded on day 92-112, the maximum variation of the ratios for channel 1 is about a factor of 10. There appears to be a temporal variation in the ratios for channel 1 during day 92-112. Generally, the ratios for the later events are larger than those of earlier events. This is especially evident at lower frequencies [see Figure 35(d)].

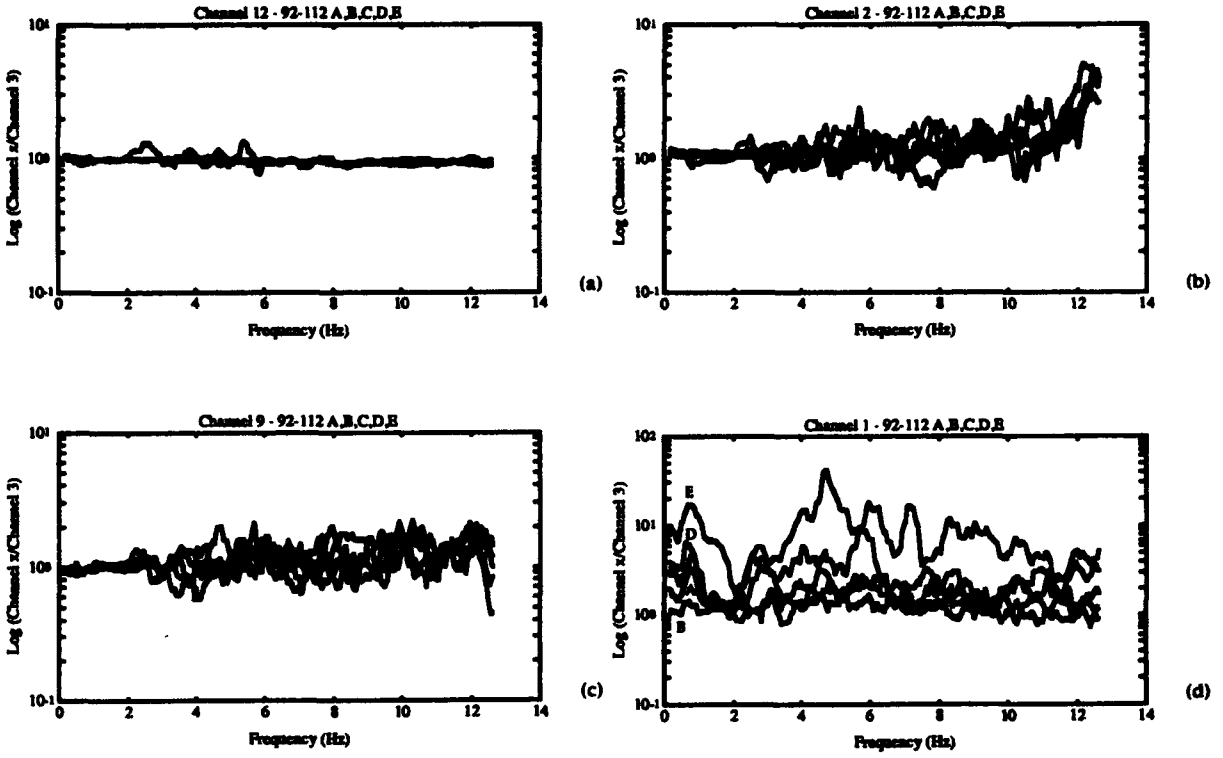

Figure 35: Ratios for pier sites for five blasts recorded on day 112 of 1992 (92-112). These events were chosen to be analyzed because they were all recorded within three hours of each other.

8. DISCUSSION

8.1 Effect of Instrument Response

Section 6 described the method used to calibrate the seismometers used in this study. The method uses both empirical and theoretical values for the instrument constants. Section 6 also described the errors associated with the different estimates of instrument response. The maximum difference between the estimates of instrument response is about 20% for frequencies under 6-Hz. Above 6-Hz the difference between the estimates becomes more significant, and the maximum difference is about 75%. In this study, a purely empirical

method of estimating the precision of the instruments was performed by placing multiple seismometers on the same pier, and comparing the spectral ratios from these instruments.

Figure 36 shows the results of comparing the amplitude spectra for channels 6 and 13 to the spectra for channel 4. These three channels are co-located on a seismic pier at site B. With the exception of the data near 1-Hz for event 91-261B, the ratios vary by no more than 5% for either channel. This compares directly with the results found for the ratios of channels 8 and 10 to channel 3, which also varied by no more than 5% (see Section 3.3). It is curious, however, that the same event (91-261B) gave anomalous results at 1-Hz for both instruments. Nonetheless, for the vast majority of data points analyzed in this study, the instruments appear to be precise to within about 5% of each other. Observed differences in amplitudes that are greater than 5%, therefore, appear to be due to factors other than instrument response.

8.2 Differences Between Soil and Pier Sites

Figure 37 shows the averages and standard deviations of the logarithms of the ratios for the pier and soils sites analyzed in this study. This figure clearly illustrates the differences between the two types of sites. The maximum standard deviation at pier sites corresponds to a variation of about 75%. At soil sites, the maximum standard deviation corresponds to a variation of about a factor of 5. Thus, soil sites are observed to cause a greater variation in seismic wave amplitudes than pier sites. While this result is not surprising, this study has demonstrated that such a difference is indeed occurring in the area surrounding Weston Observatory.

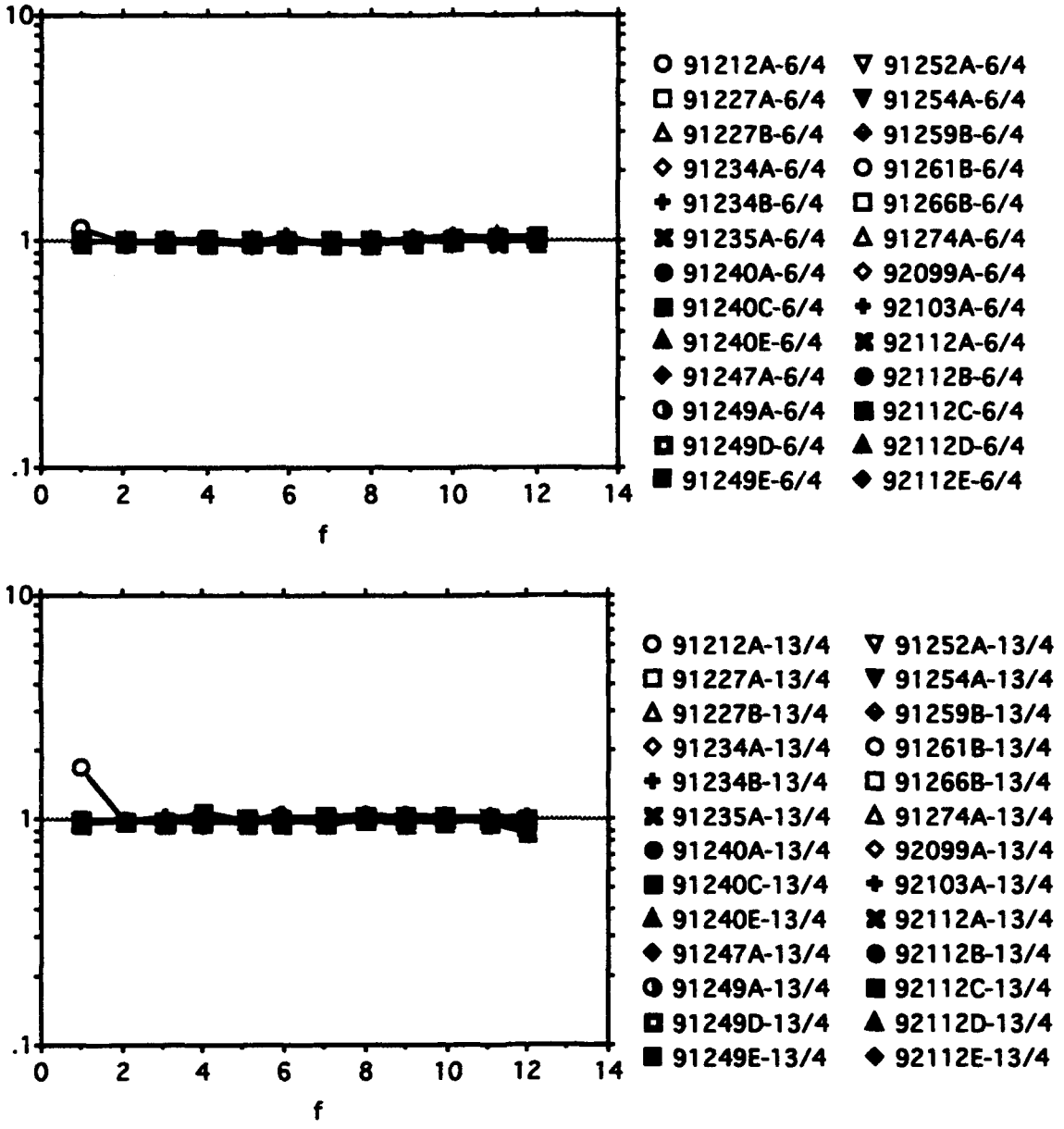

Figure 36: The results of comparing the amplitude spectra for channels 6 and 13 to the spectra for channel 4. These three channel are co-located on a seismic pier at site B. With the exception of the data around 1-Hz for event 91-261B, the ratios vary by no more than 5% for either channel. This compares directly with the results found for the ratios of channels 8 and 10 to channel 3.

The averages for the pier site channels show that, on average, site effects at the pier sites are much less significant than at soil sites. Also, at pier sites there is about the same amount of amplification as there is decrease in signal amplitudes. However, two of the soil sites (channels 1 and 2) show significant amplification throughout most of the frequency band analyzed. It is probable that some of the amplification seen on channel 1 is due to background noise rather than seismic wave amplification.

Channel 12 is a soil site which is buried within about 0.5 meters of bedrock, and within 2 meters of the reference pier. It behaves more like a pier site than a typical soil site. Figure 38 shows the averages and standard deviations for channels 8, 10 and 12. Channels 8 and 10 are co-located with the reference site. Below 6-Hz, the average for channel 12 varies by as much as 10% from channels 8 and 10. Between 6 and 10-Hz the average for channel 12 is with in 2% of the averages for channels 8 and 10, but the maximum standard deviation for this frequency band is at least 15%. Thus, it seems clear that it requires only a short distance (2 meters) and/or a small amount of sediment and weathered rock (0.5 meters) to create fairly large (15%) differences in signal amplitudes.

8.3 Amplitude Ratio as a Function Frequency

Figure 37 also summarizes the characteristics of soil and pier sites as a function of frequency. The two different types of sites behave differently in the frequency range of this study. The pier sites show the least amount of scatter at lower frequencies (below 4-Hz). Soil sites appear to vary by a smaller amount at higher frequencies (above about 9-Hz). Also, soil sites show a smaller amount of scatter near 2-Hz than at 1-Hz or between 3 and 8-Hz. The curves corresponding to the average ratios for the pier sites are similar to

each other across the entire frequency band. On the other hand, the average ratio curves for the soil sites are quite different from each other, and exhibit a distinct frequency dependence.

8.4 Variation as a Function of Distance

Figure 39(a) shows the average and standard deviation of the ratios for each pier site as a function of distance from the reference pier. In this plot, channels 8 and 10 were not included since they are co-located with the reference channel. Figure 39 seems to indicate that, at 1-Hz and in the 6 to 10-Hz frequency band, amplitude variation is not well correlated with distance from the reference pier. However, there is some indication of a systematic variation of amplitude with distance for the 2 to 4-Hz frequency band.

Figure 39(b) shows the mean and standard deviation for the spectral ratios as a function of distance for the soil sites in this study. Because of the proximity of channel 12 to bedrock, it was not included in this figure. Because of the greater amount of scatter for channel 1, it appears as if there may be some relationship between distance and spectral ratio and possibly some site amplification. However, focusing in on the channels 2 and 9 would not support that conclusion, and in light of the results found for the pier sites, I would conclude that there may be other factors which amplify signals recorded on channel 1 which are not related to distance from the reference pier. These may include background noise, a higher water table, or some other unidentified factors.

As discussed above, the channels which are co-located show only a 5% difference across the frequencies analyzed in this study. Section 8.2 discussed the differences between channel 12 and channels 8 and 10. Channels 8 and 10 are co-located with the reference channel, and channel 12 is located 2 meters

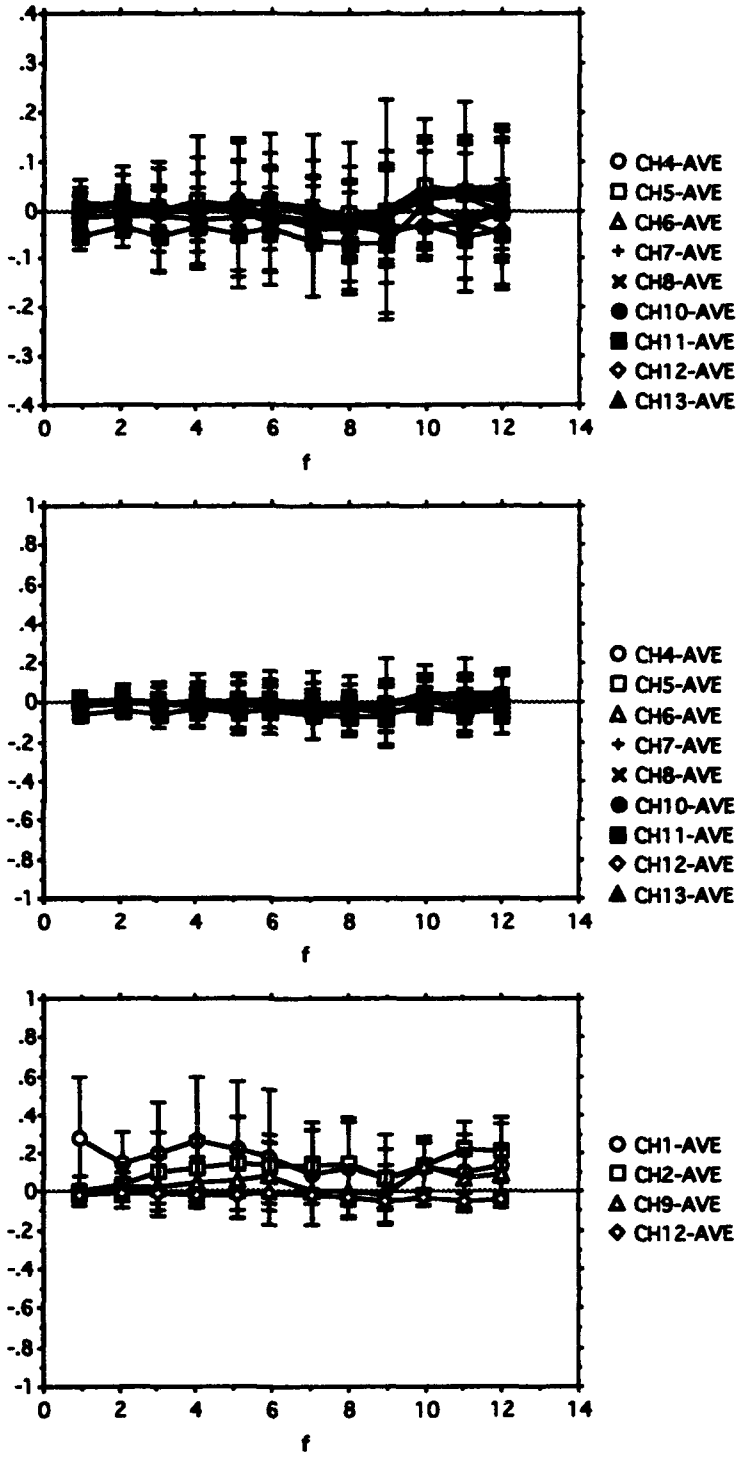

Figure 37: Averages and standard deviations for the pier and soil sites used in this study. This figure clearly illustrates the differences between the two types of sites.

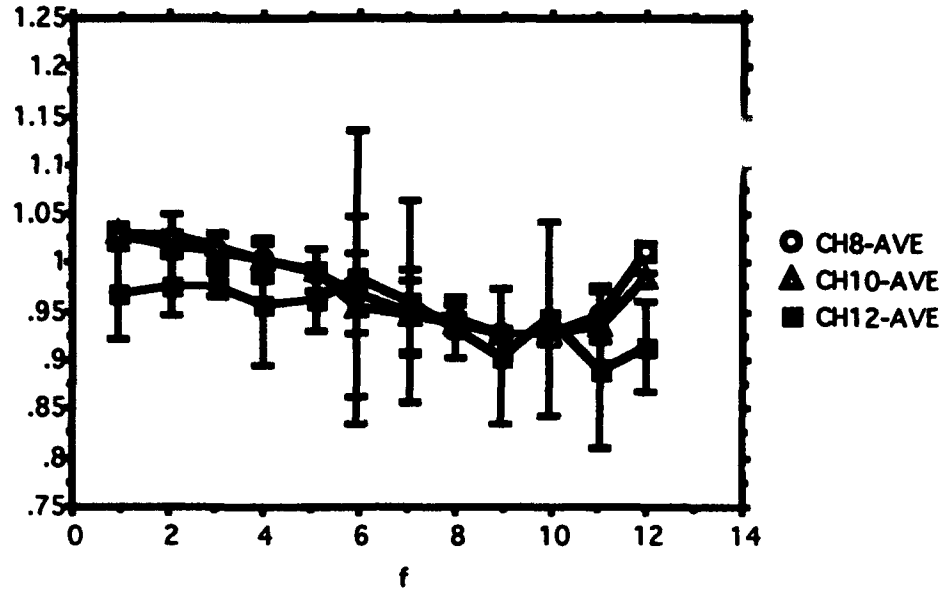

Figure 38: Averages and standard deviations for channels 8, 10 and 12. Channels 8 and 10 are co-located with the reference site. Channel 12 is located 2 meters from the reference site and within 0.5 meters from bedrock.

away from the reference channel. The differences observed between these channels may indicate the extent to which variations can be observed for channels separated at this scale. The differences may also be due to different site conditions. Channels 8 and 10 are on a seismic pier inside an enclosed shed, while channel 12 is buried within 0.5 meters of bedrock in soil, with no surrounding enclosure.

8.5 Analysis by Quarry Location:

There are a few cases in which the ratio curves (plotted as a function of frequency) appear to have characteristic shapes that are associated with events from a particular quarry. Specifically, ratio curves for San-Vel Quarry blasts recorded at channel 4, and Keating Quarry blasts recorded at channels 1, 5, 7, and 9, appear to have characteristic shapes in some frequency bands.

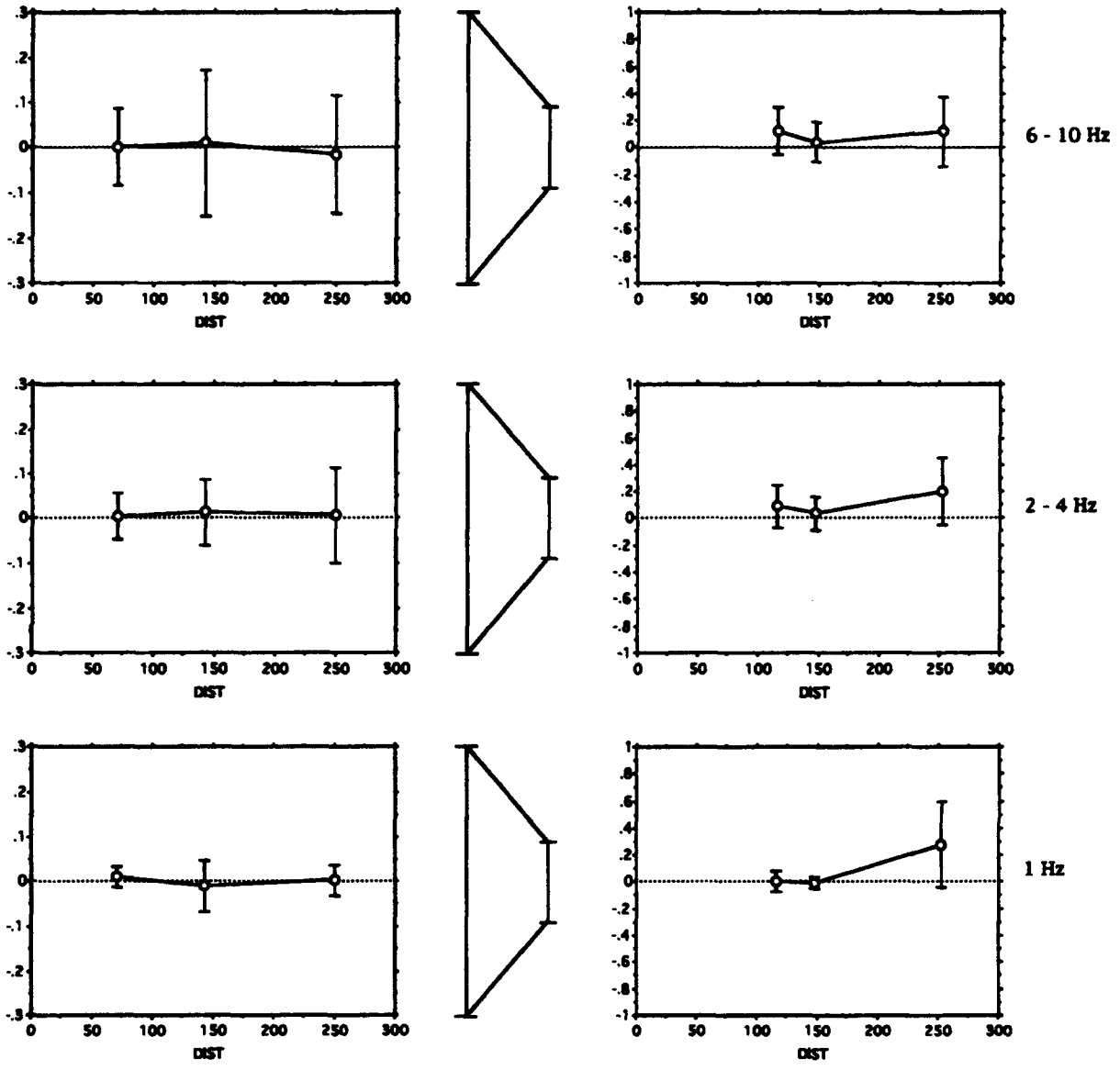

Figure 39: (a) Average and standard deviation of the ratios for each pier site as a function of distance from the reference pier. In this plot, channels 8 and 10 were not included since they are co-located with the reference channel. (b) Average and standard deviation of the ratios for each soil site as a function of distance from the reference pier. In this plot, channel 12 was not included since it is located very close to the reference channel.

San-Vel -- Channel 4: Figure 40(a) shows the ratios for this path. Between 0.5 and 1.5-Hz, the ratio curves are very flat and very close to 1.0. There appears to be a systematic shape in these ratio curves between about 3-Hz and 7-Hz. Starting near 4-Hz, the curves begin to rise to a peak that occurs at about 5-Hz. Beyond 5-Hz, the curves fall and there is a trough at about 6-Hz.

Keating -- Channel 5: Figure 40(b) shows the ratios for this path. Between 0 and 1.5-Hz, the ratio curves are very flat and very close to 1.0. There appears to be a systematic shape in these ratio curves between about 1.5-Hz and 3-Hz. Starting near 1.5-Hz, the curves begin to fall to a trough that occurs at about 2-Hz. Beyond 2-Hz, the curves rise and there is a peak at about 2.5-Hz.

Keating -- Channel 7: Figure 40(c) shows the ratios for this path. Between 0 and 1.5-Hz, the ratio curves are very flat and very close to 1.0. There appears to be a systematic shape in these ratio curves between about 1.5-Hz and 3.5-Hz. Starting near 1.5-Hz, the curves begin to fall to a trough that occurs at about 2-Hz. Beyond 2-Hz, the curves rise and there is a peak at about 2.5-Hz.

Keating -- Channel 9: Figure 40(d) shows the ratios for this path. Between 0 and 1.5-Hz, the ratio curves are very flat and very close to 1.0. There appears to be a systematic shape in these ratio curves between about 1.5-Hz and 2.5-Hz. Starting near 1.5-Hz, the curves begin to fall to a trough that occurs at about 2-Hz. Beyond 2-Hz, the curves rise and there is a peak at about 2.5-Hz.

Keating -- Channel 1: Figure 40(e) shows the ratios for this path. With the exception of one curve, the following general pattern seems to be present

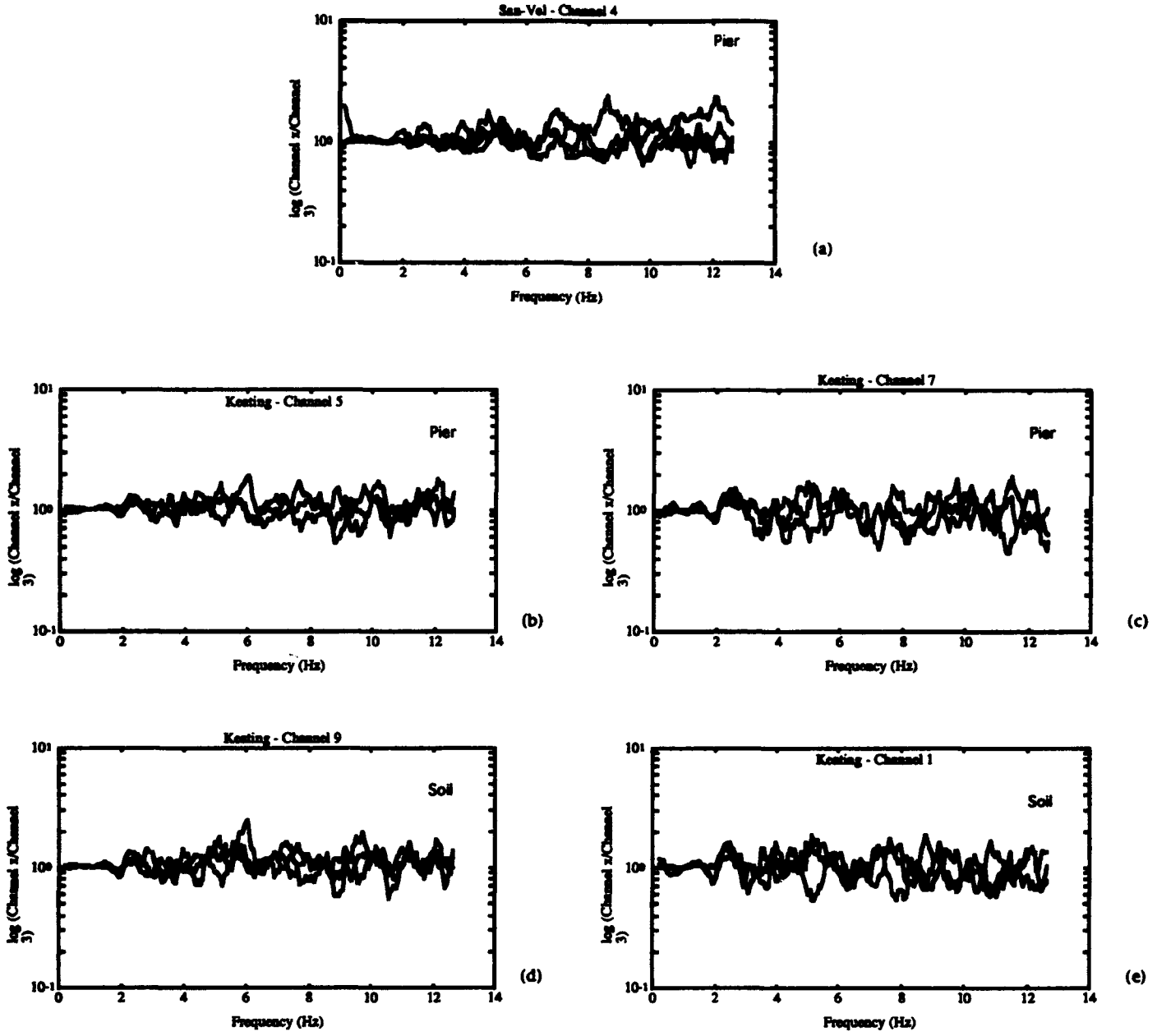

Figure 40: Examples of ratio vs. frequency curves that appear to have characteristic shapes for events from specific quarries occurs at about 2-Hz. Beyond 2-Hz, the curves rise and there is a peak at about 2.5-Hz.

in the ratio curves. Between 0 and 1.5-Hz, the ratio curves are very flat and very close to 1.0. There appears to be a systematic shape in these ratio curves between about 1.5-Hz and 2.5-Hz. Starting near 1.5-Hz, the curves begin to fall to a trough that occurs at about 2-Hz. Beyond 2-Hz, the curves rise and there is a peak at about 2.5-Hz. All the curves appear to have a general pattern between about 5.5-Hz and about 7-Hz. Starting about 5.5-Hz, the ratio curves begin to fall to a trough that occurs about 6.5-Hz. Beyond 6.5-Hz, the ratio curves rise to a trough which occurs about 7-Hz.

Between 0 and about 2.5-Hz, the ratio curves for each of these four channels appear to have a systematic pattern in response to Keating Quarry blasts. This would indicate that there may be a characteristic response of channel 3 to these blasts rather than independent, but nearly identical, responses of the four channels.

9. CONCLUSIONS

9.1 Instrument Response

Based on empirical results, the instrument corrections used in this study appear to be precise to within about 5%. The model response curves used to correct for instrument response seem to represent the shape of the instrument response sufficiently well that it is possible to make meaningful conclusions about site effects. It therefore seems reasonable to conclude that, in general, amplitude variations observed in this study that exceed 5% represent true variations in ground motion and evidence of site effects.

9.2 Pier Sites versus Soil Sites

Soil sites are observed to have a greater effect on seismic wave amplitudes than pier sites. Signal amplification up to about a factor of 5 is

observed at some of the soil sites, particularly for frequencies greater than 3-Hz. Also, seismograms recorded at soil sites are affected by background noise more than those recorded at pier sites. While these results are within the range of other studies, this study has demonstrated that such differences are indeed occurring in the area surrounding Weston Observatory, an area which is underlain by competent bedrock and is covered by (at most) about 5-6 meters of sediment.

The results for site D (the magnetic observatory) suggest that pier size and shape has an effect on signal amplitudes at frequencies greater than 6-Hz. At those higher frequencies, the variations at site D are greater than the variations at pier site C, which is farther away from the reference site than site D.

9.3 Dependence of Site Effects on Frequency

For pier sites, the maximum standard deviation of the logarithm of the ratios below 3-Hz is about 0.1, which corresponds to differences in signal amplitudes of about 26%. Above 3-Hz, the maximum standard deviation nearly twice that amount (about 0.2), which corresponds to differences of about 60%. This suggests that 3-Hz appears to be a cutoff frequency, below which signals are not significantly affected by site characteristics.

The pattern of variations at soil sites is more complicated. At frequencies between 2 and 3-Hz and between 8 and 12-Hz, soil sites show the smallest variations in amplitudes. The maximum standard deviation of the logarithms of the ratios above 8-Hz is about 0.2 (i.e. 60%). The maximum standard deviation at frequencies between 2 and 3-Hz is also about 0.2. Outside of these two frequency bands, the maximum standard deviation is about 0.4 (i.e. a factor of 2.5).

Thus, for frequencies lower than about 2-Hz, site effects may not be a very serious issue for events recorded in New England, even for soil sites (provided that the soil sites are not particularly noisy). Furthermore, for higher frequencies, pier (and bedrock) sites are probably quite reliable to within about 15% on average. The maximum error due to bedrock site effects appears to be about a factor of 2.

9.4 Dependence of Site Effects on Other Factors

Source Location: The results of examining blasts from known quarries seems to indicate that there are cases where there is a characteristic "signature" of blasts from a particular location. This type of signature is most obvious for the Keating Quarry blasts. In that case, the signature seems to be dependent on the characteristics of the reference site at least as much as it is on the characteristics of the individual sites where these signatures are observed.

Distance from Reference Site: At the scale of this array (0.25 km), propagation effects do not appear to play as significant a role as do site effects. The results for the differences between site A1 and site A suggest that there may be finer scale variations which the array was not able to resolve.

Temporal Effects and Effects of Rainfall: There appears to be as much variation for the five blasts recorded within 3 hours of each other as there was between the 26 events recorded within an entire year. This suggests that the sources of amplitude variations are probably not time dependent. One channel did show short term temporal variations. The variations of the ratios for site G during the 3 hour time period appear to be temporally dependent. This may be the result of increasing background noise during the time period analyzed.

With the exception of site G, there does not appear to be a relationship between rainfall and amplitude variations. The amplitude variations for site G appear to be slightly coincident with precipitation events, and this could possibly be due to increasing wind associated with the precipitation events.

9.5 Comparison with Previous Studies

The amount of variation in amplitudes observed around Weston Observatory is consistent with the observations reported in previous studies for other areas. Amplitude variations due to site effects reported in previous studies were as large as a factor of 20 at soil sites, and amplifications of factors of 5 to 10 are commonly reported. The difference between soil and pier sites is also consistent with that observed in previous studies. In cases where both soil and bedrock site effects have been analyzed, it is not uncommon for site effects to be greater at soil sites.

9.6 Can These Results Explain Amplitude Variations Observed in New England?

Chapter 2 discussed two examples of why this type of study is important. One example was that magnitudes based on amplitudes observed at station QUA are systematically higher than the network average. The other example was the amplitude residuals that were observed in the attenuation study. To what extent has this study addressed the issues discussed in Chapter 2?

The higher magnitudes at station QUA could very well be caused by the type of site amplification that we have observed at soil sites in this study. We have seen that, in the case of the area around station WES, site effects can cause amplitudes to vary by at least as much as a factor of 2.5 at soil sites and by at least as much as 60% at pier sites. Also, the average variation may be as much as a factor of 2 at soil sites and 10% at pier sites. The anomalously high magnitudes seen at station QUA were, on average, 0.4 magnitude units greater

than the network average (Table 1 and Figure 2). The maximum magnitude deviation in the data shown in Table 1 is 0.7 magnitude units. This represents a maximum and an average amplification of signals by factors of 5.0 and 2.7, respectively. Based on the results of this study, this amount of amplitude variation is greater than that due to site effects in the area investigated for this study. Thus, either the site effects for station QUA are greater than those for WES and/or the instrument effect at QUA has not been sufficiently constrained.

The amplitude residuals that were observed in the attenuation study described in Chapter 2 (Figure 5) were all smaller than 0.35 on a log scale (which represents a factor of 2.2 in terms of differences in signal amplitudes). Considering that the amplitudes measured for that attenuation study were not corrected for other effects, such as radiation pattern, it is not at all surprising that the amplitude residuals are as great as they are. In fact, the majority of the NESN stations are installed at soil sites, and the results of this study suggest that a large part of these observed amplitude variations could be due to site effects.

10. REFERENCES

Båth, M. (1975). Short-period Rayleigh waves from near-surface events, Physics of the Earth and Planetary Interiors, 10, 369-376.

Blaney, J.I., (1990). A Functional Description of the Geophysical Data Acquisition System, GL-TR-90-0202, ADA230032.

Blaney, J.I., (1991). Geophysical Data Acquisition System Users Manual, PL-TR-91-2138.

Blaney, J.I., (1992). Installation of a Seismic Array in the Area Surrounding Weston Observatory, (in preparation).

Cicerone, R. (1980). The Attenuation of Crustal Seismic Waves in New England, Masters Thesis, Dept. of Geology and Geophysics, Boston College, Chestnut Hill, MA.

D'Annolfo, S.E. (1992). Investigation of Lateral Variation in the Seismic Velocity Structure of the Shallow Crust Beneath Eastern Massachusetts and Southern New Hampshire, Masters Thesis, Dept. of Geology and Geophysics, Boston College, Chestnut Hill, MA.

Dwyer, J., R. Herrmann, and O. Nuttli, (1983). Spatial attenuation of the Lg wave in the Central United States, Bull. Seis Soc. Am., 73, 781-796.

Fowler, R.V., (1985). Attenuation of Rg Waves in Southern New England, Masters Thesis, Dept. of Geology and Geophysics, Boston College, Chestnut Hill, MA.

Gutenberg, B., (1957). Effects of ground motion on earthquake motion, Bull. Seis Soc. Am., 47, 221-250.

Kafka, A.L., (1990). Rg as a depth discriminate for earthquakes and explosions: a case study in New England, Bull. Seis Soc. Am., 80 No. 2 373-394.

Kafka, A.L. and A.K. Bowers, (1991). Corrections to Rg group velocity dispersion in southwestern New England (Research Note), Seism. Res. Lett., 62(3-4), 221-223

Kafka, A.L. and M. Dollin, (1985). Constraints on lateral variation in upper crustal structure beneath southern New England from dispersion of Rg waves, Geophysical Research Letters, Vol. 12, No. 5, 235-238.

Kafka, A.L. and J.W. Skehan, S.J. (1990). Major geological features and lateral variation of crustal structure in southern New England, Tectonophysics, 178: 183-192.

King, J.L. and B.E. Tucker (1984). Observed variations of earthquake motion across a sediment-filled valley, Bull. Seis Soc. Am., 74 No. 1 137-151.

Koteff, C, (1964). Surficial Geology of the Concord Quadrangle, Massachusetts, to accompany Map GQ-331, Department of the Interior, United States Geological Survey.

Koyanagi, S, K. Mayeda, and K. Aki (1992). Frequency-dependent site amplification factors using the S-wave coda for the island of Hawaii, Bull. Seis Soc. Am., 82 No. 3 1151-1185.

Mayeda, K., S. Koyanagi, and K. Aki (1991). Site amplification from S-wave coda in the Long Valley Caldera region, California, Bull. Seis Soc. Am., 81, No. 6, 2194-2213.

Nuttli, O. (1973). Seismic wave attenuation and magnitude relations for Eastern North America, Journal of Geophysical Research, 78, No. 5, 876-885.

Nuttli, O. (1978). A time-domain study of the attenuation of 10-Hz waves in the New Madrid Seismic Zone, Bull. Seis Soc. Am., 68, No. 2, 343-355.

Phillips, W.S. and K. Aki (1986). Site amplification of coda waves from local earthquakes in central California, Bull. Seis Soc. Am., 76, No. 3, 627-648.

Skehan, S.J., J.W. and P. H. Osberg (1979). The caledonides in the U. S. A., Internat. Geol. Corr. Prog. (IGCP). Project 27. Caledonides Orogen, Weston Observatory.

Stacey, F. (1969). Physics of the Earth, John Wiley and Sons, New York, 324 p.

Tucker, B.E., J.L. King, D. Hatzfeld, and I.L. Nersesov (1984). Observations of hard-rock sites effects, Bull. Seis Soc. Am., 74, 121-136.

U. S. Department of Commerce (1991). Record of River and Climatological Observations, Waltham, MA, National Oceanographic and Atmospheric Administration, National Weather Service, Asheville, NC.

Wallace, T.C. (1992). The May 21, 1992 Lop Nor Explosion: Tectonic release in the body and surface waves, Abstracts of papers presented at the 14th Annual PL/DARPA Seismic Research Symposium, p.69. PL-TR-92-2210,ADA256711

Weston Observatory (1992). List of the New England Seismic Network station gains, Weston, MA.

Prof. Thomas Ahrens
Seismological Lab, 252-21
Division of Geological & Planetary Sciences
California Institute of Technology
Pasadena, CA 91125

Prof. Keiiti Aki
Center for Earth Sciences
University of Southern California
University Park
Los Angeles, CA 90089-0741

Prof. Shelton Alexander
Geosciences Department
403 Deike Building
The Pennsylvania State University
University Park, PA 16802

Prof. Charles B. Archambeau
CIRES
University of Colorado
Boulder, CO 80309

Dr. Thomas C. Bache, Jr.
Science Applications Int'l Corp.
10260 Campus Point Drive
San Diego, CA 92121 (2 copies)

Prof. Muawia Barazangi
Institute for the Study of the Continent
Cornell University
Ithaca, NY 14853

Dr. Jeff Barker
Department of Geological Sciences
State University of New York
at Binghamton
Vestal, NY 13901

Dr. Douglas R. Baumgardt
ENSCO, Inc
5400 Port Royal Road
Springfield, VA 22151-2388

Dr. Susan Beck
Department of Geosciences
Building #77
University of Arizona
Tuscon, AZ 85721

Dr. T.J. Bennett
S-CUBED
A Division of Maxwell Laboratories
11800 Sunrise Valley Drive, Suite 1212
Reston, VA 22091

Dr. Robert Blandford
AFTAC/TT, Center for Seismic Studies
1300 North 17th Street
Suite 1450
Arlington, VA 22209-2308

Dr. Stephen Bratt
ARPA/NMRO
3701 North Fairfax Drive
Arlington, VA 22203-1714

Dr. Lawrence Burdick
IGPP, A-025
Scripps Institute of Oceanography
University of California, San Diego
La Jolla, CA 92093

Dr. Robert Burridge
Schlumberger-Doll Research Center
Old Quarry Road
Ridgefield, CT 06877

Dr. Jerry Carter
Center for Seismic Studies
1300 North 17th Street
Suite 1450
Arlington, VA 22209-2308

Dr. Eric Chael
Division 9241
Sandia Laboratory
Albuquerque, NM 87185

Dr. Martin Chapman
Department of Geological Sciences
Virginia Polytechnical Institute
21044 Derring Hall
Blacksburg, VA 24061

Mr Robert Cockerham
Arms Control & Disarmament Agency
320 21st Street North West
Room 5741
Washington, DC 20451,

Prof. Vernon F. Cormier
Department of Geology & Geophysics
U-45, Room 207
University of Connecticut
Storrs, CT 06268

Prof. Steven Day
Department of Geological Sciences
San Diego State University
San Diego, CA 92182

Marvin Denny
U.S. Department of Energy
Office of Arms Control
Washington, DC 20585

Dr. Zoltan Der
ENSCO, Inc.
5400 Port Royal Road
Springfield, VA 22151-2388

Prof. Adam Dziewonski
Hoffman Laboratory, Harvard University
Dept. of Earth Atmos. & Planetary Sciences
20 Oxford Street
Cambridge, MA 02138

Prof. John Ebel
Department of Geology & Geophysics
Boston College
Chestnut Hill, MA 02167

Eric Fielding
SNEE Hall
INSTOC
Cornell University
Ithaca, NY 14853

Dr. Petr Firbas
Institute of Physics of the Earth
Masaryk University Brno
Jecna 29a
612 46 Brno, Czech Republic

Dr. Mark D. Fisk
Mission Research Corporation
735 State Street
P.O. Drawer 719
Santa Barbara, CA 93102

Prof Stanley Flatte
Applied Sciences Building
University of California, Santa Cruz
Santa Cruz, CA 95064

Dr. John Foley
NER-Geo Sciences
1100 Crown Colony Drive
Quincy, MA 02169

Prof. Donald Forsyth
Department of Geological Sciences
Brown University
Providence, RI 02912

Dr. Art Frankel
U.S. Geological Survey
922 National Center
Reston, VA 22092

Dr. Cliff Frolich
Institute of Geophysics
8701 North Mopac
Austin, TX 78759

Dr. Holly Given
IGPP, A-025
Scripps Institute of Oceanography
University of California, San Diego
La Jolla, CA 92093

Dr. Jeffrey W. Given
SAIC
10260 Campus Point Drive
San Diego, CA 92121

Dr. Dale Glover
Defense Intelligence Agency
ATTN: ODT-1B
Washington, DC 20301

Dan N. Hagedon
Pacific Northwest Laboratories
Battelle Boulevard
Richland, WA 99352

Dr. James Hannon
Lawrence Livermore National Laboratory
P.O. Box 808
L-205
Livermore, CA 94550

Prof. David G. Harkrider
Seismological Laboratory
Division of Geological & Planetary Sciences
California Institute of Technology
Pasadena, CA 91125

Prof. Danny Harvey
CIRES
University of Colorado
Boulder, CO 80309

Prof. Donald V. Helmberger
Seismological Laboratory
Division of Geological & Planetary Sciences
California Institute of Technology
Pasadena, CA 91125

Prof. Eugene Herrin
Institute for the Study of Earth and Man
Geophysical Laboratory
Southern Methodist University
Dallas, TX 75275

Prof. Robert B. Herrmann
Department of Earth & Atmospheric Sciences
St. Louis University
St. Louis, MO 63156

Prof. Lane R. Johnson
Seismographic Station
University of California
Berkeley, CA 94720

Prof. Thomas H. Jordan
Department of Earth, Atmospheric &
Planetary Sciences
Massachusetts Institute of Technology
Cambridge, MA 02139

Prof. Alan Kafka
Department of Geology & Geophysics
Boston College
Chestnut Hill, MA 02167

Robert C. Kemerait
ENSCO, Inc.
445 Pineda Court
Melbourne, FL 32940

Dr. Karl Koch
Institute for the Study of Earth and Man
Geophysical Laboratory
Southern Methodist University
Dallas, Tx 75275

Dr. Max Koontz
U.S. Dept. of Energy/DP 5
Forrestal Building
1000 Independence Avenue
Washington, DC 20585

Dr. Richard LaCoss
MIT Lincoln Laboratory, M-200B
P.O. Box 73
Lexington, MA 02173-0073

Dr. Fred K. Lamb
University of Illinois at Urbana-Champaign
Department of Physics
1110 West Green Street
Urbana, IL 61801

Prof. Charles A. Langston
Geosciences Department
403 Deike Building
The Pennsylvania State University
University Park, PA 16802

Jim Lawson, Chief Geophysicist
Oklahoma Geological Survey
Oklahoma Geophysical Observatory
P.O. Box 8
Leonard, OK 74043-0008

Prof. Thorne Lay
Institute of Tectonics
Earth Science Board
University of California, Santa Cruz
Santa Cruz, CA 95064

Dr. William Leith
U.S. Geological Survey
Mail Stop 928
Reston, VA 22092

Mr. James F. Lewkowicz
Phillips Laboratory/GPEH
29 Randolph Road
Hanscom AFB, MA 01731-3010(2 copies)

Mr. Alfred Lieberman
ACDA/VI-OA State Department Building
Room 5726
320-21st Street, NW
Washington, DC 20451

Prof. L. Timothy Long
School of Geophysical Sciences
Georgia Institute of Technology
Atlanta, GA 30332

Dr. Randolph Martin, III
New England Research, Inc.
76 Olcott Drive
White River Junction, VT 05001

Dr. Robert Masse
Denver Federal Building
Box 25046, Mail Stop 967
Denver, CO 80225

Dr. Gary McCartor
Department of Physics
Southern Methodist University
Dallas, TX 75275

Prof. Thomas V. McEvilly
Seismographic Station
University of California
Berkeley, CA 94720

Dr. Art McGarr
U.S. Geological Survey
Mail Stop 977
U.S. Geological Survey
Menlo Park, CA 94025

Dr. Keith L. McLaughlin
S-CUBED
A Division of Maxwell Laboratory
P.O. Box 1620
La Jolla, CA 92038-1620

Stephen Miller & Dr. Alexander Florence
SRI International
333 Ravenswood Avenue
Box AF 116
Menlo Park, CA 94025-3493

Prof. Bernard Minster
IGPP, A-025
Scripps Institute of Oceanography
University of California, San Diego
La Jolla, CA 92093

Prof. Brian J. Mitchell
Department of Earth & Atmospheric Sciences
St. Louis University
St. Louis, MO 63156

Mr. Jack Murphy
S-CUBED
A Division of Maxwell Laboratory
11800 Sunrise Valley Drive, Suite 1212
Reston, VA 22091 (2 Copies)

Dr. Keith K. Nakanishi
Lawrence Livermore National Laboratory
L-025
P.O. Box 808
Livermore, CA 94550

Prof. John A. Orcutt
IGPP, A-025
Scripps Institute of Oceanography
University of California, San Diego
La Jolla, CA 92093

Prof. Jeffrey Park
Kline Geology Laboratory
P.O. Box 6666
New Haven, CT 06511-8130

Dr. Howard Patton
Lawrence Livermore National Laboratory
L-025
P.O. Box 808
Livermore, CA 94550

Dr. Frank Pilotte
HQ AFTAC/TT
1030 South Highway A1A
Patrick AFB, FL 32925-3002

Dr. Jay J. Pulli
Radix Systems, Inc.
201 Perry Parkway
Gaithersburg, MD 20877

Dr. Robert Reinke
ATTN: FCTVTD
Field Command
Defense Nuclear Agency
Kirtland AFB, NM 87115

Prof. Paul G. Richards
Lamont-Doherty Geological Observatory
of Columbia University
Palisades, NY 10964

Mr. Wilmer Rivers
Teledyne Geotech
314 Montgomery Street
Alexandria, VA 22314

Dr. Alan S. Ryall, Jr.
ARPA/NMRO
3701 North Fairfax Drive
Arlington, VA 22203-1714

Dr. Richard Sailor
TASC, Inc.
55 Walkers Brook Drive
Reading, MA 01867

Prof. Charles G. Sammis
Center for Earth Sciences
University of Southern California
University Park
Los Angeles, CA 90089-0741

Prof. Christopher H. Scholz
Lamont-Doherty Geological Observatory
of Columbia University
Palisades, NY 10964

Dr. Susan Schwartz
Institute of Tectonics
1156 High Street
Santa Cruz, CA 95064

Secretary of the Air Force
(SAFRD)
Washington, DC 20330

Office of the Secretary of Defense
DDR&E
Washington, DC 20330

Thomas J. Sereno, Jr.
Science Application Int'l Corp.
10260 Campus Point Drive
San Diego, CA 92121

Dr. Michael Shore
Defense Nuclear Agency/SPSS
6801 Telegraph Road
Alexandria, VA 22310

Dr. Robert Shumway
University of California Davis
Division of Statistics
Davis, CA 95616

Dr. Matthew Sibol
Virginia Tech
Seismological Observatory
4044 Derring Hall
Blacksburg, VA 24061-0420

Prof. David G. Simpson
IRIS, Inc.
1616 North Fort Myer Drive
Suite 1050
Arlington, VA 22209

Donald L. Springer
Lawrence Livermore National Laboratory
L-025
P.O. Box 808
Livermore, CA 94550

Dr. Jeffrey Stevens
S-CUBED
A Division of Maxwell Laboratory
P.O. Box 1620
La Jolla, CA 92038-1620

Lt. Col. Jim Stobie
ATTN: AFOSR/NL
110 Duncan Avenue
Bolling AFB
Washington, DC 20332-0001

Prof. Brian Stump
Institute for the Study of Earth & Man
Geophysical Laboratory
Southern Methodist University
Dallas, TX 75275

Prof. Jeremiah Sullivan
University of Illinois at Urbana-Champaign
Department of Physics
1110 West Green Street
Urbana, IL 61801

Prof. L. Sykes
Lamont-Doherty Geological Observatory
of Columbia University
Palisades, NY 10964

Dr. David Taylor
ENSCO, Inc.
445 Pineda Court
Melbourne, FL 32940

Dr. Steven R. Taylor
Los Alamos National Laboratory
P.O. Box 1663
Mail Stop C335
Los Alamos, NM 87545

Prof. Clifford Thurber
University of Wisconsin-Madison
Department of Geology & Geophysics
1215 West Dayton Street
Madison, WS 53706

Prof. M. Nafi Toksoz
Earth Resources Lab
Massachusetts Institute of Technology
42 Carleton Street
Cambridge, MA 02142

Dr. Larry Turnbull
CIA-OSWR/NED
Washington, DC 20505

Dr. Gregory van der Vink
IRIS, Inc.
1616 North Fort Myer Drive
Suite 1050
Arlington, VA 22209

Dr. Karl Veith
EG&G
5211 Auth Road
Suite 240
Suitland, MD 20746

Prof. Terry C. Wallace
Department of Geosciences
Building #77
University of Arizona
Tuscon, AZ 85721

Dr. Thomas Weaver
Los Alamos National Laboratory
P.O. Box 1663
Mail Stop C335
Los Alamos, NM 87545

Dr. William Wortman
Mission Research Corporation
8560 Cinderbed Road
Suite 700
Newington, VA 22122

Prof. Francis T. Wu
Department of Geological Sciences
State University of New York
at Binghamton
Vestal, NY 13901

ARPA, OASB/Library
3701 North Fairfax Drive
Arlington, VA 22203-1714

HQ DNA
ATTN: Technical Library
Washington, DC 20305

Defense Intelligence Agency
Directorate for Scientific & Technical Intelligence
ATTN: DTIB
Washington, DC 20340-6158

Defense Technical Information Center
Cameron Station
Alexandria, VA 22314 (2 Copies)

TACTEC
Battelle Memorial Institute
505 King Avenue
Columbus, OH 43201 (Final Report)

Phillips Laboratory
ATTN: XPG
29 Randolph Road
Hanscom AFB, MA 01731-3010

Phillips Laboratory
ATTN: GPE
29 Randolph Road
Hanscom AFB, MA 01731-3010

Phillips Laboratory
ATTN: TSML
5 Wright Street
Hanscom AFB, MA 01731-3004

Phillips Laboratory
ATTN: PL/SUL
3550 Aberdeen Ave SE
Kirtland, NM 87117-5776 (2 copies)

Dr. Michel Bouchon
I.R.I.G.M.-B.P. 68
38402 St. Martin D'Heres
Cedex, FRANCE

Dr. Michel Campillo
Observatoire de Grenoble
I.R.I.G.M.-B.P. 53
38041 Grenoble, FRANCE

Dr. Kin Yip Chun
Geophysics Division
Physics Department
University of Toronto
Ontario, CANADA

Prof. Hans-Peter Harjes
Institute for Geophysic
Ruhr University/Bochum
P.O. Box 102148
4630 Bochum 1, GERMANY

Prof. Eystein Husebye
NTNF/NORSAR
P.O. Box 51
N-2007 Kjeller, NORWAY

David Jepsen
Acting Head, Nuclear Monitoring Section
Bureau of Mineral Resources
Geology and Geophysics
G.P.O. Box 378, Canberra, AUSTRALIA

Ms. Eva Johannisson
Senior Research Officer
FOA
S-172 90 Sundbyberg, SWEDEN

Dr. Peter Marshall
Procurement Executive
Ministry of Defense
Blacknest, Brimpton
Reading FG7-FRS, UNITED KINGDOM

Dr. Bernard Massinon, Dr. Pierre Mechler
Societe Radiomana
27 rue Claude Bernard
75005 Paris, FRANCE (2 Copies)

Dr. Svein Mykkeltveit
NTNT/NORSAR
P.O. Box 51
N-2007 Kjeller, NORWAY (3 Copies)

Prof. Keith Priestley
University of Cambridge
Bullard Labs, Dept. of Earth Sciences
Madingley Rise, Madingley Road
Cambridge CB3 OEZ, ENGLAND

Dr. Jorg Schlittenhardt
Federal Institute for Geosciences & Nat'l Res.
Postfach 510153
D-30631 Hannover , GERMANY

Dr. Johannes Schweitzer
Institute of Geophysics
Ruhr University/Bochum
P.O. Box 1102148
4360 Bochum 1, GERMANY

Trust & Verify
VERTIC
Carrara House
20 Embankment Place
London WC2N 6NN, ENGLAND